ANALYSIS AND NETWORK SIMULATIONS OF HONEYBEE INTERNEURONS RESPONSIVE TO WAGGLE DANCE VIBRATION SIGNALS

A THESIS SUBMITTED IN FULFILLMENT OF
THE REQUIREMENTS FOR THE DEGREE OF

Doctor rerum naturalium

AT THE FACULTY OF BIOLOGY,
LUDWIG-MAXIMILIANS-UNIVERSITÄT MÜNCHEN

Ajayrama Kumaraswamy
München, 2019

This thesis was prepared under the supervision of Prof. Dr. Thomas Wachtler in the division of Computational Neurosciences at the Department of Biology, Ludwigs-Maximilians-Universität, München.

FIRST REVIEWER: PROF. DR. THOMAS WACHTLER

SECOND REVIEWER: PROF. DR. ANDREAS HERZ

DATE OF SUBMISSION: 12.02.2019

DATE OF DEFENSE: 12.07.2019

DECLARATION

I hereby declare that I have authored this thesis independently and without the use of any prohibited means. This thesis has not been submitted, either in part or full, to another examination authority. I have not attempted at any previous date to submit a doctoral thesis or appear before a doctoral examination committee.

München, 16.09.2019   ....
                           Ajayrama Kumaraswamy

CONTENTS

ABBREVIATIONS

JO   Johnston's organ

DL   dorsal lobe

PPL   posterior protocerebral lobe

mPPL   medial posterior protocerebral lobe

SEG   subesophageal ganglion

PC   protocerebrum

DC   deutocerebrum

dSEG   dorsal subesophageal ganglion

PD   pulse duration

IPI   inter-pulse interval

WP   waggle phase

PMC   primary mechanosensory center

AMMC antennal mechanosensory and motor center

LIST OF INCLUDED PUBLICATIONS

1. Kumaraswamy, A., Kai, K., Ai, H., Ikeno, H., and Wachtler, T. (2018). "Spatial registration of neuron morphologies based on maximization of volume overlap." In: *BMC Bioinformatics* 19, pp. 1–16. doi: `10.1186/s12859-018-2136-z`

2. Kumaraswamy, A., Ai, H., Kai, K., Ikeno, H., and Wachtler, T. (2019a). "Adaptations during maturation in an identified honeybee interneuron responsive to waggle dance vibration signals." In: *eNeuro* 6.5. doi: `10.1523/eneuro.0454-18.2019`

3. Ai, H., Kai, K., Kumaraswamy, A., Ikeno, H., and Wachtler, T. (2017). "Interneurons in the honeybee primary auditory center responding to waggle dance-like vibration pulses." In: *The Journal of Neuroscience* 37.44, pp. 0044–17. doi: `10.1523/JNEUROSCI.0044-17.2017`

4. [preprint] Kumaraswamy, A., Maksutov, A., Kai, K., Ai, H., Ikeno, H., and Wachtler, T. (2017a). "Network simulations of interneuron circuits in the honeybee primary auditory center." In: *bioRxiv*. doi: `10.1101/159533`

Permissions have been obtained for the reuse of the above papers, as well as for the figures in this thesis.

CONTRIBUTIONS AS CO-AUTHOR

PUBLICATION 1

This publication describes an algorithm for spatially co-registering neuron morphologies. I was the primary driver in the development of the algorithm and my main contributions were in the conception, implementation and validation of the method. Further, I contributed to the preparation of the original draft as well as the revision and finalization of the manuscript.

PUBLICATION 2

This publication describes adaptations in an identified honeybee auditory interneuron during maturation. The experimental data for this study was collected by our collaborators in Japan and I was the primary driver of the analysis part of the study. My main contributions were in deciding the methodology for comparing morphological and electrophysiological data and implementing them. Further, I contributed to the preparation of the original draft as well as the revision and finalization of the manuscript.

PUBLICATIONS 3 AND 4

Publication 3 describes 119 vibration-sensitive interneurons in the primary auditory center of the honeybee brain and categorizes them into neuron groups based on their dendritic arborization patterns and responses to antennal vibration stimuli. Further, based on experimental evidence, it proposes a putative neuronal network in the honeybee primary auditory center and highlights neural mechanisms for encoding distance information of waggle dance signals using simulations. My main contributions to this study were in the conception and implementation of simulation models for individual neurons and synapses of the proposed network as well as running simulations using the same stimulus patterns as in experiments. Publication 4 describes the simulation models and visualizes simulation results in detail. I contributed to the preparation of the original draft of Publication 4 as well as to the revision and finalization of both publications.

ABSTRACT

BACKGROUND: Honeybees have long fascinated neuroscientists with their highly evolved social structure and rich behavioral repertoire. They sense air vibrations with their antennae, which is vital for several activities during foraging, like waggle dance communication and flight.

GOALS: This thesis presents the investigation of the function of an identified vibration-sensitive interneuron, DL-Int-1. Primary goals were the investigation of (i) adaptations during maturation and (ii) the role of DL-Int-1 in networks encoding distance information of waggle dance vibration signals.

RESULTS: Visual inspection indicated that DL-Int-1 morphologies had similar gross structure, but were translated, rotated and scaled relative to each other. To enable detailed spatial comparison, an algorithm for the spatial co-registration of neuron morphologies, Reg-MaxS-N was developed and validated.

Experimental data from DL-Int-1 was provided by our Japanese collaborators. Comparison of morphologies from newly emerged adult and forager DL-Int-1 revealed minor changes in gross dendritic features and consistent, region-dependent and spatially localized changes in dendritic density. Comparison of electrophysiological response properties showed an increase in firing rate differences between stimulus and non-stimulus periods during maturation.

A putative disinhibitory network in the honeybee primary auditory center was proposed based on experimental evidence. Simulations showed that the network was consistent with experimental observations and clarified the central inhibitory role of DL-Int-1 in shaping the network output.

RELEVANCE: Reg-MaxS-N presents a novel approach for the spatial co-registration of morphologies. Adaptations in DL-Int-1 morphology during maturation indicate improved connectivity and signal propagation. The central role of DL-Int-1 in a disinhibitory network in the honeybee primary auditory center combined with adaptions in its response properties during maturation could indicate better encoding of distance information from waggle dance vibration signals.

MOTIVATION AND GOALS

Insects, in spite of having nervous systems much smaller than primates, exhibit fascinating behavior indicative of complex cognitive capabilities. The honeybee is no exception to this and several of its behaviors are unique even among insects. The foremost among such behavior is the waggle dance, which is one of the most advanced and sophisticated forms of symbolic communication among non-human animals (Munz 2005). The waggle dance is a ritualistic movement used by successful forager honeybees to communicate the distance and direction information of food sources to hive mates. Investigation of neural mechanisms underlying the sensory modalities involved in waggle dance with a focus on the encoding of waggle dance information can not only shed light on the neural principles that enable such complex communication behavior, but also inspire technologies useful for biomimetics. The research presented in this thesis looked into the antennal mechanosensory system in the honeybee, by which air vibrations produced during the waggle dance are perceived. Specifically, the research focused on the most frequently encountered vibration sensitive neuron in the honeybee primary mechanosensory center (PMC), DL-Int-1 (Ai et al. 2017) and investigated its function in processing waggle dance vibration signals in two ways. Firstly, adaptations in the structure and electric response in DL-Int-1 were studied by comparing data from young, newly emerged honeybees and mature forager honeybees. Since participation in waggle dance and foraging are mostly associated with mature foragers, adaptations in DL-Int-1 during maturation can provide insights about changes in its function for behavioral specialization. Secondly, simulations were conducted to investigate the role of DL-Int-1 in a putative network of neurons in the honeybee PMC based on experimental evidences.

1 | **INTRODUCTION**

HONEYBEES

This section presents briefly a few aspects of honeybee life, society, behavior and research that are relevant to this thesis.

Neuroscientific research in honeybees

Honeybees are among the few non-mammalian animal species that exhibit a highly evolved social structure, a rich behavioral repertoire, an exquisite navigational system, an elaborate communication system, and an extraordinary ability to learn colors, shapes, fragrances, and navigational routes quickly and accurately (Srinivasan 2010). Honeybee research has played a pioneering role in understanding the evolution of behaviors such as color vision, detection of ultraviolet and linearly polarized light, and symbolic communication in animals (Menzel 2012b). A wide spectrum of behaviors that can be examined under laboratory conditions along with the possibility of simultaneously monitoring their nervous system makes them specifically attractive to neuroscientists (Menzel 2012b). Systematic investigation of honeybee sensory perception and behaviour was pioneered by Karl von Frisch, who was awarded the Nobel Prize in 1973 for his work.

A hive of *Apis mellifera*, the widely studied species of honeybee, consists of three kinds of bees – fertile female queens, sterile female workers and male drones (Seeley 1985), and among them, the worker honeybee has fascinated neuroscientists for almost a century (Lindauer 1987). The worker honeybee performs a large number of impressive behaviors and tasks with a nervous system weighing less than a milligram and consisting of fewer than a million neurons (Srinivasan 2010; Menzel 2012b). For successfully gathering nectar and pollen, worker bees have to not only scout, identify and remember profitable food sources, but also adapt to changing environments and landscapes (Srinivasan 2010). This makes them a promising subject for studying the neural basis of a variety of behaviors such as color vision, pattern and shape recognition, communication, memory and learning, navigation and flight. Honeybees can identify colors and shapes reliably as well as learn abstract features of visual patterns (Srinivasan 2010), which they use to identify profitable food sources as well as visual landmarks during navigation. Upon returning from a nutrient-rich source, foragers communicate the location of remote sources using odor cues, taste cues as well ritualistic movement patterns called the waggle dance (Figure 1.1a, Menzel 2012b). Hive mates incorporate new information with their memories of recent excursions and fly to food sources avoiding obstacles, controlling flight speed, streamlin-

ing body posture as well as executing smooth landings (Srinivasan 2011). This rich array of capabilities and behaviors significant for the survival and proliferation of honeybee colonies provides promising opportunities to investigate neural principles and mechanisms underlying cognition.

Collective intelligence and behavior is another attractive aspect of honeybee research, which involves centralized as well as decentralized mechanisms of decision making (Menzel 2012b). Queens use special chemicals called pheromones to regulate reproduction and task prioritization of young worker bees (Beggs et al. 2007). Swarming, which involves a portion of the population of a hive moving to a new nesting site, is a prime example of collective decision making among honeybees (Visscher 2007) and involves scouting and investigation of several potential sites followed by advertisement and competition leading to the evolution of a consensus. These behaviors offer an exciting opportunity to investigate and identify the neural mechanisms underlying individual behavior and decision making that lead to collective intelligence.

The wealth of knowledge about individual and collective honeybee behavior gained through basic science research has lead to the development of more than a dozen algorithms for application in artificial intelligence (Xing and Gao 2014). Additionally, several robots have also been developed to simulate (Landgraf 2013), as well as to mimic and improvise (Y. Chen et al. 2017; Sabo et al. 2017; Srinivasan 2011) honeybee behavior.

Compared to other popular animal models such as the fly, mice and rats, genetic manipulation techniques for specific expression of proteins in honeybee neurons are still in development. Therefore, the speed and scale at which the neural foundation of honeybee behavior can be currently investigated is limited. Once ready, however, genetic manipulation techniques will enable the clarification of specific protein expression patterns leading to easier and quicker progress in understanding the role of associated neural processes in honeybee cognition and behavior (Menzel 2012b).

Different roles of the worker honeybee

Honeybees develop from eggs laid by the queen honeybee into special cells called brood cells, undergoing successively larval and pupal stages of metamorphosis before emerging as adults (Seeley 1996). Upon emergence, adult workers engage in different social roles that are generally age-dependent, which can, however, change depending on the individual and demands of the nest (Seeley 1996; Robinson 1992). For the first few days after emergence, the worker bee occupies herself with the cleaning of recently vacated brood cells.
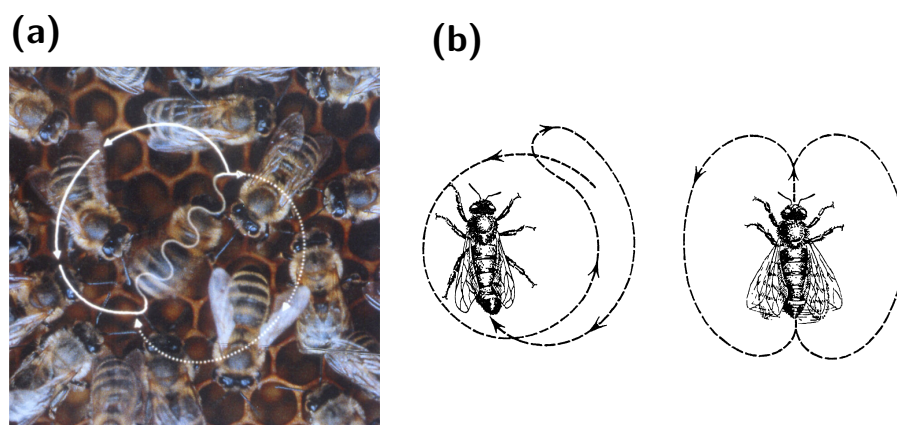
(a)

(b)

Figure 1.1: Honeybee waggle dance movements. (a) Picture of a honeybee dancing on a hive and follower bees crowding around her waggling abdomen. The movement of the dancer is shown with white lines and arrows. Modified version of Figure 1A of Chittka 2004. **(b)** Illustration of the movement patterns of the round dance (left) and the waggle dance (right). Modified version of Figure 30 of von Frisch 1973.

From the age of about 3 days, she becomes a "nurse", focusing primarily on secreting food and feeding developing honeybees, while also doing other tasks like tending to the queen and capping brood cells. From about 12 days, she moves out of the central brood nest to focus on food storage. This primarily involves receiving nectar from incoming foragers, converting it to honey using her enzymes and depositing it in storage cells. Other activities during her role as a "food storer" include packing pollen into designated cells, ventilating the hive by fanning her wings, dragging out dead honeybees, guarding the hive entrance and building new combs when required by activating her wax glands. Finally, at about 20 days, she ventures out of the hive to gather essential substances like nectar, pollen, water and resin and continues contributing till the end of her life. During this "forager" role, she could also function as a scout for exploring new nest sites if the need arises.

Waggle dance communication

A mature worker honeybee returning from a beneficial location such as a rich nutritional source or a potential nesting site advertises it to her hive mates by performing a special ritualistic movement (Figure 1.1a) in a designated part of the hive. This behavior, called "dancing", is one of the most advanced and sophisticated forms of symbolic communication in non-human animals (Munz 2005). Historically honeybee dancing has been classified into two types based on the pattern of movement – the round dance and the waggle

(a)

(b)
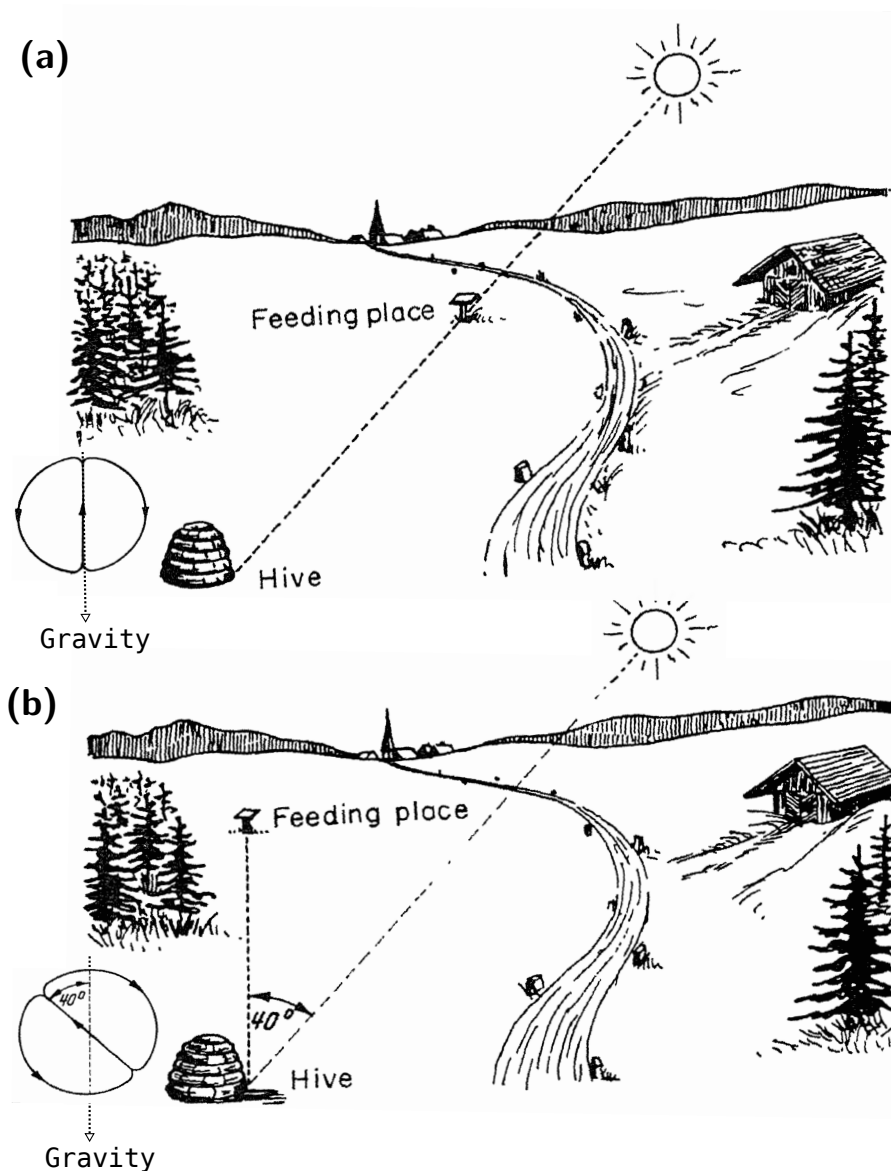
Figure 1.2: Direction encoding in waggle dance. (a) When the food source is located in the same direction as the sun from the hive, the waggle phase of the waggle dance is oriented exactly along the vertical, which is the direction opposite to gravity. **(b)** When the direction of the food source is rotated 40° anti-clockwise from the direction of the sun, the waggle phase also gets rotated by 40° anti-clockwise from the vertical. Modified version of Figure 31 of von Frisch 1973.

dance (Figure 1.1b, von Frisch 1967, Original German version: von Frisch 1965). During the round dance (Figure 1.1b left), the worker honeybee runs in a small circle that covers mostly one comb cell and its six neighbors and reverses her direction from time to time. This dance is used to indicate locations close to the hive and the target distance up to which honeybees perform the round dance ranges

from 2 m to 50 m depending on the species (Srinivasan 2011). For farther targets, she performs a dance shaped like the number '8' (Figure 1.1b, right), which is composed of a straight path as well as two curved paths. She starts by walking along the straight path, after which she returns to the beginning of the straight path along a curved path. She repeats this pattern, alternating between the two curved paths. During the straight path, she waggles her body, moving it from side to side like a pendulum. Hence, the part of the dance along the straight path is called "the waggle phase" and that along a curved path is called "the return phase". A recent study (Gardner et al. 2008) examined in detail the movement patterns of dancing bees and concluded that there was no clear switch between the two dances and that it's most meaningful to view the two dances as being at the ends of a continuum of movement patterns.

A dancing bee attracts the attention of her hive mates, who huddle around her waggling abdomen (Figure 1.1a) and follow during the dance movements(see `https://youtu.be/-7ijI-g4jHg`). After following a dance for many repetitions, worker bees fly out of the hive and visit the advertised location.

The pattern of waggle dance contains information about both the distance and direction of the target location (von Frisch 1967). Distance information is represented in the duration of the waggle phase, which is directly proportional to the distance of the target from the hive. The direction information is represented by the orientation of the straight path relative to the vertical, i.e., the direction opposite to gravity. The angle between the straight path and the vertical is the same as the angle between the flight path to sun and flight path to the target (Figure 1.2).

An advertising dancer communicates several pieces of information about the target to her hive mates through different sensory modalities. She brings back nectar from the target location in her honey stomach (Seeley 1996) and gives her hive mates samples to communicate its taste as well as scent (Farina and Wainselboim 2005). In addition, she carries the scent of the target flowers on the surface of her body, which is sensed by followers (Farina et al. 2011) and used to identify flowers, especially for close targets (von Frisch 1967). During the waggle phase, she produces pulses of sound vibrations by moving her thorax as well as by beating her wings, which travel through the honeycomb and air respectively, and are sensed by her hive mates (Hrncir et al. 2005). The temporal pattern of these sound vibration pulses has been proposed to contain information about both the distance and direction of the advertised source (von Frisch 1967; Michelsen 2003). Further, she conveys the quality of the food source by the liveliness with which

she dances (von Frisch 1967), with livelier dances having more number of loops and faster return phases (Seeley et al. 2000) as well as stronger thoracic vibrations (Hrncir et al. 2011). Additionally, a dancer releases a number of chemicals onto her abdomen as well as the air, which results in more workers flying out to forage (Thom et al. 2007).

VIBRATION SENSING IN THE HONEYBEE

This section contains a brief introduction to vibration sensing in the honeybee. It focuses on airborne vibration sensing and elaborates on associated behaviors and neural systems. It also describes briefly air vibration sensing in the fruit fly *Drosophila melanogaster*, highlighting similarities in vibration stimuli associated with communication behavior and the underlying neural systems.

Types of vibration sensing

Honeybees, like many other insect species, are pre-adapted for noisy environments (Claridge 2005; Henry 2005) and have developed specialized systems for sensing vibrations. These systems play an important role in honeybee social communication and are classified into two types based on the medium of propagation – substrate and airborne vibrations (Hrncir et al. 2005). Substrate-borne vibrations are produced by rhythmic thoracic oscillations that are transmitted to the substrate through their legs and honeybees sense them using subgenual organs on their legs. Airborne vibrations are produced by wing beats and honeybees sense them using the Johnston's organ (JO) located in the pedicel of their antennae (Figure 1.3b), which forms the initial part of the honeybee antennal mechanosensory system.

Behaviors involving antennal vibrations

Airborne vibrations produced by wing beats are associated with several insect behaviors such as species recognition based on flight sounds in swarming mosquitoes and courtship dances in Drosophila (Claridge 2005). In honeybees, as in flies, the perception of such vibrations by the JO was long associated primarily with the detection of flight speed (Heran 1959; Hrncir et al. 2005). A recent study in honeybees has also linked it to the modulation of body posture during flight (Taylor et al. 2013). However, air vibration sensing through the JO in the honeybee has been most investigated in the context of waggle dance communication. During the waggle phase of the waggle dance (Section 1.1.3), the worker honeybee beats her wings to produce jets of air according to a consistent temporal pattern (Figure 1.3a, Wenner 1962; Esch 1961; Hrncir et al. 2011) and these air jets propagate tailwards beyond her abdomen towards follower bees. These pulses are about 15 ms long (pulse duration, PD) and are separated by silent phases of about 15 ms (inter-pulse interval, IPI). The frequency of air vibration during these pulses is in the range 200–300 Hz. These air vibration pulses have been shown

to be crucial for recruiting hive mates to the advertised location (von Frisch 1967; Kirchner 1993) and mechanical models imitating waggle dancing honeybees have been able to recruit foragers (Michelsen et al. 1992; Landgraf et al. 2011).

Thus, there is evidence indicating that airborne vibration is central to multiple honeybee behaviors and is importantly essential for waggle dance communication. This motivates investigation of the neural mechanisms behind transduction and processing of air vibration signals in the honeybee.

Peripherial sensory system

Honeybees sense airborne vibrations in the environment using the JO, which is located in the pedicel of the antenna (Figure 1.3b, Yack 2004). The outermost part of the honeybee antenna, the flagellum, is not rigidly connected to the rest of the antenna and hence oscillates in response to vibrations in the air. These oscillations are transduced by sensory neurons of the JO and relayed to the honeybee brain (Ai et al. 2007; Tsujiuchi et al. 2007). Notably, Tsujiuchi et al. (2007) showed that the mechanical properties of the flagellum, as well as the sensory neurons of the JO in forager honeybees, were tuned to detect frequencies in the range 250–300 Hz, which are produced during waggle dance communication.

Primary Mechanosensory Center

Sensory neurons of the JO send their afferents to the primary mechanosensory center (PMC) of the honeybee brain, which consists of medial PPL and the AMMC and the latter is made up of the DL and dorsal subesophageal ganglion (SEG) (Figure 1.3b, Ai et al. 2007). To investigate the spatial distribution of neurons arborizing in these areas, Ai et al. (2009) injected a dye into the DL and allowed it to diffuse into neurons arborizing in it (Figure 1.3c). They found a large number of neurons with cell bodies in the protocerebrum (PC), the deutocerebrum (DC) and the SEG. Among them, three neuron types have been studied in detail – a local interneuron DL-Int-1, a projection neuron DL-Int-2 and a descending neuron PPL-D-1.

DL-Int-1

The soma of DL-Int-1 (Ai et al. 2009), which is also called AMMC-Int-1 (Ai and Itoh 2012), is located in the PC. A single neurite emanates from the soma and projects to the DL where it trifurcates into secondary dendrites (Figure 1.4a). One of these dendrites

arborizes profusely in the DL, a second in dorsal subesophageal ganglion (dSEG) and a third in medial posterior protocerebral lobe (mPPL). The arborization in mPPL has a small number of fine spines while those in the AMMC of the honeybee brain has fine spines as well as blebs. The dendrites of DL-Int-1 run close to the afferents of JO sensory neurons. DL-Int-1 are spontaneously active and respond to vibration stimulus applied to the ipsilateral antenna with on-phasic excitation, tonic inhibition and off-phasic rebound (Figure 1.4b). Further, the response is affected by the frequency of antennal vibration as well as light and olfactory stimuli. However, the response pattern to stimuli of waggle dance frequency (about 265 Hz) remained qualitatively unchanged when stimulus length was varied in the range 0.5–1.5 s (Ai et al. 2009).

DL-Int-2

The soma of DL-Int-2 (Ai et al. 2009), also called AMMC-Int-2 (Ai and Itoh 2012), is located in the DC. A single neurite emanates from the soma and projects to the DL where it arborizes profusely (Figure 1.4c, Ai et al. 2009). Three thick branches emanate from the DL and one of them extends towards the lateral PPL and has many fine blebs ("z" in Figure 1.4c). A second extends towards dSEG and has extensive arborization with numerous fine spines ("x" in Figure 1.4c) with a third extending towards lateral PPL ("y" in Figure 1.4c). DL-Int-2 show weak inconsistent spontaneous activity and respond to vibration stimulus applied to the ipsilateral antenna with on-phasic and tonic excitation (Figure 1.4d). The response pattern also varied based on the frequency and duration of the stimulus (Ai et al. 2009).

PPL-D-1

The soma of PPL-D-1 (Ai 2013), also called SPS-D-1 (Ai and Itoh 2012), is located in the SEG. A single neurite emanates from the soma and projects to dSEG where it bifurcates into secondary branches (Figure 1.4e, Ai 2013). One branch arborizes in ipsilateral PPL while the other arborizes in the contralateral PPL and dSEG. PPL-D-1 is a descending neuron, with a thick branch descending from the brain to the body of the honeybee along the ventral nerve cord. PPL-D-1 does not respond to vibration stimulus of frequency 265 Hz applied to the ipsilateral antenna. However, when citral olfactory stimulus was applied to the contralateral antenna simultaneously with vibration stimulus at 265 Hz to the ipsilateral antenna, PPL-D-1 responded with long-lasting excitation (Ai 2013).

Similarities with Drosophila vibration sensing

Airborne vibration sensing in the Drosophila has many similarities with that in the honeybee. The most studied behavior in the context of airborne vibration sensing in Drosophila is the courtship ritual, during which males exhibit a sequence of stereotyped behavior (Ishikawa and Kamikouchi 2016) and produce courtship songs by vibrating their wings which typically alternates between sine and pulse songs. The pulse songs have however attracted more research interest as males and females exposed to pulse songs show behavior associated with courtship and copulation (Ishikawa and Kamikouchi 2016).

The antennal mechanosensory system in Drosophila has several commonalities with that in the honeybee. Although the JO is present in the antenna of most insect species, it is specialized for detecting near-field air vibrations in some Hymenoptera including honeybees and many Diptera including Drosophila (Yack 2004). Drosophila have a feather-like protrusion called "arista" attached to the third segment of their antenna which vibrates in response to airborne vibrations (Ishikawa and Kamikouchi 2016) and causes the basal part of the third antennal segment to rotate relative to the second antennal segment. These rotations are transduced by the JO present in the second antennal segment and relayed to the brain.

Similar to the honeybee, the afferents of JO sensory neurons in Drosophila project to the PMC, which consists of the AMMC, the wedge and the SEG. Several types of local, projection and descending neurons arborizing in the PMC have been identified and studied (Ishikawa and Kamikouchi 2016) and neural silencing studies using genetic tools have shown two of these neuron types to be necessary for courtship song responses (Vaughan et al. 2014). Higher order auditory neurons and their connectivity have also been investigated (Ishikawa and Kamikouchi 2016).
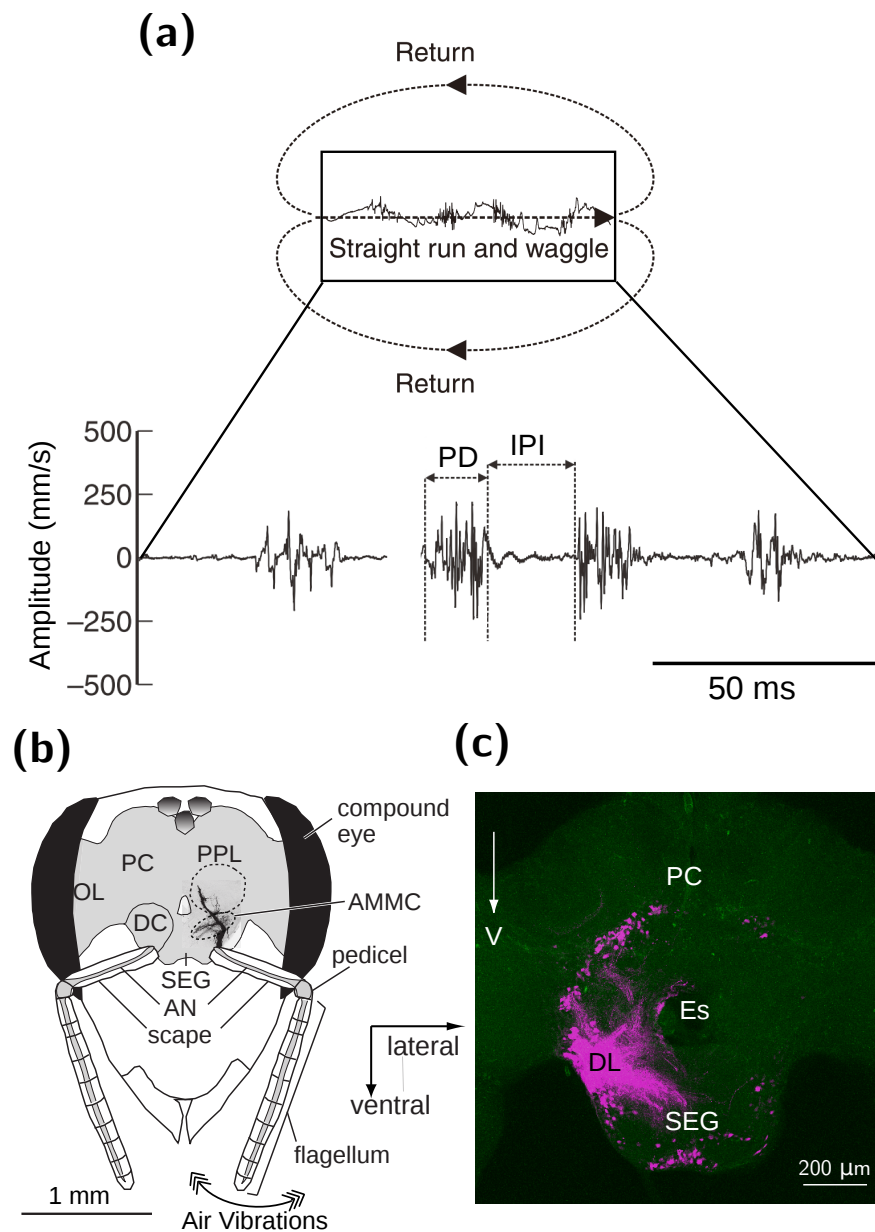
Figure 1.3: Waggle dance signals and the antennal mechanosensory system (a) Waggle dance vibration signals. During the waggle phase (WP), dancer honeybees produce a series of air vibration pulses of frequency 200–300 Hz and duration 15 ms (PD), separated by about 15 ms intervals (IPI). Modified from Figure 1L of Ai et al. 2018. **(b)** Antennal mechanosensory system. Oscillations of flagellum caused by air vibrations are picked up by the JO in the pedicel and relayed to the PMC of the honeybee brain consisting of AMMC and medial PPL. Modified from Figure 1C of Ai et al. 2007. **(c)** A fluorescence image of a honeybee brain in which dextran-tetramethylrhodamine was injected into the right DL. About 200 interneurons were stained in this sample, with cell bodies located in many regions of the ipsilateral and contralateral hemispheres. Modified from Figure 2A of Ai et al. 2009. *OL: optic lobe; AN: antennal nerve; Es: esophagus*
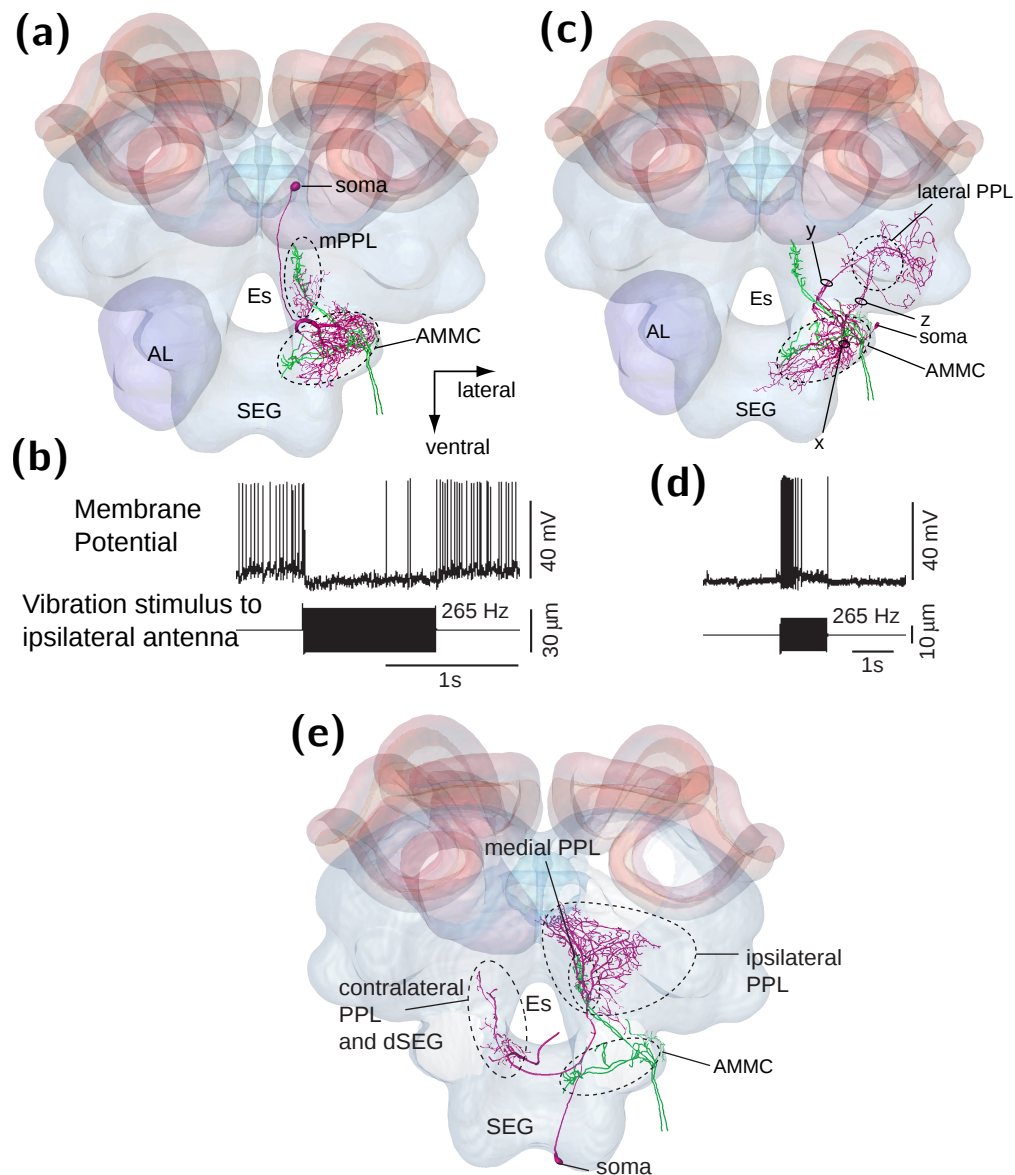
Figure 1.4: PMC neurons. **(a)** Arborization pattern of DL-Int-1. Its dendrites (maroon) run close to JO afferents (green). Modified from Figure 5A of Ai 2013. **(b)** A response trace of DL-Int-1 to vibration stimulus showing on-phasic excitation, tonic inhibition and offset rebound. Modified from Figure 6E of Ai et al. 2009. **(c)** Arborization pattern of DL-Int-2. Modified from Figure 6A of Ai 2013. **(d)** A response trace of DL-Int-2 to vibration stimulus showing on-phasic and tonic excitation. Modified from Figure 13F of Ai et al. 2009. **(e)** Arborization pattern of PPL-D-1. Modified from Figure 7A of Ai 2013.

CONTEXT OF DOCTORAL RESEARCH

This section introduces the context in which the doctoral research was carried out, with brief descriptions of the parent project "Gin-Jang", goals of the thesis within the parent project and the data involved.

The GinJang project

"GinJang" is a German-Japanese research collaboration project that investigates the neural basis of hearing in honeybees, focusing on neural circuitry in the honeybee primary auditory center that processes air vibration signals involved in waggle dance communication. Prof. Hiroyuki Ai[1] at Fukuoka University leads experimental investigations of the project using intracellular recording and staining as well as imaging. Prof. Hidetoshi Ikeno[2] at the University of Hyogo leads the segmentation and reconstruction of the three-dimensional structure of neurons as well as the construction of a honeybee standard brain focused on primary auditory center (Ikeno et al. 2018b). Prof. Thomas Wachtler[3] at Ludwig-Maximilians-Universität München leads the computational analysis and modeling of the data produced at the labs of Dr. Ai and Prof. Ikeno.

Goals of doctoral research

As part of the GinJang project, the overall direction of the thesis was the investigation of the function of an identified vibration-sensitive interneuron DL-Int-1 in processing waggle dance vibration signals and this consisted of two sub-projects. Firstly, adaptations in the morphology and physiology of DL-Int-1 during maturation were investigated, by comparing 3D structural data and intracellular recoding traces from newly emerged adult honeybees and mature, forager honeybees (see Section 1.1.2). Since waggle dance communication and foraging are generally associated with mature foragers, adaptations in DL-Int-1 during maturation can provide insights about adaptations in its function relevant for processing waggle dance signals. The second sub-project investigated the function of DL-Int-1 in a proposed network of neurons in the honeybee PMC. This was undertaken by building models for DL-Int-1 and other PMC neurons along with the synapses connecting them

---

1 http://resweb2.jhk.adm.fukuoka-u.ac.jp/FukuokaUnivHtml/info/3855/R110E.html
2 https://www.researchgate.net/profile/Hidetoshi_Ikeno
3 http://neuro.bio.lmu.de/members/comp_neuro_wachtler/wachtler_t/index.html

based on experimental observations, followed by simulations with behaviorally relevant stimuli.

Data involved

Experiments were carried out in the lab of Prof. Hiroyuki Ai at Fukuoka University using newly emerged adult and forager honeybees. Sharp electrodes were inserted into the honeybee PMC to record intracellularly from neurons that responded to antennal vibration. Traces of the neuron membrane potential, vibration stimulus and current injected through the electrode into the cell were recorded for the duration of the experiments using Spike2 software (Cambridge Electronic Design Limited, Cambridge, England) and saved in SMR Files. Experimental metadata such as details of the subject honeybee, types and characteristics of stimuli applied and amplifier gain variations were stored in excel files. These data were used to investigate the changes in DL-Int-1 physiology during maturation as well as for building spiking models of DL-Int-1 and DL-Int-2.

Fluorescent dyes were injected into the neurons after electrophysiological recordings. Honeybee brains were extracted and imaged using laser scanning microscopy (LSM) to obtain 3D image stacks containing singly stained neurons. Information about the shape and structure of neurons were extracted from the image stacks using a newly developed method (Ikeno et al. 2018a) at the lab of Prof. Ikeno and stored as SWC morphologies (Cannon et al. 1998). The resulting SWC files of newly emerged adult and forager DL-Int-1 were used to investigate changes in morphology during maturation.

All experimental data and processed data were collected in an online database for sharing among collaborators.

COMPARATIVE ANALYSIS OF NEURON MORPHOLOGY

This section contains brief introductions into the acquisition and modeling of neuron morphology, various existing methods for comparing morphologies and detailed morphological analysis based on spatial registration. Comparing the morphology of DL-Int-1 neurons between newly emerged adults and foragers was one of the goals of the doctoral research and these topics provide foundations for the parts of Methods and Results that describe morphological comparisons.

Acquiring and modeling neuron morphology

Neuron morphology is the description of shape and structure of neurons. It is recorded by introducing an agent into a neuron that, when imaged, stands out against the surrounding tissue. The most commonly used highlighting agents are fluorescent dyes (Turner et al. 1993) and genetically introduced fluorescent proteins (Livet et al. 2007). Most commonly used imaging methods are light (Sanderson et al. 2014; Sigrist and Sabatini 2012) and electron microscopy (Briggman and Bock 2012). From the resulting three dimensional images, a model representing the structure of the neuron is extracted (Meijering 2010) using manual (J. R. Glaser and E. M. Glaser 1990; Magliaro et al. 2017), semi-automatic (Feng et al. 2015) or completely automatic methods (Donohue and Ascoli 2011; Acciai et al. 2016; Peng et al. 2015; Peng et al. 2015). The most widely used model format is the SWC format (Cannon et al. 1998), in which the structure of the neuron is represented by a set of nodes connected in a tree structure, where each node represents a point in three-dimensional space and contains information about its location and thickness.

Comparison based on whole cell measures

A commonly applied approach for comparing neuron morphologies is the statistical testing of differences between whole cell scalar measures. These measures are mainly of two types – topological and metric (Uylings and Pelt 2002). Topological measures do not consider spatial aspects of morphologies such as length, diameter and angle. They view morphologies only as trees, with each tree consisting of a root node, branch nodes, branch segments and terminal nodes. They quantify measures like the degree of a node, which is the total number of terminal nodes contained in the subtree emanating from the node and the centrifugal order, which is the number of branch segments contained in the path between

the root and the node. On the other hand, metric measures consider information about the length, thickness and angle of dendritic branches in addition to topological aspects in their calculations. Examples of metric measures are average diameter, total surface area and total volume of the morphology. Such measures are evaluated for every dendritic branch and bifurcation of a morphology and reduced to one number using functions such as mean, minimum and maximum.

These measures transform information about all dendrites and bifurcations of a morphology into one number and hence the comparisons based on these scalar measures can only detect net overall differences. They could overlook differences that are not spatially homogeneous in sign, as the calculation of whole cell measures collapses such inhomogeneities. Nonetheless, depending on the morphologies, such comparisons result either in large significant differences, which indicate that the morphologies are widely different, or small and possibly significant differences, which could then be used to choose the direction of further analysis.

There are several software tools for calculating whole cell scalar measures, prominent ones being Vaa3d[4] (Peng et al. 2010), btmorph[5] (Torben-Nielsen 2014), and L-Measure[6] (Scorcioni et al. 2008). Most tools have implemented a few specific measures in addition to a set of common measures. The L-Measure help webpage[7] provides a comprehensive list of commonly implemented measures and their definitions.

Comparison based on radially distributed measures

Another widely used approach for comparing neuron morphologies is based on Sholl Analysis (Sholl 1953), which divides morphologies into radial subregions using spherical shells (Uylings and Pelt 2002). Shells are constructed equally thick and centered about a common prominent landmark on each morphology. Scalar measures are calculated for each shell and either compared separately or combined together to form radial distributions, which are subsequently compared.

Although such measures localize differences at a finer spatial scale than whole cell measures, they overlook differences that are inhomogeneous in sign over a shell. For cases where differences at the level of spherical shells are small and not highly significant,

---

4 `vaa3d.org`
5 `https://github.com/btorb/btmorph_v2`
6 `http://cng.gmu.edu:8080/Lm`
7 `http://cng.gmu.edu:8080/Lm/help/index.htm`

analysis at an even finer spatial scale, such as that using 3D voxels could be required.

Spatial co-registration and detailed comparison

One approach to spatial localization of differences between morphologies involves division of morphologies into subregions and comparing scalar measures restricted to individual subregions. Such analysis, however, requires the dendritic arborizations of all morphologies in a subregion to correspond to each other, which is achieved by a process called spatial registration that removes differences in translation, rotation and scaling between morphologies.

Some analyses do not require all spatial differences between morphologies to be removed. A prominent example is Sholl analysis, which uses spherical shells for dividing morphologies and hence is invariant to rotational differences as long as translational and scale differences are removed. Thus a common approach for registering morphologies before Sholl analysis is to align prominent landmarks such as the center of the soma (O'Neill et al. 2015; Langhammer et al. 2010; Coskren et al. 2014) or prominent branching points (Mizrahi et al. 2000; Cuntz et al. 2008).

However, if the subregions are not invariant to rotation differences, for example 3D voxels, a more precise spatial registration of morphologies is required. Several different approaches have been used to achieve this. One approach uses the standard brain, which is the average of a large number of whole brain images in which prominent landmarks have been labeled (Menzel 2012a; Evans et al. 2012). Morphologies of individual neurons are then recorded along with landmarks in their surrounding tissues, which are then used to register the morphologies into the standard brain. Other approaches have been used when standard brains were not available or applicable. Mizrahi et al. (2000) registered morphologies by translating them to match landmarks and rotating them about one axis. BlastNeuron (Wan et al. 2015) used an affine registration method based on pointwise Euclidean distances and RANSAC sampling for establishing the detailed spatial and topological correspondence between morphologies. Several Iterative Closest Point based methods from computer vision and biomedical imaging are also applicable, specifically the ones that can handle morphologies scaled differently along different axes (Maier-Hein et al. 2012; E. Chen et al. 2015).

2 | METHODS AND RESULTS

ORGANIZATION

The methods and results of the doctoral research have been included in four publications. This section describes how the contents of the four publications map onto the two goals of the thesis (Section 1.3.2).

Adaptations during maturation

When visualized together, newly emerged adult and forager DL-Int-1 morphologies showed similar overall shape and branching pattern, but were rotated, translated and scaled with respect to each other. Detailed spatial comparison of the morphologies required the removal of these differences and hence, a new method for the spatial registration of neuron morphologies was developed. Publication 1 presents a detailed description of the new method as well as its validation, which was done by comparing its performance with that of other existing methods on a large data set of insect morphologies. Application of the new method to DL-Int-1 morphologies and detailed spatial comparison of their dendritic features are presented in Publication 2.

Electrophysiological data of newly emerged adult and forager DL-Int-1 were processed along with experimental metadata to identify and organize important parts of response traces. Comparison of several response features between the two maturation levels is presented in Publication 2.

Network Function of DL-Int-1

Dendritic projection patterns, electrophysiological responses and immunohistochemistry of DL-Int-1 and DL-Int-2 suggest a circuitry of excitatory and inhibitory neurons for encoding honeybee communication signals. The setup and simulation of this network as well as the comparison of simulated and experimental response traces of DL-Int-1 and DL-Int-2 to waggle dance-like stimuli are presented in Publication 4. These computational results have been included in Publication 3, which proposes and discusses this network after a detailed experimental characterization of DL-Int-1, DL-Int-2 and other neurons in the honeybee PMC.

PUBLICATION 1

Citation

1. Kumaraswamy, A., Kai, K., Ai, H., Ikeno, H., and Wachtler, T. (2018). "Spatial registration of neuron morphologies based on maximization of volume overlap." In: *BMC Bioinformatics* 19, pp. 1–16. doi: `10.1186/s12859-018-2136-z`

Context

This publication describes a method for spatial registration of neuron morphologies. It is especially suited for stereotypic insect neurons like DL-Int-1.

When visualized together, newly emerged adult and forager DL-Int-1 morphologies had similar shape and branching patterns and this was confirmed by preliminary analysis using whole cell measures. Before investigating spatially localized differences, the morphologies were required to be co-registered by the removal of translation, rotation and scale differences and hence an algorithm called "Reg-MaxS-N" was developed. This publication presents this algorithm in detail. Comparison of Reg-MaxS-N with six state-of-the-art algorithms using five diverse sets of test insect morphologies showed that Reg-maxS-N had the best performance for most test sets and highlighted the test cases for which Reg-MaxS-N was particularly suitable.

This algorithm was applied to co-register newly emerged adult and forager DL-Int-1 morphologies and identify local differences in dendritic density, which is presented in Publication 2.

BMC Bioinformatics

METHODOLOGY ARTICLE   **Open Access**

CrossMark

Spatial registration of neuron morphologies based on maximization of volume overlap

Ajayrama Kumaraswamy[1]* , Kazuki Kai[2], Hiroyuki Ai[2], Hidetoshi Ikeno[3] and Thomas Wachtler[1]

Abstract

Background: Morphological features are widely used in the study of neuronal function and pathology. Invertebrate neurons are often structurally stereotypical, showing little variance in gross spatial features but larger variance in their fine features. Such variability can be quantified using detailed spatial analysis, which however requires the morphologies to be registered to a common frame of reference.

Results: We outline here new algorithms — Reg-MaxS and Reg-MaxS-N — for co-registering pairs and groups of morphologies, respectively. Reg-MaxS applies a sequence of translation, rotation and scaling transformations, estimating at each step the transformation parameters that maximize spatial overlap between the volumes occupied by the morphologies. We test this algorithm with synthetic morphologies, showing that it can account for a wide range of transformation differences and is robust to noise. Reg-MaxS-N co-registers groups of more than two morphologies by iteratively calculating an average volume and registering all morphologies to this average using Reg-MaxS. We test Reg-MaxS-N using five groups of morphologies from the *Droshophila melanogaster* brain and identify the cases for which it outperforms existing algorithms and produce morphologies very similar to those obtained from registration to a standard brain atlas.

Conclusions: We have described and tested algorithms for co-registering pairs and groups of neuron morphologies. We have demonstrated their application to spatial comparison of stereotypic morphologies and calculation of dendritic density profiles, showing how our algorithms for registering neuron morphologies can enable new approaches in comparative morphological analyses and visualization.

Keywords: Spatial registration, Neuron morphology

Background

Since Ramon y Cajal's 'Neuron Theory' [1], neuronal morphology has been a prominent field of study in Neuroscience. With early hand-drawn illustrations, later camera lucida tracings and more recent digital reconstructions [2], scientists have investigated the structure of individual nerve cells to better understand its role in neuronal function and pathology. Using modern imaging techniques and reconstruction algorithms, labs from around the world are producing huge numbers of detailed 3D morphologies [3, 4], and databases have been developed to collect and host such data [5].

A prominent application of neuron morphology is in comparative studies aiming to quantify the inter-group and intra-group variability of neurons. Neuronal shape and structure have been known to vary widely, even across specimens of a single species, making their characterization and classification a very difficult task [6]. Although long investigated [7, 8], the general principles underlying such diverse structures have largely been elusive, with a few widely applicable ones being uncovered only in the last decade [9–12]. Many different approaches with increasingly complex methods have therefore been used in the investigation of neuronal shape and structure.

*Correspondence: ajayramak@bio.lmu.de
[1]Department of Biology II, Ludwig-Maximilians-Universität München, Grosshadernerstr. 2, Planegg-Martinsried 82152 Germany
Full list of author information is available at the end of the article

Kumaraswamy *et al. BMC Bioinformatics*   (2018) 19:143

Page 2 of 16

A common approach has been to statistically test the variance of whole cell scalar measures ([13, 14]) of neuronal morphologies within and between groups. Although these methods have been successful in some cases [15–17], they have proven unsuitable for quantifying finer changes in topology and morphology [15, 18].

The next finer level of quantification involves dividing each morphology into concentric disks or shells about pre-identified centering points, grouping topologically or morphologically equidistant regions from different individuals and computing statistical variability of morphological and topological measures like the number of dendrites [19–21] within and across groups to characterize morphologies. For each such set of corresponding regions, statistical variability of morphological and topological measures like the number of dendrites [19–21] are used to characterize morphologies. Although this approach has been successfully used to quantify inter-group and intra-group variability in several studies of specific cell types [22–25], it has been found to be inadequate for morphologies that have similarly complex structures but differ in fine spatial distributions of morphological and topological features [15, 18]. For such cases, Mizrahi et al. [18] illustrated the use of Hausdorff Distance based features by quantifying the overall spatial dissimilarity between morphologies at different spatial scales. More recently, Kanari et al. [26] proposed a novel feature based on radial distance and topological "persistence" of dendrites and showed that a distance measure based on it could distinguish groups of complex morphologies with fine differences. A shortcoming of these approaches is that regions that are morphologically or topologically equidistant are lumped together for analysis, which can lead to dilution or cancellation of differences. Another drawback of this approach is the requirement for identification of corresponding centering points across different specimens, especially for invertebrates for which the somas are "segregated" [27] and variably located (for example, see Additional file 1 that visualizes classified groups of morphologies from *Drosophila melanogaster*).

For localization of inter-group and intra-group differences in morphological features, a spatial correspondence needs to be established between regions, in other words, the morphologies need to be co-aligned or co-registered. Several recent studies have proposed methods for such co-registration of morphologies and used them to compare morphologies.
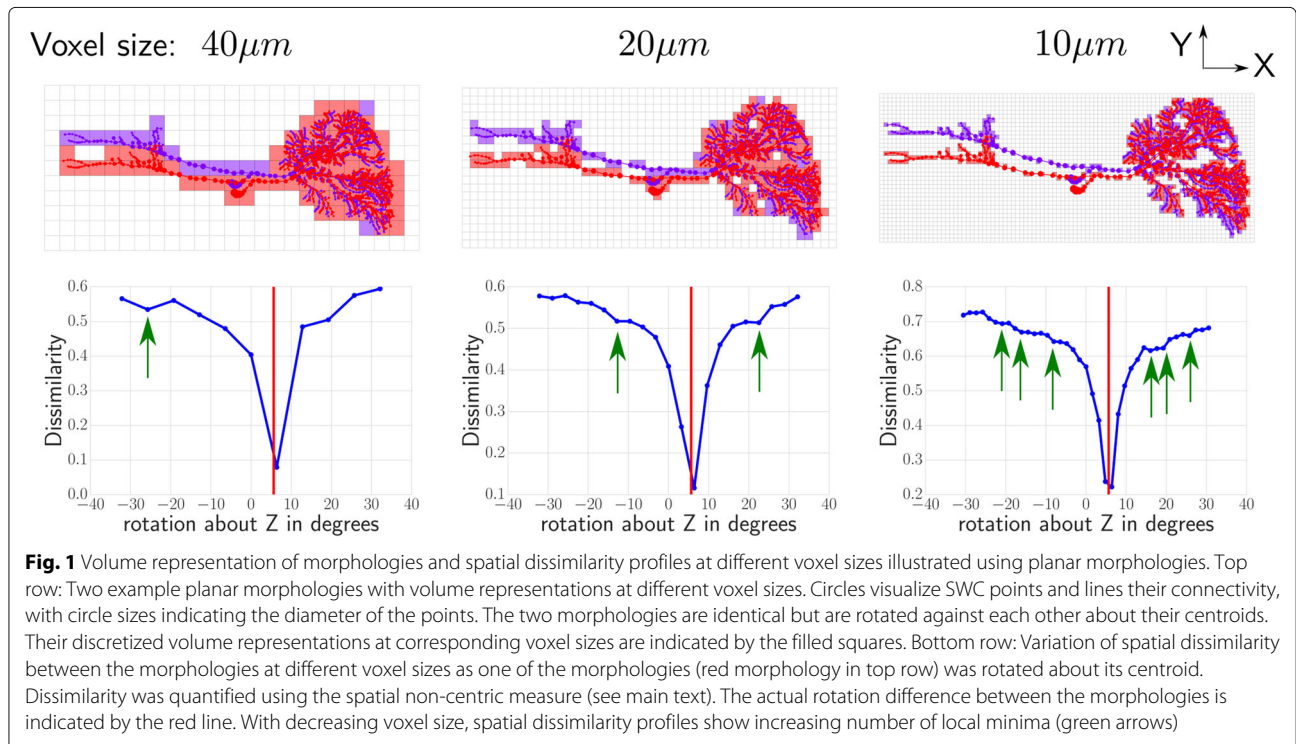
Fiduciary markers can be used to register the original image data to a standard brain before extracting morphologies [28, 29]. Although this approach is very effective for brain regions with an existing standard brain [30–32], construction of a new standard brain is beyond the means of individual researchers as it requires a huge concerted effort. Furthermore, even for the cases where brain atlases are available, registration of individual morphologies can be ineffective due to lack of sufficient fiduciary markers in the brain region of interest. Hence methods that co-register morphologies without requiring external information are needed.

Other studies have presented co-registration methods that do not need fiduciary markers. Mizrahi et al. [18] implemented a method consisting of a translation for matching landmarks and rotation about one axis based on radii of ganglia. BlastNeuron [33] uses an affine registration method based on pointwise Euclidean distances and RANSAC sampling [34] as a preprocessing step for establishing detailed spatial and topological correspondence between morphologies. Several Iterative Closest Point (ICP) based methods from computer vision and biomedical imaging are also applicable, specifically the ones that can handle morphologies scaled differently along different axes [35, 36]. All these methods use measures of dissimilarity based on pointwise Euclidean distances for registration and hence seek a solution of point-to-point or surface-to-surface overlap, which can be hard to achieve for neuron morphologies, due to natural biological variation in their fine spatial structures. This has also been a major consideration in the construction and application of brain atlases [37]. Even neurons that have highly consistent global spatial features show considerable variation in their lower order branches [18, 37]. Moreover, the spatial region occupied by dendritic arbor has been shown to be important for the classification and synthesis of morphologies [15] and for investigating the role of single neuron morphology in the population [38]. This is consistent with dendrites and axons occupying specific spatial regions for making synaptic connections, while, within these regions, there can be variability in the exact arborization patterns at fine spatial scales [10]. Therefore, our approach aims to match the volume occupied by dendritic arbors at different spatial scales instead of seeking a point-to-point match between morphologies. Specifically, affine transformations are applied to blurred volume representations of morphologies at different spatial scales (Fig. 1) to maximize spatial overlap between volumes occupied by them. Using this approach, we present Reg-MaxS (**Reg**istration based on **Max**imization of **S**patial overlap) and Reg-MaxS-N for co-registering pairs and groups of morphologies, respectively.

Methods

We describe here algorithms for co-registration of morphologies based on maximizing spatial overlap and such an approach requires defining a measure of spatial dissimilarity between morphologies and describing a strategy for finding a transformation that minimizes this dissimilarity. We discuss these aspects in the following subsections.

Kumaraswamy *et al. BMC Bioinformatics* (2018) 19:143

Page 3 of 16

Fig. 1 Volume representation of morphologies and spatial dissimilarity profiles at different voxel sizes illustrated using planar morphologies. Top row: Two example planar morphologies with volume representations at different voxel sizes. Circles visualize SWC points and lines their connectivity, with circle sizes indicating the diameter of the points. The two morphologies are identical but are rotated against each other about their centroids. Their discretized volume representations at corresponding voxel sizes are indicated by the filled squares. Bottom row: Variation of spatial dissimilarity between the morphologies at different voxel sizes as one of the morphologies (red morphology in top row) was rotated about its centroid. Dissimilarity was quantified using the spatial non-centric measure (see main text). The actual rotation difference between the morphologies is indicated by the red line. With decreasing voxel size, spatial dissimilarity profiles show increasing number of local minima (green arrows)

Measures of spatial dissimilarity

Our algorithms approach spatial dissimilarity based on the overlap between volumes occupied by morphologies at different spatial scales. The following definition for volume occupied by morphologies is used.

Representing the volume of a morphology

A common way of representing a neuron's three dimensional structure is by using the SWC format [14, 39], which represents a binary tree embedded in three dimensional space. Each point or node has, apart from its three spatial coordinates, a radius associated with it. With these features, every parent-child pair of nodes can be used to construct a frustrum, and consequently a set of connected frustra can be constructed from a tree structure which then represents the neuronal morphology. In our algorithms, to extract a volume representation of a morphology described in the SWC format, the three dimensional space containing the morphology is discretized into a set of equally sized cubic voxels (Fig. 1 top row). The voxels are positioned so that there is a voxel with its center at the origin of the space and the edge length of a voxel, which we term "voxel size", is the most important parameter of this volume discretization. Among these voxels, those that contain at least one point of the morphology are identified and the resulting set of voxels is used to represent its volume.

Measures of spatial dissimilarity for two morphologies

Given two morphologies *A* and *B*, we define spatial dissimilarity (*D*) from their volume representations *setA* and *setB* as:

$$D(setA, \ setB) = \frac{n(setA \ - \ setB) + n(setB \ - \ setA)}{n(setA \ \cup \ setB)}$$
$$= 1 - \frac{n(setA \ \cap \ setB)}{n(setA \ \cup \ setB)}$$

where $n()$ represents the number of elements in a set, and $\cup$ and $\cap$ represent the set union and set intersection operators, respectively. This measure essentially quantifies the spatial overlap between two morphologies normalized by their total volume.

Our algorithms use two measures of spatial dissimilarity, which we call "centric" and "non-centric" measures. The non-centric measure calculates the spatial dissimilarity between morphologies based on the values given, without applying any transformations. This measure is used when estimating translation and rotation differences between morphologies. The centric measure first translates one of the morphologies so that its centroid coincides with that of the other and calculates spatial dissimilarity using the volumes of the resulting morphologies. This measure is used when estimating scaling differences.

Kumaraswamy *et al. BMC Bioinformatics*   (2018) 19:143

Page 4 of 16

Measures of spatial dissimilarity for a group of morphologies

We define a measure for more than two morphologies based on voxel occupancy in the following paragraphs.

Given a group of morphologies, occupancy of a voxel is defined as the total number of morphologies of the group that have at least one point belonging to the voxel. A histogram of voxel occupancy values is calculated using all voxels with non-zero occupancy. A weighted histogram is created by multiplying each count of the histogram by its voxel occupancy. A normalized histogram is created by normalizing the weighted histogram by its sum.

It is desirable that a perfectly co-registered group of morphologies, i.e., a group with each morphology occupying the same set of voxels, has a spatial dissimilarity of zero. The normalized histogram of such a group would have a value of one at voxel occupancy equal to the size of the group and zero for all other values of voxel occupancy. Larger deviation from such a normalized histogram indicates larger spatial dissimilarity. Therefore, we define spatial dissimilarity of a group of morphologies as the distance between its normalized histogram and the normalized histogram corresponding to perfect spatial overlap, quantified by Earth-Mover-Distance [40].

Estimating best transformations

In our approach, morphologies are co-registered by repeatedly removing rotation, scaling or translation differences. These differences are estimated using a multi-scale method based on exhaustive searches, which are described in the following paragraphs. Since the measures defined above show multiple local minima over the space of transformations, especially when working at low voxel sizes (Fig. 1), gradient based optimization techniques are not suitable.

Exhaustive search

Exhaustive search is a basic search algorithm where all candidates from the search space are sequentially generated and tested to find the solution which optimizes a certain criteria. To illustrate this with the example of estimating the rotational difference between two morphologies, exhaustive search can be formulated as sequentially generating all possible rotations, applying them to one of the morphologies, calculating spatial dissimilarity for each of them with the reference and choosing that rotation which leads to the least dissimilarity. However, the number of possible rotations is infinite. Therefore, an approximate estimate is obtained by generating a discrete set of equally spaced rotations from a plausible region of the rotation space and exhaustively searching among these rotations for the optimal rotation. This can be implemented by parametrizing rotation, sampling the plausible range of each parameter uniformly with a certain inter-sample-interval, and exhaustively searching all

combinations of the resulting parameters (for implementation details see Additional file 2).

Multi-scale estimation

Using exhaustive search on a discretized search space imposes a trade-off between accuracy of the resulting estimate and the computational cost associated with its calculation. To reduce this computational cost, our algorithms use the strategy of hierarchical or multi-resolution matching [41, 42] which has been successfully used to speed up and reduce errors of 3D image registration methods. Starting at the largest voxel size, it runs an exhaustive search over an equally spaced discrete set of plausible parameters to find an estimate. The exhaustive search at the next lower voxel size is run over a smaller region around this estimate determined by its uncertainty (see Additional file 2 for more details). Thus estimates are progressively refined by running exhaustive searches over a sequence of discretized volumes generated using decreasing values of voxel size.

Reg-MaxS

Using this multi-scale estimation method to determine transformation differences between morphologies, Reg-MaxS iteratively applies transformations to remove determined differences until no transformation reduces the spatial dissimilarity between the morphologies any further. It first translates one of the morphologies so that its center coincides with the other. It then applies a sequence of translation, rotation and scaling transforms to minimize the spatial dissimilarity between morphologies. The order in which the different transformations are applied is determined based on how the application of one transformation influences the subsequent estimation of another transformation difference.

Rotation and translation do not affect each other, i.e., if there are only rotation and translation differences between morphologies, it does not matter whether the rotation difference is removed first and then the translation difference or vice versa. However, scaling and rotation/translation affect each other, i.e., applying a scaling affects a subsequent estimation of a translation/rotation difference and vice versa. Hence, Reg-MaxS applies a sequence of translation/rotation transforms until no translation or rotation can reduce spatial dissimilarity further. Then it applies a scaling transform. This is followed again by a set of translation/rotation transforms which is then followed again by a scaling. This iteration of alternatively applying a set of translation/rotation and scaling is continued until none of the transforms can decrease the spatial dissimilarity between the morphologies any further. Finally, the iteration at which spatial dissimilarity was minimized is chosen as the final solution.

Kumaraswamy *et al. BMC Bioinformatics* (2018) 19:143

Page 5 of 16

(see Additional file 2 for actual algorithm). Note that Reg-MaxS does not handle reflections. Any reflections must be removed before the algorithm is applied.

Reg-MaxS-N

Reg-MaxS-N is an algorithm for co-registering multiple morphologies. It uses Reg-MaxS for co-registering pairs of morphologies and is based on "iterative averaging" [43] which has been successfully used to generate several standard brain atlases [43–45]. It is an iterative algorithm, which in each iteration uses a reference volume and registers all morphologies to it. From the resulting registered morphologies, it generates an "average volume", which is then used as the reference in the following iteration. For the first iteration, volume occupied of one of the morphologies to be registered is chosen as the initial reference. The iteration stops when all pairwise registrations of an iteration are rejected (see "Accepting a pairwise registration" section) Finally, the iteration at which the occupancy based measure of the morphologies was minimized is chosen as the final solution (see Additional file 2 for actual algorithm).

Computing the average volume

There are several ways of generating an average volume from a group of registered morphologies. In image stack registration paradigms, where voxel values are multi-valued and numerical (E.g.: for grayscale image stacks), an average of a set of images is generated by averaging the value for each voxel across the set of images. In other problems where voxel values are non-numerical (string labels for example, as in [43]), a democratic policy is used, where the most frequently occurring value is chosen for each voxel. However, in our formulation each voxel takes one of two values, '1' or '0', indicating whether it contains at least one point of the morphology or not. Using a democratic policy would mean that the average retains only those voxels for which more morphologies have '1's than '0's. For those cases where some parts of the morphologies have not yet overlapped at the end of the first iteration, this policy would remove those parts from the average. Since the morphologies are registered to this average in the following iteration, those parts would no longer be taken into account for registration. Instead, we use a more conservative approach and assign a voxel in the average volume to be '1' if at least one of the morphologies being averaged has a value '1'. In other words, the average volume of a given set of morphologies is calculated as the union of the voxel sets of all the morphologies. This ensures that each morphology is completely represented in the average and thereby contributes equally in determining the final registration.

Initial approximate registration

For the first iteration, an initial approximate registration is performed by matching centroids. For all subsequent iterations, no initial registration is applied.

Restricting total scaling

In every iteration, Reg-MaxS-N uses Reg-MaxS for registering morphologies to an average volume. A parameter of Reg-MaxS is the range of values of scales over which Reg-MaxS searches to find the scale that, when applied to the test morphology, minimizes its spatial dissimilarity with the reference. However, if this range of possible scales is constant, and Reg-MaxS-N repeatedly aligns the morphologies to the average volume of the previous iteration, it would scale the morphologies larger and larger to stretch the dimensions which show high spatial dissimilarity. If such scaling is not constrained, the morphologies would become disproportionately and unrealistically large to achieve a high similarity value. Hence, Reg-MaxS-N constrains the total scaling that is applied to a morphology. It keeps track of the total scaling that has been already applied to a morphology at the end of each iteration and reduces the amount of scaling that can be applied to it in the next iteration. This prevents the total scaling from becoming unrealistic.

Normalizing final morphologies

As explained above, since Reg-MaxS-N repeatedly registers morphologies to the average of the previous iteration, the final morphologies would have translation, rotation and scaling differences with the initial reference morphology, i.e., the reference morphology of the first iteration. For further analysis on these final registered morphologies, it is convenient to transform them such that they are comparable to the original reference morphology. Thus, Reg-MaxS-N calculates the sum total of all translation, rotation and scaling transforms applied to the original reference morphology over all iterations and applies the inverse of this total transformation to all the final registered morphologies. This makes all of them comparable with the original reference morphology.

Accepting a pairwise registration

At each step, Reg-MaxS uses the multi-scale method for determining transformation differences. In the multi-scale method, the final estimate is determined at the lowest voxel size of the algorithm. Thus, Reg-MaxS tries to minimize spatial dissimilarity between two morphologies at this lowest voxel size. Doing so could lead to an increase in spatial dissimilarity at a higher voxel size. This is acceptable, since we want an exact or a very large overlap between the volumes of the morphologies. However, when working iteratively with a group of morphologies,

Kumaraswamy *et al. BMC Bioinformatics* (2018) 19:143

Page 6 of 16

the reference corresponds to an actual morphology only for the first iteration. For all other iterations, it is a conservative "average" representing the union of the volumes of several morphologies, which does not represent any single morphology. Sacrificing spatial overlap at a higher voxel size for spatial overlap at a lower voxel size can cause over-fitting, in the sense that parts which do not necessarily correspond to each other would end up being randomly matched. Hence, a morphology registered to an average is accepted only if spatial dissimilarity at the highest voxel size has decreased. If the spatial dissimilarity at the highest voxel size has remained the same, then the spatial dissimilarity at the next highest voxel size is considered, and so on. When a registration is not accepted, the test morphology is itself designated as the registered morphology.

Testing the methods

To validate Reg-MaxS and Reg-MaxS-N, we tested them on several groups of morphologies. We defined measures for quantifying performance and calculated them for each of the test cases. Comparing these measures, we identified the cases where the algorithms performed poorly and investigated the reason behind them. In this section, we describe the morphologies and performance measures used for testing the algorithms.

Morphologies used for testing

Synthetic Morphologies used to test Reg-MaxS To illustrate its working and explore its limitations, we applied Reg-MaxS to synthetic data generated from a morphology of a visual neuron from the blowfly [15] (Fig. 2b green) obtained from NeuroMorpho.org [2]. The morphology is nearly two dimensional and has a dense dendritic arbor with a thick axon which projects to a couple of nearby regions.

We first created a set of 10 noisy morphologies by adding independent zero-mean Gaussian noise of standard deviations (std) 1, 3, 5, ...,17, 19 μm to the points of the morphology. Next, 100 different random transformations were constructed by drawing translations from a uniform distribution over [-20, 20]μm, rotations from a uniform distribution over [-30, 30] degrees and scaling from a uniform distribution over [0.5, 1/0.5]. Each transformation was applied to the set of ten noisy morphologies to generate one hundred such sets. In addition, 1000 noiseless morphologies were generated by applying 1000 different random transformations constructed as above to the original noiseless morphology. To summarize, we used 2000 transformed morphologies: (1000 without noise) + (100 with noise of std 1μm) + (100 with noise of std 3μm) +....+ (100 with noise of std 19μm).

Morphologies used to test Reg-MaxS and Reg-MaxS-N

Table 1 describes the five groups of neuron morphologies from *Drosophila melanogaster* used for testing Reg-MaxS and Reg-MaxS-N. Morphologies within a group have stereotypic structure but each group shows a different three dimensional dendritic arborization (see Additional file 1).

All the morphologies were generated from image stacks of the FlyCircuit Database [31]. The morphologies reconstructed without registering to any standard brain atlas ("non-standard" morphologies) were obtained from NeuroMorpho.org [2]. Morphologies which were reconstructed after registering to a Drosophila standard brain [30, 46] ("standardized" morphologies) were obtained from Dr. Gregory Jefferis.

Measures for quantifying performance of Reg-MaxS

Reg-MaxS was evaluated by applying it to register a test morphology to a reference and calculating residual errors based on the Euclidean distances of corresponding point pairs between result and reference morphologies. When synthetic morphologies were used, the test morphologies were randomly transformed versions of the reference and hence a pointwise correspondence was readily available. When real morphologies were used, test and reference morphologies were from the group 'LCInt' and no such correspondence was available. In this case, correspondences were defined by choosing the nearest neighbor among the test SWC points for every SWC point of the reference morphology.

Measures of performance: The residual error above between result and reference morphologies was quantified as follows. Given a reference morphology P and a result morphology Q_1, let $\{p_1, p_2, \cdots, p_m\}$ be the SWC points of P and $\{q_{p_1}, q_{p_2}, \cdots, q_{p_m}\}$ be their corresponding points in Q_1. From these points, a set of Euclidean distances $\left\{d_1^{Q_1}, d_2^{Q_1}, \cdots, d_m^{Q_1}\right\}$ were calculated as follows:
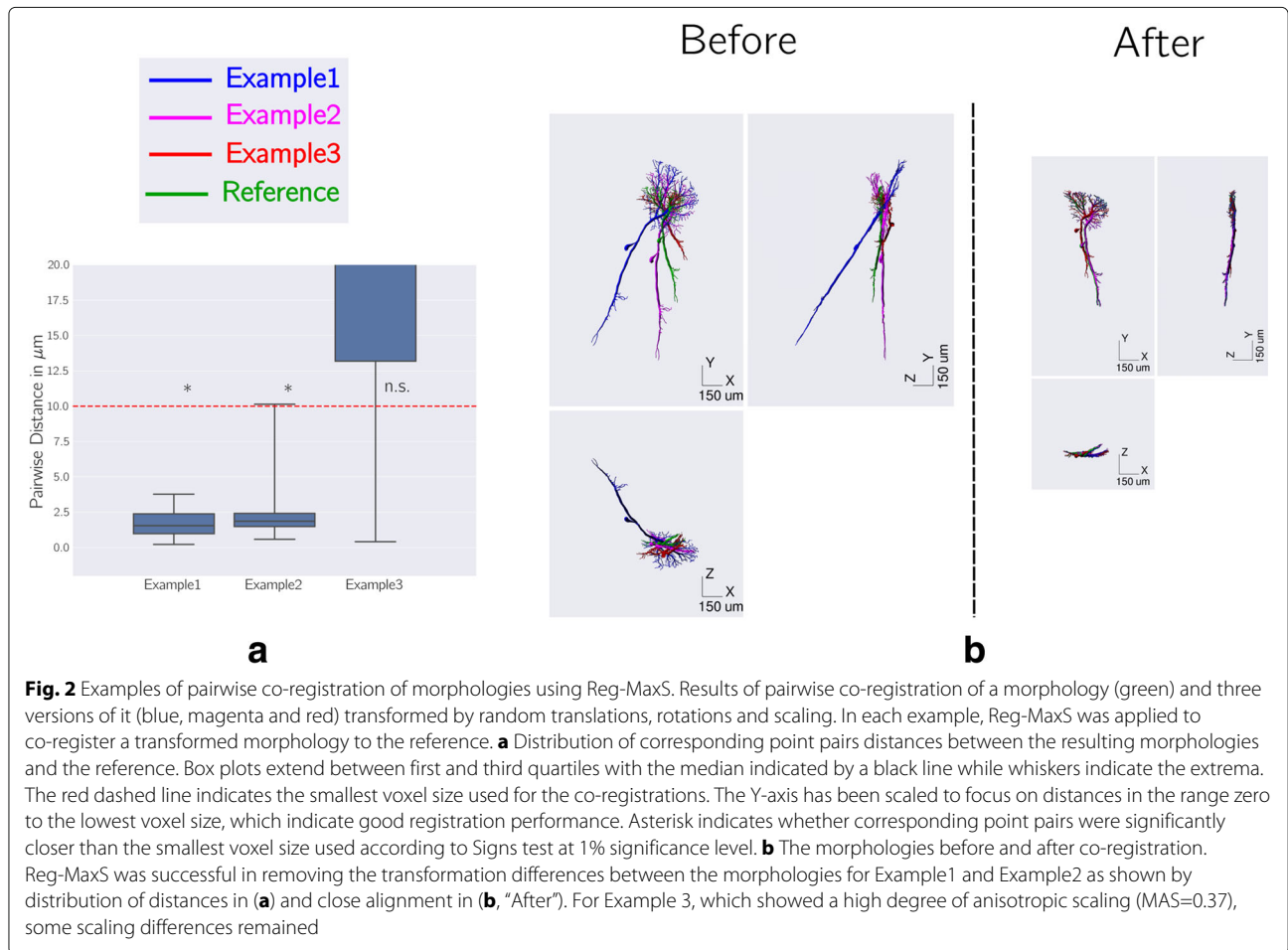
$$d_i^{Q_1} = \sqrt{\left(p_i^x - q_{p_i}^x\right)^2 + \left(p_i^y - q_{p_i}^y\right)^2 + \left(p_i^z - q_{p_i}^z\right)^2}$$

$$\text{for } i \text{ in } \{1, 2, 3, \cdots, m\}$$

where the superscripts x, y and z indicate coordinates in space. We used multiple tests for validation and therefore given a set of tests $\{Q_1, Q_2, Q_3..., Q_n\}$, a set of Euclidean distances as shown below were calculated.

$$\left\{\begin{array}{cccc} d_1^{Q_1}, & d_2^{Q_1}, & \cdots, & d_m^{Q_1}, \\ d_1^{Q_2}, & d_2^{Q_2}, & \cdots, & d_m^{Q_2}, \\ \cdots, & \cdots, & \cdots, & \cdots, \\ d_1^{Q_n}, & d_2^{Q_n}, & \cdots, & d_m^{Q_n} \end{array}\right\}$$

Since the finest spatial scale at which Reg-MaxS registers morphologies is the smallest voxel size used, distances

Kumaraswamy *et al. BMC Bioinformatics* (2018) 19:143

Page 7 of 16

Fig. 2 Examples of pairwise co-registration of morphologies using Reg-MaxS. Results of pairwise co-registration of a morphology (green) and three versions of it (blue, magenta and red) transformed by random translations, rotations and scaling. In each example, Reg-MaxS was applied to co-register a transformed morphology to the reference. **a** Distribution of corresponding point pairs distances between the resulting morphologies and the reference. Box plots extend between first and third quartiles with the median indicated by a black line while whiskers indicate the extrema. The red dashed line indicates the smallest voxel size used for the co-registrations. The Y-axis has been scaled to focus on distances in the range zero to the lowest voxel size, which indicate good registration performance. Asterisk indicates whether corresponding point pairs were significantly closer than the smallest voxel size used according to Signs test at 1% significance level. **b** The morphologies before and after co-registration. Reg-MaxS was successful in removing the transformation differences between the morphologies for Example1 and Example2 as shown by distribution of distances in (**a**) and close alignment in (**b**, "After"). For Example 3, which showed a high degree of anisotropic scaling (MAS=0.37), some scaling differences remained

less than the smallest voxel size indicate good registration. We regrouped these distances in two ways to quantify two kinds of performances:

1. Performance for every test across SWC points, using

Table 1 Neurons from *Drosophila melanogaster* used for testing Reg-MaxS and Reg-MaxS-N

Group name	No. of morphologies	Description	NBLAST Cluster [46]
LCInt	8	Interneuron of the fly Lobula complex	246
ALPN	14	Neuron projecting from the antennal lobe to the mushroom body	458
OPInt	23	Interneuron of the fly Optic lobe	209
AA1	12	Interneuron of fly ventrolateral protocerebum	921
AA2	9	Neuron of the fly antennal mechanosensory and motor center	803

$$\left\{ \left\{ d_1^{Q_1}, d_2^{Q_1}, \cdots, d_m^{Q_1} \right\}, \left\{ d_1^{Q_2}, d_2^{Q_2}, \cdots, d_m^{Q_2} \right\}, \cdots, \left\{ d_1^{Q_n}, d_2^{Q_n}, \cdots, d_m^{Q_n} \right\} \right\}$$

2. Performance for every SWC point of the reference morphology across tests, using,

$$\left\{ \left\{ d_1^{Q_1}, d_1^{Q_2}, \cdots, d_1^{Q_n} \right\}, \left\{ d_2^{Q_1}, d_2^{Q_2}, \cdots, d_2^{Q_n} \right\}, \cdots, \left\{ d_m^{Q_1}, d_m^{Q_2}, \cdots, d_m^{Q_n} \right\} \right\}$$

These performance measures were calculated as the percentage of tests or SWC points for which distances were significantly smaller than the smallest voxel size used. Since only distance values smaller than the smallest voxel size were relevant, we used the one-tailed Wilcoxon test, also known as the Signs test with a significance level cutoff of one percent.

Measure of anisotropic scaling: Some preliminary tests with Reg-MaxS indicated that performance of the algorithm was affected by different scaling along different axes of the morphologies relative to each other (see "Results" section). To quantify such differences in

Kumaraswamy *et al. BMC Bioinformatics* (2018) 19:143

Page 8 of 16

scaling along axes, we defined the following Measure of Anisotropic Scaling (MAS):

$$\text{MAS} = 1 - \frac{1}{3}\left(\frac{s_1}{s_2} + \frac{s_1}{s_3} + \frac{s_2}{s_3}\right)$$

where s_1, s_2, s_3 are the scaling differences along the axes arranged in ascending order. MAS has a value of zero when the scaling differences along all axes are equal, and increase gradually to one as the scales become more and more different.

Comparing Reg-MaxS-N with other methods

We compared the performance of Reg-MaxS-N with Reg-MaxS and four other methods for co-registering morphologies from recent studies:

- **PCA:** A method using Principal Component Analysis based on a similar method for image stacks [47].
- **PCA + RobartsICP:** The PCA method above followed by Anisotropic-Scaled Iterative Closed Point [36].
- **BlastNeuron:** The affine transformation step of BlastNeuron [33].
- **Standardized:** A method using a standard brain [30].

Code for BlastNeuron and RobartsICP was obtained from the respective authors. Morphologies registered to a standard brain were provided by Dr. Gregory Jefferis. The PCA method was implemented as follows. Given a test and a reference morphologies, we assumed that they have similar dendritic density profiles and were oriented similarly in space. Based on this, the method assumes a correspondence between the first principal axes (principal axes corresponding to the largest principal factors), second principal axes and the third principal axes of the two morphologies. This method translates the test morphology so that its center coincides with that of the reference and rotates it so that their corresponding principal axes align. Scaling differences are determined based on the variances of the morphologies along the corresponding principal axes and the test morphology is appropriately scaled.

Each registration method was applied to each of the five groups of morphologies with the standardized version of one of the morphologies as the initial reference. Performance was quantified using the occupancy-based measure defined above. The results of PCA, PCA + RobartsICP, Reg-MaxS and Reg-MaxS-N were in the same frame of reference as the standardized morphologies allowing direct comparison. The results of BlastNeuron however were in a different frame of reference.

In addition, the above registration tests were repeated three times for each method and each group using different morphologies as initial references and performances were quantified in each case.

Computing density profiles from sets of registered morphologies for visualization

We visualized the results of PCA, BlastNeuron and Reg-MaxS-N along with the standardized morphologies by constructing density profiles from each of them and by maximal projections of these density profiles along two orthogonal planes. These density profiles were generated using the method described in [30]. For each set of morphologies that were co-registered, a density profile was constructed discretized with a voxel size of $0.25\mu m \times 0.25\mu m \times 0.25\mu m$. Each morphology was resampled so that the distance between any pair of connected points was at most $0.1\mu m$. Each voxel that contained at least one point of the morphology was assigned a value of 1 and all others were assigned 0. This binary density profile was smoothed using a unity sum 3D discrete Gaussian Kernel. The standard deviation of this kernel was chosen individually for each group of morphologies. Density profiles so calculated for each morphology were averaged across morphologies to obtain a density profile for the set of morphologies.

Results

Testing Reg-MaxS with synthetic morphologies

Testing Reg-MaxS with noiseless morphologies

We first used the synthetically generated noiseless morphologies for testing Reg-MaxS. In each of these test registrations, the respective original morphology was always used as the reference while a transformed version of the original morphology was used as the test. The smallest voxel size used was 10 μm for all the tests. When pointwise distance statistics were calculated for each test registration across SWC points, 675 of 1000 tests (67.5%) had final distances that were significantly smaller than the smallest voxel size (n=1290, Signs Test, 1% significance level). When pointwise distance statistics were calculated for each SWC point across test registrations, 1287 of 1290 SWC points (99.76%) had final distances that were significantly smaller than the smallest voxel size (n=1000, Signs Test, 1% significance level). Thus, although Reg-MaxS fails to register a significant number of SWC points in a third of the test registrations, the number of points for which it consistently fails across tests is small.

Three example tests are illustrated in Fig. 2. Reg-MaxS failed for the test morphology "Example3", especially in removing scaling differences. This was caused by the heavy anisotropic scaling in this morphology (scaling differences: 1.12 along X, 0.61 along Y and 1.27 along Z, MAS=0.37). We analyzed this further by separating morphologies based on their level of anisotropic scaling (see "Effect of anisotropic scaling" section below).

In these tests the morphologies used had nearly planar densities. However, Reg-MaxS also performed well on

Kumaraswamy *et al. BMC Bioinformatics*   (2018) 19:143

Page 9 of 16

morphologies with 3D extent. This is demonstrated in the "Testing Reg-MaxS with real reconstructions" section using LCInt morphologies which have a non-planar dendritic density profile.

Effect of anisotropic scaling

To investigate the effect of the level of anisotropic scaling on the performance of Reg-MaxS, we calculated statistics only for the tests with low levels of anisotropic scaling, i.e., for cases where Measure of Anisotropic Scaling (MAS) was less than 0.2. Across SWC points, 166 of 193 tests (86%) had significant numbers of final distances smaller than the smallest voxel size (n=1290, Signs Test, 1% significance level). Across test registrations, 1290 of 1290 SWC points (100%) had final distances less than smallest voxel size (n=193, Signs Tests, 1% significance level). This shows that Reg-MaxS performs better for cases with low levels of anisotropic scaling, i.e, for cases where the MAS is less than 0.2.

Testing Reg-MaxS with noisy morphologies

Reg-MaxS was designed to co-register morphologies so that their spatial characteristics can be compared, assuming that the morphologies have very similar structure and belong to the same stereotypic neuron group but are obtained from different specimens. Even stereotypical neurons exhibit natural biological variability in the exact location of their dendrites from individual to individual, especially for higher order dendrites. Thus, in order to properly register such morphologies, Reg-MaxS must be able to tolerate such variability in dendritic position. We tested this by applying Reg-MaxS to morphologies where noise was added to each point of the morphology.

As described in "Methods" section, we generated noisy synthetic morphologies by first adding independent Gaussian noise to each point of a reference morphology M (Fig. 3a) to generate a noisy morphology N(M), shown in Fig. 3b. Then we randomly transformed N(M) to obtain the morphology TN(M), shown in Fig. 3c together with the original morphology M. We then ran Reg-MaxS with M as reference and TN(M) as the test to produce the morphology RTN(M), shown in Fig. 3d. Since the best expected registration of TN(M) to M is N(M), we compared RTN(M) to N(M) and calculated point-wise distances and registration accuracy accordingly. This was done for ten different values of standard deviation and a hundred different transforms. Figure 3e show the results of these tests. Reg-MaxS showed about 85% success for values of noise standard deviation less than the smallest voxel size.

Testing Reg-MaxS with real reconstructions

Reg-MaxS applies affine transforms for reducing spatial dissimilarity between morphologies. However, multiple morphologies of the same stereotypical neuron obtained from different specimens could show non-affine differences as well, if the brains of the specimens show non-affine differences. This is taken into account while constructing brain atlases that use both affine and non-affine transforms (e.g., [43]). To test if the limitation to affine transforms is a major drawback for Reg-MaxS, we registered non-standard versions of LCInt morphologies (see Additional file 1 for its 3D structure) to their corresponding standardized versions. Since a pointwise correspondence between the morphologies was not available in this case, we used distance statistics of nearest point pairs of the reference morphology and the registered morphology for quantifying algorithm performance. The algorithm performed well on all neurons, with significant number of nearest point pairs closer than the smallest voxel size ($117 \leq n \leq 276$, Signs test, 1% significance level). However, these tests showed slightly larger final distances ($5.51 \pm 4.49 \ \mu m$) compared to tests using noiseless synthetic morphologies with only affine transformation differences ($3.08 \pm 3.35 \ \mu m$). The distributions of nearest point distances also showed more outliers compared to noiseless synthetic tests because of non-rigid differences between the non-standard and standardized morphologies.

Testing Reg-MaxS-N with groups of morphologies

For evaluating Reg-MaxS-N, we compared its performance with that of five other methods (see "Methods" section). We applied the six methods to five groups of morphologies, repeating each case for four different initial references. Results of applying the methods are visualized in Fig. 4 using one sample morphology per group. Performance was quantified using occupancy-based dissimilarity (see "Methods" section) and averaged across initial references as shown in Fig. 5. Reg-MaxS-N outperformed PCA, BlastNeuron and PCA+RobartsICP for four of the five groups – LCInt, ALPN, OPInt and AA. For AA2, a group of neurons with unusually high structural stereotypy, BlastNeuron and PCA+RobartsICP showed slightly higher performance than Reg-MaxS-N (see "Applicability" in "Discussion" section for more). The density profiles calculated from the result morphologies of Reg-MaxS-N were very similar to those obtained using methods relying on a standard brain (Fig. 6). Furthermore, the performance of Reg-MaxS-N across initial references was less variable than BlastNeuron, PCA-Based+RobartsICP and Reg-MaxS for all groups as seen from the error bars in Fig. 5 (also see Additional file 3). Although PCA showed lower variance across initial references for ALPN and AA1 morphologies, its median performance was lower. Thus Reg-MaxS-N showed higher average performance and lower sensitivity to initial reference than other existing methods in a large majority of our tests.
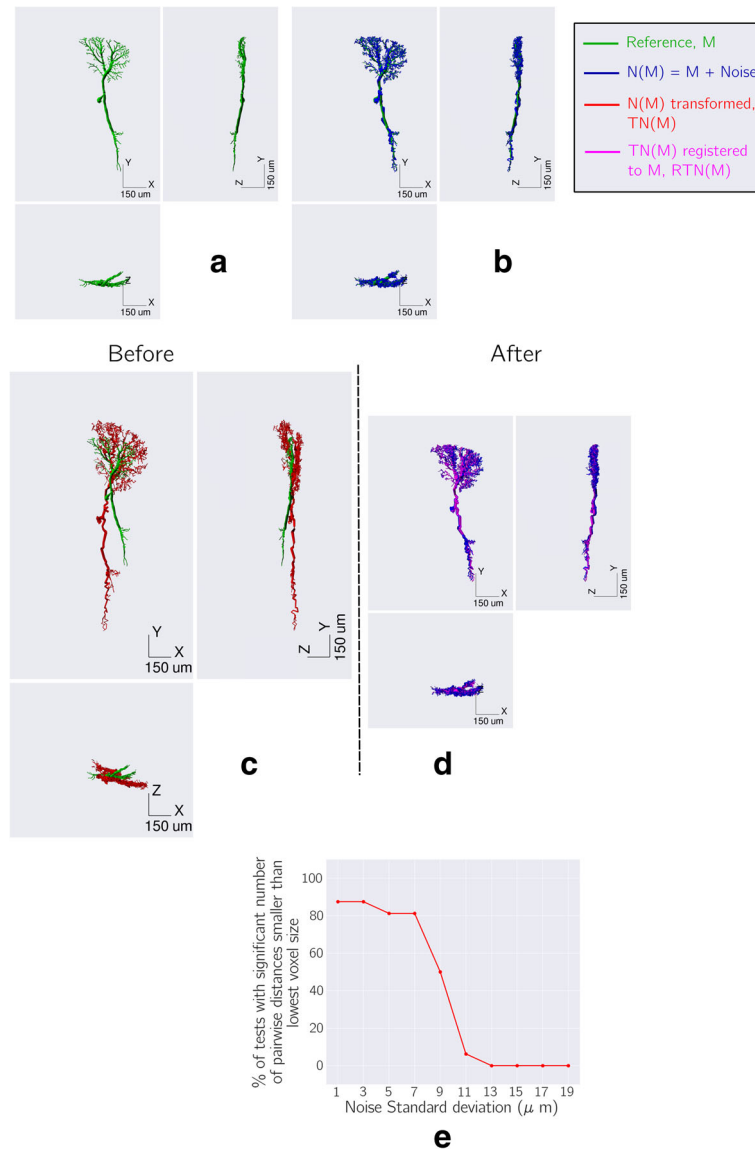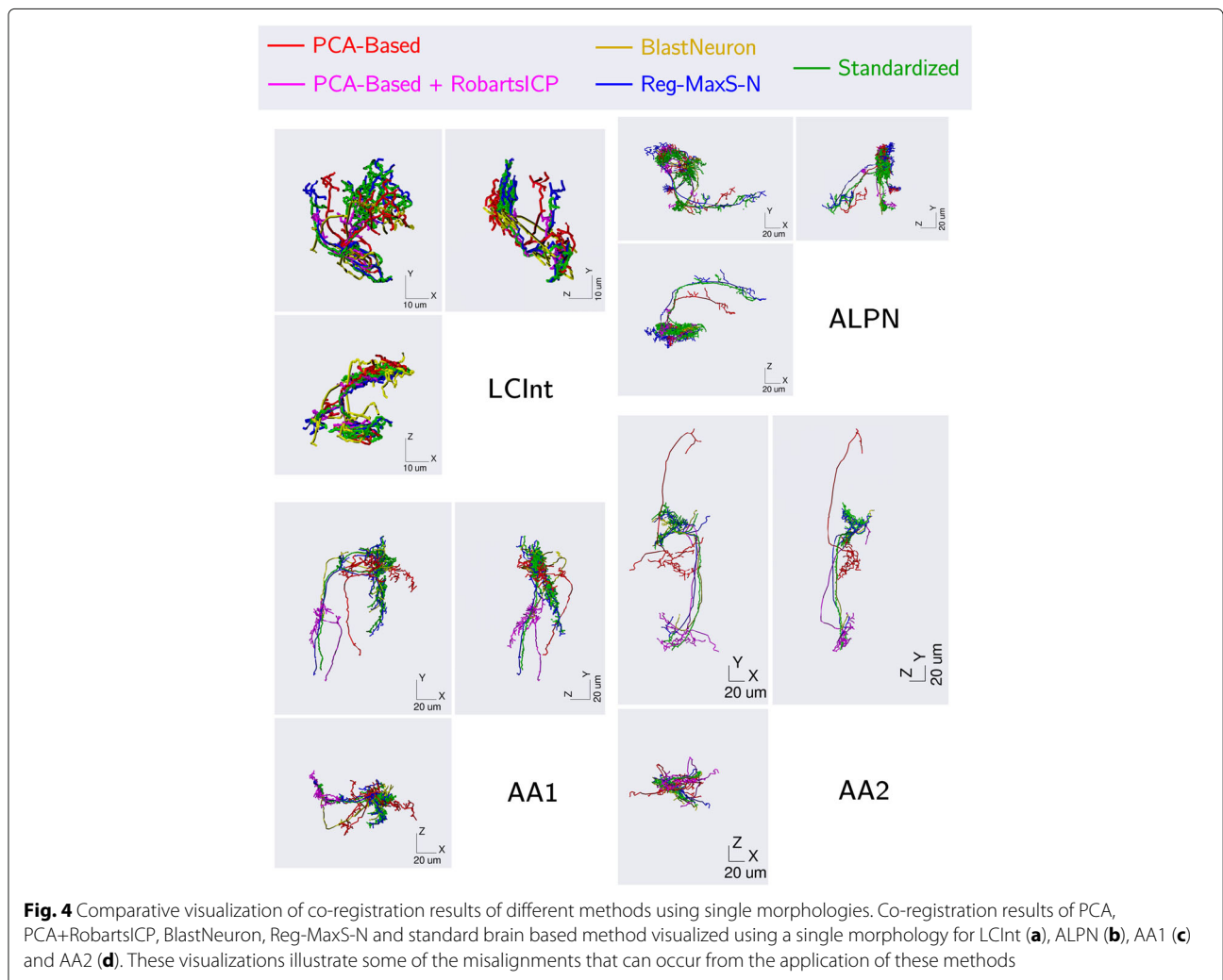
Kumaraswamy *et al. BMC Bioinformatics*   (2018) 19:143

Page 10 of 16

Fig. 3 Testing Reg-MaxS with noisy morphologies. **a** The reference morphology M. **b** M (green) and the morphology N(M) (blue), which was obtained by adding independent Gaussian noise of standard deviation $7\mu m$ to each point of M. **c** M (green) and the morphology TN(M) (red), which was obtained by applying random translation, scaling and rotation to N(M). **d** N(M) (blue) and RTN(M) (violet), which was obtained by registering TN(M) to M using Reg-MaxS. The process was repeated using multiple random transformations and different values of noise standard deviations (see "Methods" section). **e** Performance of Reg-MaxS as a function noise standard deviation. Reg-MaxS performance was calculated as the percentage of tests for which the distribution of resulting pointwise distances was significantly smaller than the smallest voxel size (10 μm). Reg-MaxS-N showed high performance for noise with standard deviation below the smallest voxel size

Discussion

We have presented Reg-MaxS and Reg-MaxS-N, algorithms for co-registering pairs and groups of neuron morphologies, respectively, by maximizing spatial overlap. We have quantified the performance of Reg-MaxS using synthetic and real morphologies. We have tested Reg-MaxS-N on different groups of morphologies with different initial references and quantified its performance for each case.

Initialization

Spatial registration is a global optimization problem usually consisting of multiple local minima. Most registration algorithms therefore initialize using an approximate solution before minimizing dissimilarity. Several different strategies have been developed for initialization of registration algorithms [48]. However, initialization is required only when the objects being registered are expected to have large transformation differences. Neuron

Kumaraswamy *et al. BMC Bioinformatics*   (2018) 19:143

Page 11 of 16

Fig. 4 Comparative visualization of co-registration results of different methods using single morphologies. Co-registration results of PCA, PCA+RobartsICP, BlastNeuron, Reg-MaxS-N and standard brain based method visualized using a single morphology for LCInt (**a**), ALPN (**b**), AA1 (**c**) and AA2 (**d**). These visualizations illustrate some of the misalignments that can occur from the application of these methods

morphologies of the same type obtained from different individuals do no usually have large transformation differences other than translations caused by arbitrary choice of origin. Hence Reg-MaxS uses centroid alignment for initialization. Nonetheless, Reg-MaxS can be easily modified to include an appropriate initialization if an application demands it.

Reg-MaxS vs Reg-MaxS-N
Compared to Reg-MaxS, Reg-MaxS-N has mainly two additional components in its procedure — iterative registration and final normalization. While Reg-MaxS registers all morphologies once to the initial reference, Reg-MaxS-N applies multiple iterations of such registrations, calculating a new reference in each iteration. This iterative strategy reduces the effect of the choice of initial reference on algorithm performance. In our tests, Reg-MaxS-N performed better than Reg-MaxS for most cases, and showed less variability across different initial references compared to Reg-MaxS (see Figs. A31 and A35

of Additional file 3), indicating better suitability for these cases.

For ALPN, OPInt and AA1 morphologies, the performance of Reg-MaxS-N was nearly the same as that of Reg-MaxS . In these cases, Reg-MaxS-N chose the morphologies at the end of its first iteration as the solution, i.e., the same solution as Reg-MaxS. However, the solution morphologies for Reg-MaxS-N were additionally normalized so that they were comparable to the initial reference and this caused the observed reduction in performance of Reg-MaxS-N compared to Reg-MaxS in some of these cases. The normalization was applied mainly for the purpose of visualization and comparison with other methods, and can therefore be excluded when analyzing single groups of morphologies.

Computational cost
Reg-MaxS applies a sequence of transformations for maximizing spatial overlap between two morphologies. It estimates transformation differences at each step using

Kumaraswamy *et al. BMC Bioinformatics*   (2018) 19:143

Page 12 of 16

Fig. 5 Performance comparison of registration methods. Performance of six registration methods for five different groups of morphologies. Error bars indicate 95% confidence intervals of median performance, calculated across values for four initial references. BlastNeuron performance for OPInt morphologies are not shown as the program provided by the authors stopped after a time limit of 30 min and produced no results. In most cases, Reg-MaxS and Reg-MaxS-N outperform the other methods

a measure of spatial overlap based on the set of voxels occupied by each morphology. However, the set of voxels occupied by a morphology can change with every rotation or scaling. This makes it hard to predict the computational cost of estimating transformation differences at each step and thus to estimate the total computational cost of Reg-MaxS. Furthermore, Reg-MaxS and Reg-MaxS-N are both iterative algorithms which stop only when spatial overlap between morphologies cannot be improved further. This further complicates the prediction of total number of iterations and total computational cost.

We compared the run times per morphology of Reg-MaxS, Reg-MaxS-N and other methods for co-registration of groups of neurons with different settings of initial reference (Table 2). Run times for Reg-MaxS-N were many times longer than those of the other methods. This is because Reg-MaxS-N iteratively registers morphologies many times, refining their spatial alignment and incorporating features of all morphologies. Therefore Reg-MaxS-N is expected to run longer than methods that register each morphology to the reference only once. A more suitable comparison is between Reg-MaxS and the other methods, since all of them register each morphology once. These run times were comparable, differing by factors between 0.25 and 5. The main reason for the
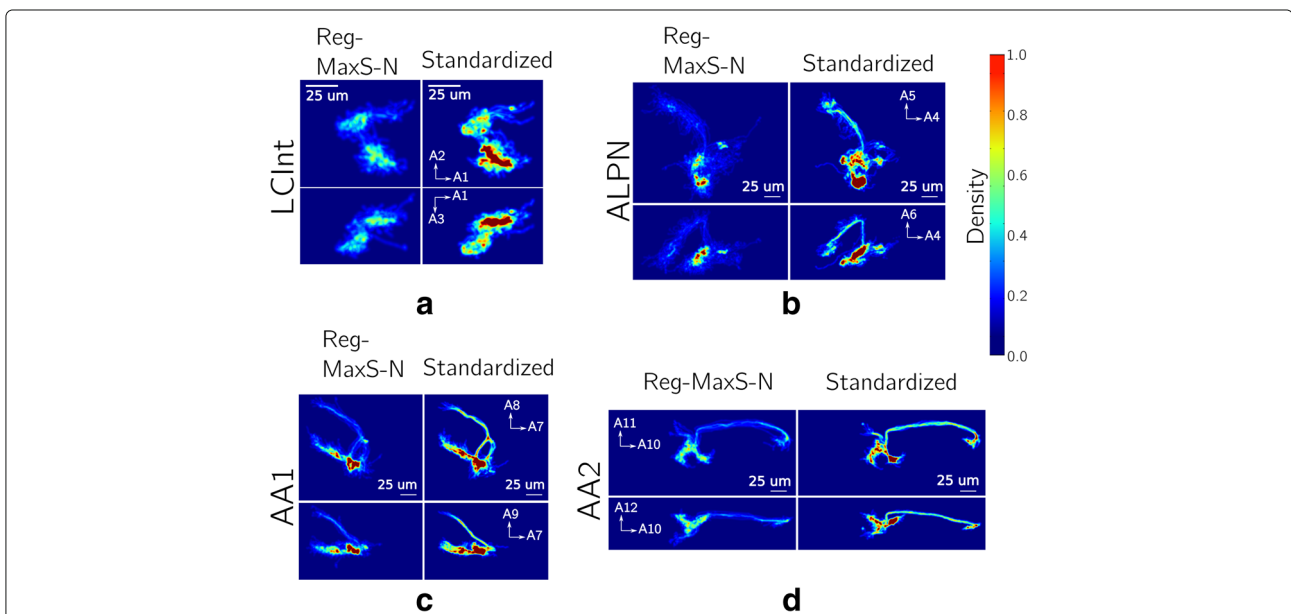
Fig. 6 Comparison of dendritic density profiles generated using Reg-MaxS-N and brain altas based method. **a** Two dimensional projections of morphological densities after registration with Reg-MaxS-N (left columns) and standard brain based registration (right columns). Densities were calcuated for voxels of size $0.25 \mu m$. Color indicates the fraction of morphologies that, after registration, had at least one dendrite in the particular voxel. For illustration purposes, densities have been smoothed by a 3D Gaussian kernel with standard deviation of $1.25 \mu m$. **a** Densities for eight LCInt morphologies. A1, A2 and A3 correspond to the principal axes of the standardized LCInt morphology used as initial reference. **b** Densities for fourteen ALPN morphologies. A4, A5 and A6 correspond to the principal axes of the standardized ALPN morphology used as initial reference. **c** Densities for twelve AA1 morphologies. A7, A8 and A9 correspond to the principal axes of the standardized AA1 morphology used as initial reference. **d** Densities for nine AA2 morphologies. A10, A11 and A12 correspond to the principal axes of the standardized AA2 morphology used as initial reference. In all cases, Reg-MaxS-N produced densities very similar to that produced by standard brain based method

Kumaraswamy *et al. BMC Bioinformatics*   (2018) 19:143

Page 13 of 16

Table 2 Comparison of average runtimes per morphology for different registration algorithms

Method	Average runtimes per morphology (s)				
	LCInt	ALPN	OPInt	AA1	AA2
PCA	0.07	0.08	0.45	0.59	0.25
PCA + RobartsICP	189.63	318.18	287.02	68.07	39.03
BlastNeuron	19.48	319.32	N.A.	115.95	185.78
Reg-MaxS	98.44	239.20	474.88	90.45	46.89
Reg-MaxS-N	1141.81	605.82	2796.96	883.670	633.44

The runtimes per morphology for each method and test group averaged across initial references. The runtimes of BlastNeuron for OPInt group of morphologies were unavailable as the program provided by the authors of BlastNeuron stopped execution after an internally defined time limit without producing output

variabilities seen both in the run times of each algorithm and in the relative run times between algorithms is that all the algorithms except PCA use iterative routines for finding optimal transformations and their run times can vary substantially and differently depending on properties of the morphologies like size, number of SWC nodes and spatial structure.

Choice of voxel sizes

The most important parameters of Reg-MaxS and Reg-MaxS-N are the set of voxel sizes over which transformation difference estimates are refined during co-registration of morphologies. The largest and the smallest voxel sizes define the coarsest and the finest spatial scales, respectively, at which the algorithms register morphologies. The algorithms consider a voxel to be occupied by a morphology if it contains one or more of its SWC points and align morphologies by applying transformations to match the sets of occupied voxels. Thus morphological features at scales finer than that defined by the smallest voxel size are ignored by the algorithms. Therefore, a good choice for the smallest voxel size is the spatial scale below which morphological features are not expected to match.

In our preliminary tests involving morphologies of different sizes and dendritic densities, we found a smallest voxel size of $10\mu m$ to be a good compromise and therefore used it for evaluating algorithm performances. To investigate the effect of reducing the value of the smallest voxel size, we repeated the tests by setting the value of smallest voxel size to $5\mu m$. The results are summarized in Additional file 4. For pairwise co-registration of test morphologies that were larger in size and that had fewer features at scales smaller than $10\mu m$ than other test morphologies, the performance of Reg-MaxS reduced from 67.5% at $10\mu m$ to 32.2% at $5\mu m$. On the other hand, for pairwise co-registration of test morphologies that were smaller in size and had more features at scales smaller than $10\mu m$, performance of Reg-MaxS showed only a minor improvement. Furthermore, performance of Reg-MaxS and Reg-MaxS-N in co-registration of groups of

morphologies did not show any substantial changes when smallest voxel size was changed from $10\mu m$ to $5\mu m$ (Additional file 4, Fig. A41). Thus, the value of smallest voxel size can influence the performance of our algorithms depending on the size and the sparsity of structural features of morphologies being registered, and should be chosen accordingly.

Applicability

Reg-MaxS repeatedly applies a set of rotation/translations followed by a scaling to maximize spatial overlap between morphologies. Scales are estimated after aligning centroids of morphologies. In other words, Reg-MaxS seeks a solution of close centroid alignment. Therefore Reg-Max-S and consequently Reg-MaxS-N are best applicable to morphologies that are complete and have similarly situated centroids. Their application to partial morphologies or largely incomplete reconstructions is not straightforward and requires caution and consideration. For more efficient handling of such cases, the algorithms could be modified so that they do not depend heavily on centroid alignment.

Reg-MaxS-N was outperformed by PCA+RobartsICP and BlastNeuron for one out of five of our test groups of morphologies, AA2. Importantly, this was not due to poor performance of Reg-MaxS-N, but due to untypically good performance of BlastNeuron and PCA+RobartsICP. A reason for this could lie in the unusually high structural stereotypy of AA2 morphologies, which is also reflected by lower values of occupancy-based dissimilarity compared to other groups (Fig. 5, also see Fig. A35 of Additional file 3). This high structural stereotypy indicates the existence of a solution with very close point-to-point alignment, and hence BlastNeuron and PCA + RobartsICP, which are based on pointwise distance statistics, performed better. Under most realistic conditions, however, neuron morphologies will have a non-negligible biological variability in their fine spatial features, and therefore we would expect Reg-MaxS-N to perform better than the other methods considered here, as was the case for the other four test groups. However, since our sample sizes were small (n=4) we could not establish statistical significance for the differences in performance.

Calculating dendritic density profiles using Reg-MaxS-N

Applying Reg-MaxS-N to three groups of stereotypic neuron morphologies from the *Droshophila melanogaster* brain, we have shown that Reg-MaxS-N can co-register groups of neuron morphologies. Without the need for an external reference like a standard brain atlas, the registration results were very similar to morphologies registered conventionally, using such a reference. Dendritic density profiles can be calculated from

Kumaraswamy *et al. BMC Bioinformatics*   (2018) 19:143

Page 14 of 16

groups of registered morphologies by spatial averaging (see "Methods" section). Thus Reg-MaxS-N can be used to calculate dendritic density from profiles of stereotypic neurons (Fig. 6). Such density profiles are useful in analyzing spatial variances in different subregions of neurons and can provide insights about the brain regions surrounding neurons [11]. Furthermore, density profiles so calculated could be used in generative models of neuron morphology [10, 49, 50]. Such models usually assume simple density profiles like a uniform density over the region of arborization. The availability of better spatial density profile estimates can improve such existing models and also enable the development of new models.

Possible improvements

Reg-MaxS applies a sequence of translation, rotation and scaling transformations to maximize the spatial overlap between morphologies. We tested Reg-MaxS with synthetic morphologies that had random translation, rotation and scaling differences and demonstrated its ability to revert these transformations. Other affine differences like shear would be expected to be compensated approximately by combinations of rotation and anisotropic scaling transformations. However, specifically including shear in the sequence of transformations applied could speed up the registration process and possibly result in better performance.

Topological features play an important role in determining neuronal function [51, 52] and hence are indispensable in the study of neuron morphology. Some recent studies [26, 33] have illustrated the effectiveness of the combined use of spatial and topological features for characterization and classification of morphology. Since Reg-MaxS-N can provide better spatial registration of morphologies than existing methods, it could be used as preprocessing to remove spatial differences for algorithms that subsequently estimate topological differences. Further, incorporating topological features into its formulation could lead to even more powerful methods for analyzing neuron morphologies.

Conclusion

We have addressed the problem of co-registering neuron morphologies, which is a crucial requirement for visualization and spatial analysis of stereotypical neurons, by formulating algorithms based on maximizing spatial overlap. Our tests using synthetic and real groups of morphologies have indicated that our algorithms can be used for registering stereotypic neuron morphologies that show considerable spatial variability in their fine structures as long as they are similarly scaled along different axes. The dendritic densities of stereotypic neurons calculated using our algorithms were very similar to those produced using

a standard brain, demonstrating the potential of our algorithms in detailed spatial comparison of neuron morphologies.

Additional files

Additional file 1: Figure showing the five groups of neuron morphologies used for evaluating Reg-MaxS-N registered to a standard brain (a) Interneurons in the Lobula complex (b) Antennal lobe projection neurons (c) Interneurons of ventrolateral protocerebum (d) Neuron of the antennal mechanosensory and motor center (e) Interneurons in the optic lobe. Figures from http://flybrain.mrc-lmb.cam.ac.uk/si/nblast/clusters/. (PNG 2101 kb)

Additional file 2: Implementation details of Reg-MaxS and Reg-MaxS-N. (PDF 306 kb)

Additional file 3: Performance comparison of Reg-MaxS-N and other methods for different initial references plotted separately for each group of morphologies. (PDF 593 kb)

Additional file 4: Tests Results of Reg-MaxS and Reg-MaxS-N with smallest voxel size set to 5μm. (PDF 181 kb)

Availability of data materials

The morphologies reconstructed without registering to any standard brain atlas ("non-standard" morphologies) were obtained from NeuroMorpho.org (http://dx.doi.org/10.1038/nrn1885). The corresponding registered ("standardized") morphologies were part of NBLAST (http://dx.doi.org/10.1016/j.neuron.2016.06.012) and were obtained from Dr. Gregory Jefferis (jefferis@mrc-lmb.cam.ac.uk). The names of all the neurons used in this study are provided below.
Visual Neuron From Blow Fly: HSN-fluoro01;
LCInt: Gad1-F-000062, Cha-F-000012, Cha-F-300331, Gad1-F-600000, Cha-F-000018, Cha-F-300051, Cha-F-400051, Cha-F-200000;
ALPN: VGlut-F-700500, VGlut-F-700567, VGlut-F-500471, Cha-F-000353, VGlut-F-600253, VGlut-F-400434, VGlut-F-600379, VGlut-F-700558, VGlut-F-500183, VGlut-F-300628, VGlut-F-500085, VGlut-F-500031, VGlut-F-500852, VGlut-F-600366;
OPInt: Trh-F-000047, Trh-M-000143, Trh-F-000092, Trh-F-700009, Trh-M-000013, Trh-M-000146, Trh-M-100009, Trh-F-000019, Trh-M-000081, Trh-M-900003, Trh-F-200035, Trh-F-200015, Trh-M-000040, Trh-M-600023, Trh-M-100048, Trh-M-700019, Trh-F-100009, Trh-M-400000, Trh-M-000067, Trh-M-000114, Trh-M-100018, Trh-M-000141, Trh-M-900019, Trh-M-800002;
AA1: VGlut-F-300181.CNG, VGlut-F-400545.CNG, VGlut-F-500778.CNG, VGlut-F-300196.CNG, VGlut-F-300288.CNG, VGlut-F-600290.CNG, VGlut-F-600499.CNG, VGlut-F-400665.CNG, VGlut-F-300142.CNG, VGlut-F-500147.CNG, VGlut-F-600181.CNG, VGlut-F-700190.CNG
AA2: Trh-F-700063.CNG, Trh-F-500050.CNG, Trh-F-500106.CNG, Trh-M-500051.CNG, Trh-F-600071.CNG, Trh-F-500093.CNG, Trh-F-500148.CNG, Trh-F-500154.CNG, Trh-F-700018.CNG
Programs for applying Reg-MaxS and Reg-MaxS-N to SWC files are available at https://github.com/wachtlerlab/Reg-MaxS. doi: https://doi.org/10.12751/g-node.feee47.

Kumaraswamy *et al. BMC Bioinformatics*   (2018) 19:143

Page 15 of 16

Authors' contributions

Ethics approval and consent to participate

Not applicable.

Consent for publication

Images used in Additional file 1 have been reproduced from http://flybrain.mrc-lmb.cam.ac.uk with written permission from Dr. Gregory Jefferis.

Competing interests

The authors declare that they have no competing interests.

Publisher's Note

Springer Nature remains neutral with regard to jurisdictional claims in published maps and institutional affiliations.

Author details

[1]Department of Biology II, Ludwig-Maximilians-Universität München, Grosshadernerstr. 2, Planegg-Martinsried 82152 Germany. [2]Department of Earth System Science, Fukuoka University, 8-19-1 Nanakuma, Jonan-ku, Fukuoka-shi, 814-0180 Fukuoka, Japan. [3]School of Human Science and Environment, University of Hyogo, 1-1-12 Shinazaike-Honcho, Himeji, Hyogo, 670-0092, Japan.

References

1. López-Muñoz F, Boya J, Alamo C. Neuron theory, the cornerstone of neuroscience, on the centenary of the Nobel Prize award to Santiago Ramón y Cajal. Brain Res Bull. 2006;70(4–6):391–405. Available from: https://doi.org/10.1016/j.brainresbull.2006.07.010.

2. Ascoli GA. Mobilizing the base of neuroscience data: the case of neuronal morphologies. Nat Rev Neurosci. 2006;7(4):318–24. Available from: https://doi.org/10.1038/nrn1885.

3. Halavi M, Hamilton KA, Parekh R, Ascoli GA. Digital reconstructions of neuronal morphology: three decades of research trends. Front Neurosci. 2012;6:49. Available from: https://doi.org/10.3389/fnins.2012.00049.

4. Peng H, Hawrylycz M, Roskams J, Hill S, Spruston N, Meijering E, et al. BigNeuron: Large-Scale 3D Neuron Reconstruction from Optical Microscopy Images. Neuron. 2015;87(2):252–256. Available from: https://doi.org/10.1016/j.neuron.2015.06.036.

5. Parekh R, Ascoli GA. Neuronal morphology goes digital: a research hub for cellular and system neuroscience. Neuron. 2013;77(6):1017–38. Available from: https://doi.org/10.1016/j.neuron.2013.03.008.

6. DeFelipe J, López-Cruz PL, Benavides-Piccione R, Bielza C, Larrañaga P, Anderson S, et al. New insights into the classification and nomenclature of cortical GABAergic interneurons. Nat Rev Neurosci. 2013;14(3):202–216. Available from: https://doi.org/10.1038/nrn3444.

7. Smit GJ, Uylings HBM. The morphometry of the branching pattern in dendrites of the Visual Cortex Pyramidal cells. Brain Res. 1975;87:41–53. Available from: https://doi.org/10.1016/0006-8993(75)90777-5.

8. Uylings HBM, Smit GJ. 3-dimensional branching structure of pyramidal cell dendrites. Brain Res. 1975;87(1):55–60. Available from: https://doi.org/10.1016/0006-8993(75)90778-7.

9. Teeter CM, Stevens CF. A General Principle of Neural Arbor Branch Density. Curr Biol. 2011;21(24):2105–2108. Available from: https://doi.org/10.1016/j.cub.2011.11.013.

10. Cuntz H, Forstner F, Borst A, Häusser M. One rule to grow them all: a general theory of neuronal branching and its practical application. PLoS Comput Biol. 2010;6(8). Availa2ble from: https://doi.org/10.1371/journal.pcbi.1000877.

11. Cuntz H. The dendritic density field of a cortical pyramidal cell. Front Neuroanat. 2012;6:2. Available from: https://doi.org/10.3389/fnana.2012.00002.

12. Kubota Y, Karube F, Nomura M, Gulledge AT, Mochizuki A, Schertel A, et al. Conserved properties of dendritic trees in four cortical interneuron subtypes. Sci Rep. 2011;1:89. Available from: https://doi.org/10.1038/srep00089.

13. Uylings HBM, van Pelt J. Measures for quantifying dendritic arborizations. Netw (Bristol, England). 2002;13(3):397–414. Available from: https://doi.org/10.1088/0954-898X/13/3/309.

14. Ascoli GA, Alonso-Nanclares L, Anderson SA, Barrionuevo G, Benavides-Piccione R, Burkhalter A, et al. Petilla terminology: nomenclature of features of GABAergic interneurons of the cerebral cortex. Nat Rev Neurosci. 2008;9(7):557–568. Available from: https://doi.org/10.1038/nrn2402.

15. Cuntz H, Forstner F, Haag J, Borst A. The morphological identity of insect dendrites. PLoS Comput Biol. 2008;4(12):e1000251. Available from: https://doi.org/10.1371/journal.pcbi.1000251.

16. Rautenberg PL, Grothe B, Felmy F. Quantification of the three-dimensional morphology of coincidence detector neurons in the medial superior olive of gerbils during late postnatal development. J Comp Neurol. 2009;517(3):385–396. Available from: https://doi.org/10.1002/cne.22166.

17. Conjeti S, Mesbah S, Negahdar M, Rautenberg PL, Zhang S, Navab N, et al. Neuron-Miner: An Advanced Tool for Morphological Search and Retrieval in Neuroscientific Image Databases. Neuroinformatics. 2016. Available from: https://doi.org/10.1007/s12021-016-9300-2.

18. Mizrahi A, Ben-Ner E, Katz MJ, Kedem K, Glusman JG, Libersat F. Comparative analysis of dendritic architecture of identified neurons using the Hausdorff distance metric. J Comp Neurol. 2000;422(3):415–428. Available from: https://doi.org/10.1002/1096-9861(20000703)422:3<415::AID-CNE8>3.0.CO;2-T.

19. Sholl DA. Dendritic organization in the neurons of the visual and motor cortices of the cat. J Anat. 1953;87(Pt 4):387–406.1. Available from: http://www.ncbi.nlm.nih.gov/pmc/articles/PMC1244622/.

20. Langhammer CG, Previtera ML, Sweet ES, Sran SS, Chen M, Firestein BL. Automated Sholl analysis of digitized neuronal morphology at multiple scales: Whole cell Sholl analysis versus Sholl analysis of arbor subregions. Cytom Part A. 2010;77 A(12):1160–1168. Available from: https://doi.org/10.1002/cyto.a.20954.

21. Garcia-Segura LM, Perez-Marquez J. A new mathematical function to evaluate neuronal morphology using the Sholl analysis. J Neurosci Methods. 2014;226:103–109. Available from: https://doi.org/10.1016/j.jneumeth.2014.01.016.

22. Billeci L, Pioggia G, Vaglini F, Ahluwalia A. Assessment and comparison of neural morphology through metrical feature extraction and analysis in neuron and neuron-glia cultures. J Biol Phys. 2009;35(4):447–464. Available from: https://doi.org/10.1007/s10867-009-9150-3.

23. Coskren PJ, Luebke JI, Kabaso D, Wearne SL, Yadav A, Rumbell T, et al. Functional consequences of age-related morphologic changes to pyramidal neurons of the rhesus monkey prefrontal cortex. J Comput Neurosci. 2014;263–283. Available from: https://doi.org/10.1007/s10827-014-0541-5.

24. Xu HP, Sun JH, Tian N. A general principle governs vision-dependent dendritic patterning of retinal ganglion cells. J Comp Neurol. 2014;522(15):3403–3422. Available from: https://doi.org/10.1002/cne.23609.

25. O'Neill KM, Akum BF, Dhawan ST, Kwon M, Langhammer CG, Firestein BL. Assessing effects on dendritic arborization using novel Sholl analyses. Front Cell Neurosci. 2015;9:285. Available from: https://doi.org/10.3389/fncel.2015.00285.

26. Kanari L, Dłotko Pawełand Scolamiero M, Levi R, Shillcock J, Hess K, Markram H. A Topological Representation of Branching Neuronal Morphologies. Neuroinformatics. 2017. Available from: https://doi.org/10.1007/s12021-017-9341-1.

27. Rivera-alba M, Peng H, Polavieja GGD, Chklovskii DB. Wiring economy can account for cell body placement across species and brain areas. Curr Biol. 2014;24(3):R109–R110. Available from: https://doi.org/10.1016/j.cub.2013.12.012.

28. Brandt R, Rohlfing T, Rybak J, Krofczik S, Maye A, Westerhoff M, et al. Three-dimensional average-shape atlas of the honeybee brain and its applications. J Comp Neurol. 2005;492(1):1–19. Available from: https://doi.org/10.1002/cne.20644.

29. Ashburner J. Computational neuroanatomy. Nat Methods. 2000;8(6):493–500. Available from: https://doi.org/10.1038/nmeth.1602.

Kumaraswamy *et al. BMC Bioinformatics* (2018) 19:143

Page 16 of 16

30. Jefferis GSXE, Potter CJ, Chan AM, Marin EC, Rohlfing T, Maurer CR, et al. Comprehensive maps of Drosophila higher olfactory centers: spatially segregated fruit and pheromone representation. Cell. 2007;128(6): 1187–203. Available from: https://doi.org/10.1016/j.cell.2007.01.040.

31. Chiang AS, Lin CY, Chuang CC, Chang HM, Hsieh CH, Yeh CW, et al. Three-Dimensional Reconstruction of Brain-wide Wiring Networks in Drosophila at Single-Cell Resolution. Curr Biol. 2011;21(1):1–11. Available from: https://doi.org/10.1016/j.cub.2010.11.056.

32. Kohl J, Ostrovsky AD, Frechter S, Jefferis GSXE. A Bidirectional Circuit Switch Reroutes Pheromone Signals in Male and Female Brains. Cell. 2013;155(7):1610–1623. Available from: https://doi.org/10.1016/j.cell.2013.11.025.

33. Wan Y, Long F, Qu L, Xiao H, Hawrylycz M, Myers EW, et al. BlastNeuron for Automated Comparison, Retrieval and Clustering of 3D Neuron Morphologies. Neuroinformatics. 2015;13(4):487–499. Available from: https://doi.org/10.1007/s12021-015-9272-7.

34. Schnabel R, Wahl R, Klein R. Efficient RANSAC for Point-Cloud Shape Detection. Comput Graph Forum. 2007;26(2):214–226. Available from: https://doi.org/10.1111/j.1467-8659.2007.01016.x.

35. Maier-Hein L, Franz AM, Dos Santos TR, Schmidt M, Fangerau M, Meinzer HP, et al. Convergent iterative closest-point algorithm to accomodate anisotropic and inhomogenous localization error. IEEE Trans Pattern Anal Mach Intell. 2012;34(8):1520–1532. Available from: https://doi.org/10.1109/TPAMI.2011.248.

36. Chen ECS, McLeod aJ, Baxter JSH, Peters TM. Registration of 3D shapes under anisotropic scaling. Int J CARS. 2015;10(6):867–878. Available from: https://doi.org/10.1007/s11548-015-1199-9.

37. Livneh Y, Mizrahi A. A time for atlases and atlases for time. Front Syst Neurosci. 2010;3(17):. Available from: https://doi.org/10.3389/neuro.06.017.2009.

38. Schneider CJ, Cuntz H, Soltesz I. Linking Macroscopic with Microscopic Neuroanatomy Using Synthetic Neuronal Populations. PLoS Comput Biol. 2014;10(10):. Available from: https://doi.org/10.1371/journal.pcbi.1003921.

39. Cannon RC, Turner DA, Pyapali GK, Wheal HV. An on-line archive of reconstructed hippocampal neurons. J Neurosci Methods. 1998;84(1-2): 49–54. Available from: https://doi.org/10.1016/S0165-0270(98)00091-0.

40. Rubner Y, Tomasi C, Guibas LJ. Earth mover's distance as a metric for image retrieval. Int J Comput Vis. 2000;40(2):99–121. Available from: https://doi.org/10.1023/A:1026543900054.

41. Thevenaz P, Ruttimann UE, Unser M. Iterative multi-scale registration without landmarks. Proc Int Conf Image Process. 1995;3:228–231. Available from: https://doi.org/10.1109/ICIP.1995.537622.

42. Je C, Park HM. Optimized hierarchical block matching for fast and accurate image registration. Signal Process Image Commun. 2013. Available from: https://doi.org/10.1016/j.image.2013.04.002.

43. Rohlfing T, Brandt R, Maurer CR, Menzel R. Bee brains, B-splines and computational democracy: generating an average shape atlas. Proc IEEE Workshop Math Meth Biomed Image Anal (MMBIA 2001). 2001;2001: 187–194. Available from: https://doi.org/10.1109/MMBIA.2001.991733.

44. Egger R, Narayanan RT, Helmstaedter M, de Kock CPJ, Oberlaender M. 3D Reconstruction and Standardization of the Rat Vibrissal Cortex for Precise Registration of Single Neuron Morphology. PLOS Comput Biol. 2012;8(12): 1–18. Available from: https://doi.org/10.1371/journal.pcbi.1002837.

45. Ikeno H, Kazawa T, Namiki S, Miyamoto D, Sato Y, Haupt SS, et al. Development of a Scheme and Tools to Construct a Standard Moth Brain for Neural Network Simulations. Comput Intell Neurosci. 2012;2012. Available from: https://doi.org/10.1155/2012/795291.

46. Costa M, Manton JD, Ostrovsky AD, Prohaska S, Jefferis GSXE. NBLAST: Rapid, Sensitive Comparison of Neuronal Structure and Construction of Neuron Family Databases. Neuron. 2016. Available from: https://doi.org/10.1016/j.neuron.2016.06.012.

47. Alpert NM, Bradshaw JF, Kennedy DN, Correia JA. The Principal Axes Transformation - A method for Image Registration. J Nucl Med. 1990;31: 1717–1722. Available from: http://jnm.snmjournals.org/content/31/10/1717.long.

48. Tam GKL, Cheng ZQ, Lai YK, Langbein FC, Liu Y, Marshall D, et al. Registration of 3D Point Clouds and Meshes: A Survey From Rigid to Non-Rigid. IEEE Trans Vis Comput Graph. 2013;19(7):1–20. Available from: https://doi.org/10.1017/CBO9781107415324.004.

49. Torben-Nielsen B, De Schutter E. Context-aware modeling of neuronal morphologies. Front Neuroanat. 2014;8:92. Available from: https://doi.org/10.3389/fnana.2014.00092.

50. van Pelt J, van Ooyen A. Estimating neuronal connectivity from axonal and dendritic density fields. Front Comput Neurosci. 2013;7:160. Available from: https://doi.org/10.3389/fncom.2013.00160.

51. Chen JY. A simulation study investigating the impact of dendritic morphology and synaptic topology on neuronal firing patterns. Neural Comput. 2010;22(4):1086–111. Available from: https://doi.org/10.1162/neco.2009.11-08-913.

52. Ferrante M, Migliore M, Ascoli GA. Functional Impact of Dendritic Branch-Point Morphology. J Neurosci. 2013;33(5):2156–2165. Available from: https://doi.org/10.1523/JNEUROSCI.3495-12.2013.

PUBLICATION 2

Citation

2. Kumaraswamy, A., Ai, H., Kai, K., Ikeno, H., and Wachtler, T. (2019a). "Adaptations during maturation in an identified honeybee interneuron responsive to waggle dance vibration signals." In: *eNeuro* 6.5. doi: `10.1523/eneuro.0454-18.2019`

Context

This publication presents the adaptations in morphology and physiology of DL-Int-1 as honeybees mature from newly emerged adults to foragers.

Morphological comparisons revealed region specific pruning and outgrowth of dendrites that could indicate to improved connectivity and signal propagation. Comparison of electrophysiological responses indicated stronger inhibition relative to spontaneous activity and enhanced postinhibitory rebound during maturation.

Extensive analysis of DL-Int-1 responses provided insights that were instrumental in constructing spiking models for it.

Development

Adaptations during Maturation in an Identified Honeybee Interneuron Responsive to Waggle Dance Vibration Signals

Ajayrama Kumaraswamy,[1] Hiroyuki Ai,[2] Kazuki Kai,[2] Hidetoshi Ikeno,[3] and Thomas Wachtler[1]

https://doi.org/10.1523/ENEURO.0454-18.2019

[1]Department of Biology II, Ludwig-Maximilians-Universität München, Planegg-Martinsried, 82152, Germany, [2]Department of Earth System Science, Fukuoka University, Fukuoka, 814-0180, Japan, and [3]School of Human Science and Environment, University of Hyogo, Himeji, 670-0092, Japan

Abstract

Honeybees are social insects, and individual bees take on different social roles as they mature, performing a multitude of tasks that involve multi-modal sensory integration. Several activities vital for foraging, like flight and waggle dance communication, involve sensing air vibrations through their antennae. We investigated changes in the identified vibration-sensitive interneuron DL-Int-1 in the honeybee *Apis mellifera* during maturation by comparing properties of neurons from newly emerged adult and forager honeybees. Although comparison of morphological reconstructions of the neurons revealed no significant changes in gross dendritic features, consistent and region-dependent changes were found in dendritic density. Comparison of electrophysiological properties showed an increase in the firing rate differences between stimulus and nonstimulus periods in foragers compared with newly emerged adult bees. The observed differences in neurons of foragers compared with newly emerged adult honeybees suggest refined connectivity, improved signal propagation, and enhancement of response features possibly important for the network processing of air vibration signals relevant for the waggle dance communication of honeybees.

Key words: adaptation; honeybee; maturation; neuron morphology

---

Significance Statement

In the darkness of the hive, honeybees inform each other about profitable food sources using stereotypic movements accompanied by specific sound patterns produced by wing-beats. Here we present a study of an identified vibration-sensitive neuron, named DL-Int-1, in the honeybee brain focusing on structural and functional adaptations by comparing data from young, newly emerged adult and mature forager honeybees. We found region-dependent changes in the morphological structure of DL-Int-1 as well as specific changes in its response properties, which suggest an adaptation process during maturation leading to a refinement in network connectivity and improved processing of waggle dance signals in the honeybee brain.

Introduction

Perception of vibrations and sounds is very important for social insects (Hunt and Richard, 2013) and among them, honeybees are unique in that they use air-borne vibrations for communication (Kirchner, 1997). Among

several intra-hive communication behaviors linked to air-borne vibration sensing (Barth et al., 2005; Hunt and Richard, 2013; Nieh, 2010), the waggle dance behavior, which is used to communicate the distance, direction and profitability of food sources, has been extensively studied

in the honeybee *Apis mellifera* (von Frisch 1965, 1967; Kirchner and Towne 1994; Brockmann and Robinson, 2007; Hrncir et al., 2011; Couvillon, 2012). Waggle dance behavior consists of alternative repetitions of two movements; a straight onward movement called the "waggle phase" during which honeybees produce air vibrations by oscillating their abdomen from side to side and beating their wings; and a curved movement called the "return phase" during which they return to the starting point of the onward phase. The neural mechanisms underlying the processing and decoding of the waggle dance vibration signals have so far not been uncovered.

Air vibrations behind dancing honeybees are detectable only up to 15–20 mm (Michelsen, et al., 1987) and consist of low (12–25 Hz) and high (200–300 Hz) frequencies from two sources (Wenner, 1962). Vibrations produced by the wagging abdomen only contain low frequencies, whereas jets of air vibration produced by wing beats have a pulse train pattern and contain both low and high frequencies (Michelsen et al., 1987; Michelsen, 2003). Both kind of vibrations have been shown to be relevant for waggle dance communication (Michelsen et al., 1989, 1992). Honeybees can detect air vibrations using various mechanosensory organs on their bodies. Among them, the Johnston's Organ (JO) located in the pedicel of the antennae (Fig. 1a) has been shown to be the primary sensory organ for detecting near-field vibrations of the waggle dance (Dreller and Kirchner, 1993). Sensory afferents of the JO project into the honeybee brain, specifically in medial posterior protocerebral lobe (mPPL) and the antennal mechanosensory and motor center (AMMC), which consists of the dorsal lobe (DL) and dorsal subesophageal ganglion (dSEG; Fig. 1a; Ai et al., 2007).

More than 10 groups of interneurons belonging to three categories have been identified and characterized in these regions (Ai et al., 2009, 2017; Ai, 2010, 2013) and have been shown to respond to antennal vibrations similar to those produced by air vibration jets of the waggle dance (Ai et al., 2017). In particular, a group of GABAergic interneurons called DL-Int-1 has been studied intensively and has been characterized in detail (Ai et al., 2009, 2017; Ai, 2013). However, neural responses to low-frequency vibrations produced by abdomen waggling has not yet been characterized.

Correspondence should be addressed to Ajayrama Kumaraswamy at Ajayramak@bio.lmu.de or Thomas Wachtler at Wachtler@bio.lmu.de.

DL-Int-1 somata are located in the rind of the protocerebrum and have single neurites branching and projecting to the DL, the dSEG and the mPPL, where they further branch into dense arborizations that run close to afferents (Fig. 1b; Ai et al., 2009). DL-Int-1 are spontaneously active and respond to vibration stimuli applied to the ipsilateral antenna. Their responses to vibration stimuli are characterized by on-phasic excitation to stimulus onset, tonic inhibition during continuous stimulation, and rebound spiking after vibration offset (Ai et al., 2009). DL-Int-1 neurons are thought to play a role in encoding the duration of the waggle phase (Ai et al., 2017), which correlates with the distance of the advertised food source from the hive (von Frisch, 1967).

As they mature, adult honeybees engage in four primary social roles—cleaners, nursers, food storers, and foragers—and perform different tasks in different roles (Seeley, 1996). Several studies have investigated the neural basis of such behavioral versatility by studying structural changes in the honeybee brain with age and social role, mainly focusing on the mushroom body (Groh, et al., 2006, 2012; Groh and Meinertzhagen, 2010). Although most developmental changes in the honeybee brain occur during pupal and larval stages (Devaud and Masson, 1999; Ganeshina et al., 2000), considerable age-dependent and experience-dependent anatomic changes have been described at the level of subregions in the adult honeybee antennal lobe (Winnington et al., 1996; Sigg et al., 1997; Morgan et al., 1998; Brown et al., 2004; Andrione et al., 2017; Arenas et al., 2013) and the mushroom body (Withers et al., 1993, 1995; Durst et al., 1994; Fahrbach et al., 1998; Wolschin et al., 2009), as well as at the level of single mushroom body neurons (Farris et al., 2001). In addition, electrophysiological properties of honeybee neurons also mature with age and experience in the antennal lobe (Wang et al., 2005) and in the mushroom body (Kiya et al., 2007). Adaptations in neural processing could be especially crucial during the transition to foraging, because, compared with in-hive activities, foraging entails several new and complex behaviors such as attending to waggle dancers, sensing the waggle dance vibration signals and decoding target location, using such information on foraging trips, and advertising newly found locations to hivemates through the waggle dance. Honeybees start following waggle dances only after 1 week after emergence (Ai et al., 2018b). Mechanosensory neurons in the JO of the antennae become more responsive to high-frequency waggle dance vibrations as honeybees mature from newly emerged adults to foragers (Tsujiuchi et al., 2007). It is unclear, however, to what extent neurons in central circuits processing waggle dance vibration signals show such adaptation. We therefore investigated morphological and electrophysiological changes of neurons in the primary mechanosensory center of the honeybee, focusing on DL-Int-1 neurons. To identify maturation-related adaptations in DL-Int-1, we analyzed and compared reconstructed morphologies and electrophysiological properties of neurons from newly emerged adult bees and foragers bees.
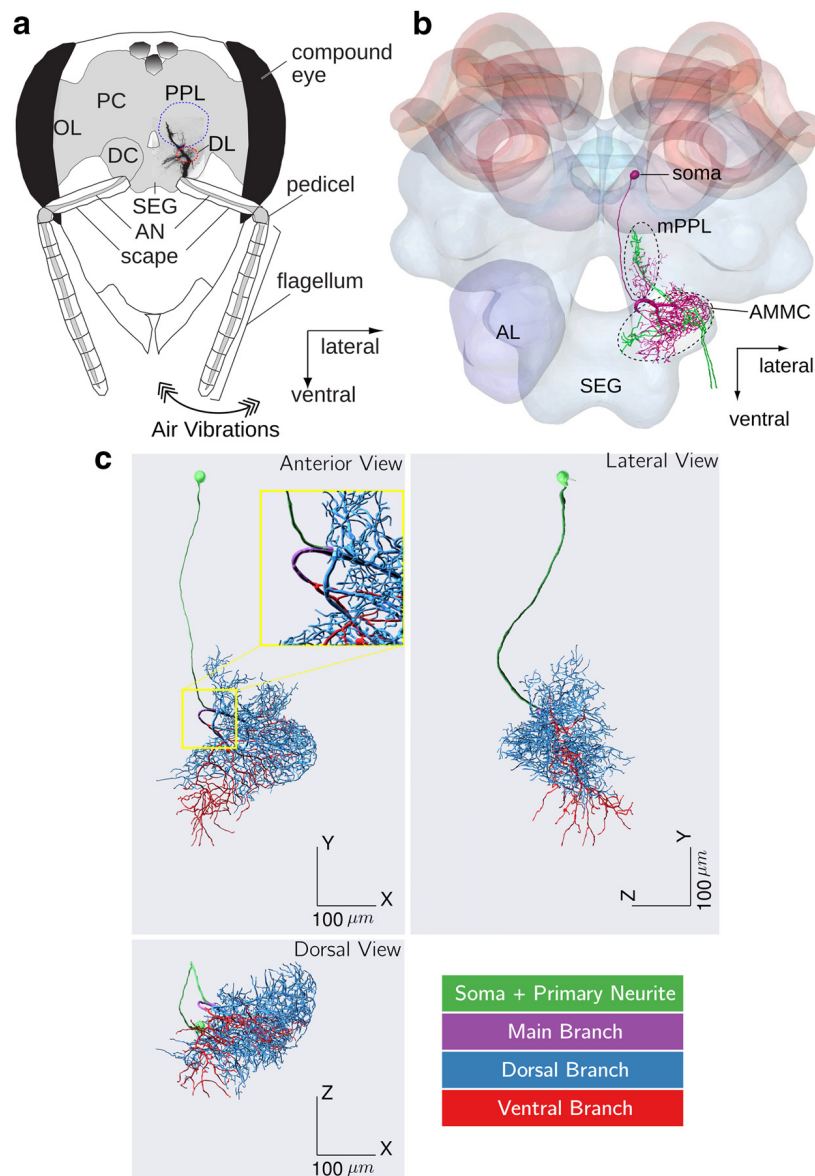
Figure 1. Vibration sensing, primary mechanosensory center and DL-Int-1 interneuron in the honeybee. *a*, Airborne vibration jets produced during the waggle dance are picked up by the flagellum are transduced by sensory neurons of the JO in the pedicel and transmitted to the primary mechanosensory center of the honeybee brain, which consists of the mPPL, DL, and dSEG. Modified with permission from Ai et al. (2007), their Figure 1. *b*, Projection patterns of sensory afferents (green) and DL-Int-1 (magenta) in the primary mechanosensory center of the honeybee brain. DL-Int-1 has dendrites running close to sensory afferents in the DL. Modified from Ai (2013), their Figure 5. *c*, Morphology of DL-Int-1 visualized using three 2D projections. We divided DL-Int-1 morphology into four subregions for analysis. Inset, Magnified version of the region around the Main Branch. OL, Optic lobe; PC, protocerebrum; DC, deutocerebrum; AN, antennal nerve; AL, antennal lobe.

Materials and Methods

Honeybees

Honeybees (*Apis mellifera*) reared at Fukuoka University between 2012 and 2014 were used in this study. Experiments were conducted on more than 300 bees for investigating neurons in the primary mechanosensory center of the honeybee brain. Collected data included electrophysiological recordings and laser scanning microscopy images, which were stored in a database and classified into multiple neuron groups based on electrophysiological and morphological characteristics (Ai et al., 2017, their Table 1). In the current study, we used DL-Int-1 data from the database belonging to honeybees of two stages of maturation:

- **Newly emerged adults (age 1-3 d):** female honeybees shortly after emerging from their cell in the hive. Before the experiments, these bees were kept in isolated cages containing sugar solution and pollen.
- **Foragers (older than 10 d):** female honeybees returning from foraging with pollen on their hindlegs.

Experimental procedure

The experimental procedure for generating image stacks and electrophysiological response traces from

Table 1. Scalar morphometric measures showing significant differences

Measure	Morphological subregion	Newly emerged (NE, n = 6)	Forager (F, n = 6)	Change in median value [(F-NE)/NE]	p
Width (along x), μm	Main branch	10.4, 22.1, 26.5	25.2, 34.1, 61.4	+54.3%	0.004
Height (along y), μm	Dorsal branch	152, 236, 263	212, 268, 294	+13.6%	0.041
Total dendritic volume, $\times 10^3 (\mu m)^3$	Main branch	0.183, 0.409, 0.803	0.301, 0.829, 0.967	+103%	0.041
Average partition asymmetry	Whole arborization	0.597, 0.661, 0.653	0.561, 0.576, 0.636	−12.86%	0.041
Maximum centrifugal order	Ventral branch	13, 30, 43	12, 16, 20	−46.7%	0.043
Hausdorff fractal dimension	Ventral branch	1.14, 1.24, 1.35	1.11, 1.14, 1.2	−8.07%	0.041

Summary statistics of six scalar morphometric and topological parameters that show significant differences for at least one morphological subregion. The triplets in columns three and four represent minimum, median, and maximum values. P values were calculated using Mann–Whitney U test and a cutoff of 5% was used. Summary statistics for all 19 scalar measures and for all 4 subregions are provided in Extended data Table 1-1, Table 1-2, Table 1-3, and Table 1-4. Morphologies showed significant differences for a few scalar measures, with width, total dendritic volume, and maximum centrifugal order showing large changes.

honeybee vibration-sensitive interneurons has been presented in detail by Ai et al. (2017) and we describe it here briefly. After immobilization and head fixing using bee's wax, the frontal surface of the honeybee brain was exposed by cutting away a small rectangular window between the compound eyes. Borosilicate glass electrodes filled at the tip with a dye were inserted into the primary mechanosensory center to record from individual neurons. Three dyes were used: Lucifer yellow CH dilithium salt (catalog number L0259, Sigma-Aldrich), Dextran tetramethylrhodamine solution (3000 molecular weight, anionic, lysine fixable; catalog number D3308, ThermoFisher Scientific), and AlexaFluor 647 hydrazide (catalog number A20502, ThermoFisher Scientific). With the electrode stably inserted into a vibration-sensitive interneuron, sinusoidal vibration stimuli of frequency 265 Hz and duration 1 s were applied to the right antenna and responses were recorded intracellularly. Electrical signals were amplified using an amplifier (MEZ8301, Nihon Kohden), filtered to remove frequencies higher than 20 kHz and recorded using Spike2 (Cambridge Electronic Design; RRID: SCR_000903) at a sampling rate of 20.833 kHz. After recording electrical activity, a hyperpolarizing current (2–5 nA for 2–10 min) was applied to inject the dye into the neuron. Thereafter, the brains were dissected out, fixed in 4% paraformaldehyde for 4 h at room temperature, and then rinsed in phosphate buffer solution, dehydrated, and cleared in methyl salicylate for subsequent observation and imaging.

The cleared specimen containing intracellularly stained neurons were viewed from the posterior side of the brain under a confocal laser-scanning microscope (LSM 510, Carl Zeiss) with a Zeiss Plan-Apochromat 25×/numerical aperture 0.8 oil lens objective (working distance, 0.57 mm). Image stacks of the AMMC and the mPPL were taken at a resolution of 0.36 μm on the imaging plane

using 1-μm-thick optical sections and stitched together digitally to obtain image stacks of complete neurons.

Morphological subregions of DL-Int-1

To refer to specific subregions of the DL-Int-1 morphology, we adopt the following definitions (Fig. 1c; Ai et al., 2017):

- **Soma and primary neurite (SPN):** consists of the soma and its primary neurite until bifurcation.
- **Main branch (MB):** consists of the two daughter branches of the primary neurite until they bifurcate.
- **Dorsal branch (DB):** consists of the remaining dendritic arborization originating from the dorsal end of the MB.
- **Ventral branch (VB):** consists of the remaining dendritic arborization originating from the ventral end of the MB.
- **Whole arborization (WA):** consists of the MB, the DB, and the VB.

Reconstruction of morphologies

The reconstruction procedure has been described in detail by Ikeno et al. (2018). Briefly, image stacks with single dye-filled neurons were de-convolved to reduce image blurring and noise. Regions of each image stack containing the dendritic subtrees emerging from the dorsal and ventral daughter branches of SPNs (Ikeno et al., 2018, their Fig. 6E) were identified based on continuity of branching structure and dendritic thickness and were converted into custom image masks. Applying these masks, two image stacks were created that separately contained the identified dorsal and ventral subtrees of SPN. Morphologies of these subtrees were reconstructed from their image stacks by segmentation, pruning and smoothing using SIGEN software (Minemoto et al., 2009; RRID:SCR_016284) and combined to form the recon-

struction of WA. WA was manually separated into MB, DB, and VB based on the first branching points on the two daughter branches of the primary neurite and stored in separate SWC files (Cannon et al., 1998) for morphometric analyses.

Morphological comparison using scalar measures

Morphologies of DL-Int-1 neurons from newly emerged adult and forager honeybees were compared using 19 widely used metric and topological measures (Uylings and van Pelt, 2002; Scorcioni et al., 2008; Peng et al., 2014). These measures were calculated using a modified version of the BTMORPH software v2.2.1 (Torben-Nielsen 2014; RRID:SCR_003566; code: https://github.com/wachtler-lab/btmorph_v2), Vaa3d v3.447 (Peng et al., 2014; RRID: SCR_002609), and pyVaa3d (code: https://github.com/ajkswamy/pyVaa3d, v0.4). Mann–Whitney U test was used for calculating the significance of differences between the maturation levels with a cutoff of 5%.

Spatial registration

Preliminary visual comparisons indicated that DL-Int-1 morphologies had differences in translation, rotation and scaling that could have resulted from structural differences between honeybee brains as well as from fixation and dehydration artifacts caused during experimentation. Therefore, we coregistered all DL-Int-1 morphologies to a common frame of reference using the Reg-MaxS-N software (Kumaraswamy et al., 2018; code https://doi.org/10.12751/g-node.feee47; RRID:SCR_016257). Reg-MaxS-N estimates and removes differences between morphologies by translation, rotation, and scaling, successively refining estimates of differences at multiple spatial resolutions. In this study we used spatial resolutions of 160, 80, 40, and 20 μm. Morphologies from newly emerged adult and forager bees were coregistered in two steps. First, newly emerged adult and forager morphologies were coregistered separately using Reg-MaxS-N (Kumaraswamy et al., 2018). Then, the two resulting groups of morphologies were brought to the same frame of reference by coregistering the unions of the points of all morphologies in a maturation group using Reg-MaxS (Kumaraswamy et al., 2018).

To control for parameter choice during spatial registration, the procedure above was repeated using multiple parameter sets. Newly emerged adult and forager morphologies were each coregistered separately using three initial references to generate three sets of registered morphologies for each maturation level. Taking all possible combinations of these sets, nine sets of all 12 morphologies were created, which were in turn registered together. All other parameters remained the same for the nine sets (for all parameters, see Extended data Fig. 2-1).

Morphological comparison using spherical shells

The radial distribution of dendritic length was compared between the two maturation levels by dividing the space containing the morphologies into spherical shells of thickness 20 μm, similar to Sholl analysis (Sholl 1953; Uylings and van Pelt, 2002; Langhammer et al., 2010; Garcia-Segura and Perez-Marquez, 2014), which has been

shown to be effective in analyzing morphologies (Cuntz et al., 2008; Luebke et al., 2015; O'Neill et al., 2015). As a natural extension of Sholl analysis, we used the measure dendritic length to quantify changes in dendritic arborization during maturation. For every shell, we calculated PDL_{shell}, which is the percentage of dendritic length of a morphology contained in the shell. Using two-way ANOVA (Wobbrock et al., 2011), we tested whether, in each shell, PDL_{shell} (1) was significantly different between newly emerged adults and foragers and (2) showed no significant dependence between the effects caused by maturation and registration parameters. The tests used a cutoff level of significance of 5% after Bonferroni correction (Bland and Altman, 1995; McDonald, 2014). This analysis was not applied to MB morphologies because most of them had no branching points and comprised of single stretches of dendrites spanning less than 50 μm.

Morphological comparison using 3D voxels

To compare the morphologies with an even finer spatial granularity, we analyzed non-overlapping 3D voxels of size 20 μm. For each voxel, we calculated PDL_{voxel}, which is the percentage dendritic length of a morphology contained in the voxel. Note that, because all the voxels had the same volume, changes in PDL_{voxel} are proportional to changes in average dendritic density. The same criteria as in the previous analysis were used for identifying voxels for which PDL_{voxel} changed significantly during maturation, independent of registration parameters. To visualize the changes in dendritic density, we calculated for each voxel the normalized change in PDL_{voxel} as follows:

$$\triangle PDL_{voxel}^{norm} = \frac{\overline{PDL_{voxel}^{f}} - \overline{PDL_{voxel}^{n}}}{\overline{PDL_{voxel}}} ,$$

where, for a given voxel, $\overline{PDL_{voxel}^{f}}$ is the average PDL_{voxel} for forager morphologies across registration parameters and honeybee samples, $\overline{PDL_{voxel}^{n}}$ is the average PDL_{voxel} for newly emerged adult morphologies across registration parameters and honeybee samples; and $\overline{PDL_{voxel}}$ is the average PDL_{voxel} across all maturation levels, registration parameters, and honeybee samples.

Morphological comparison using proximal and distal partitions

We divided the space containing the morphologies into proximal and distal partitions based on the remoteness of morphological nodes from their roots, which was quantified using the measure %PL:

$$\%PL = 100 \times \frac{PL_{root}}{PL_{root} + PL_{term}^{max}} ,$$

where PL_{root} is the distance along the dendritic tree, also called path-length, between the node and the root; and PL_{term}^{max} is the maximum of the path-lengths between the node and all terminals in the sub-tree emanating from the node. A voxel was classified to be distal if the median value of %PL, calculated across maturation levels, registration parameters and honeybee samples

was more than 90. The significance of differences in PDL_{voxel} between newly emerged adults and foragers were calculated separately for proximal and distal partitions using aligned rank transform (ART) two-way ANOVA (Wobbrock et al., 2011) and the same criteria as in previous analysis.

Analysis of electrophysiology

The physiological response of DL-Int-1 to continuous vibration stimuli applied to the antenna consisted of on-phasic excitation followed by a tonic inhibition and offset rebound (Ai et al., 2009). We defined four time periods for analyzing the electrophysiological activity of DL-Int-1 (Fig. 4b):

- **Spontaneous activity:** 3 s period preceding stimulus onset.
- **On-phasic response:** first 75 ms after stimulus onset.
- **Inhibitory response:** from the end of on-phasic response until stimulus offset.
- **Rebound response:** a 75 ms period after a delay of 25 ms from stimulus offset.

Raw data of electrophysiological recordings were read from Spike2 files using NEO v0.5 (Garcia et al., 2014; RRID:SCR_000634), stored using the NIX format v1.4.5 (Stoewer et al., 2014; RRID:SCR_016196) and analyzed using custom Python scripts. Trials were time-aligned to stimulus onset and time-resolved estimates of average firing rates were generated using adaptive kernel density estimation (Shimazaki and Shinomoto, 2010; Implementation: https://github.com/cooperlab/AdaptiveKDE). The distribution of spike train features such as spike rates and spike times were visualized using the "violinplot" function of the Python package seaborn (Waskom et al., 2018). This function uses kernel density estimation to estimate continuous distributions using Gaussian kernels and Scott's formula for bandwidth calculation (Härdle et al., 2004, p 73). Mann–Whitney U test was used for calculating the significance of differences in response features with a cutoff of 5%.

We quantified the strength of inhibition relative to spontaneous activity by calculating Relative Inhibition, defined as follows:

$$Relative\ Inhibition = 1 - \frac{Firing\ Rate\ during\ Inhibitory\ Response\ period}{Firing\ Rate\ during\ Spontaneous\ Activity\ period}$$

Computational environment, code, and data availability

Data preprocessing and analysis were conducted on a desktop computer with an 8-core Intel i7 Processor, 16 GB of RAM running Ubuntu 16.04. The data used for this study are available online on the repository GIN (https://doi.org/10.12751/g-node.e70cb4). Analysis of morphologies and electrophysiological activities was done using custom Python (RRID:SCR_008394) scripts, which are available online (https://github.com/wachtlerlab/GJEphys and https://github.com/wachtlerlab/GJMorph, respectively; Extended Data 1).

Results

Data collection

Sharp electrodes were inserted into DL-Int-1 neurons in the honeybee brain to record electrophysiological activity as well as to inject dye for imaging neuron morphology. Only about 10% of electrode insertions yielded useful data because honeybee brains were not transparent enough for visually targeted electrode insertion and DL-Int-1 neurons were encountered in about one-third of such insertions (Ai et al., 2017). Furthermore, maintaining the electrode within the neuron long enough to obtain sufficient electrophysiological data were difficult especially for newly emerged adult honeybees, as their brains were soft and infirm. Our data of DL-Int-1 neurons from newly emerged adults were therefore limited to six samples with sufficient data for analysis. For the comparative analysis, we chose six forager samples from our database matching the response pattern of the neurons from newly emerged adults.

Morphological adaptations

The four subregions of DL-Int-1 morphology—the WA, MB, DB, and VB (see Materials and Methods, Reconstruction of morphologies)—were compared separately to investigate changes during maturation.

Analysis 1: scalar morphometrics

We first compared the morphologies using whole-cell scalar measures, which detect net overall changes in morphological subregions as they combine data from all dendrites. Table 1 lists the measures that showed significant differences between the morphologies of newly emerged adult and forager DL-Int-1 neurons for at least one subregion (for summary statistics of WA, MB, DB, and VB, see Extended data Table 1-1, Table 1-2, Table 1-3, and Table 1-4, respectively). MB and VB showed significant differences between newly emerged and forager DL-Int-1 neurons for two measures each, whereas DB and WA had one measure each with a significant difference. The changes were neither consistent across morphological subregions nor highly significant (p-values between 1 and 5%) and the number of measures showing significant differences were consistent with the number false-positives expected. Hence, at the level of whole-neuron morphological measures, significant changes could not be detected. However, these results did not exclude the possibility of localized changes in dendritic arborization. Therefore we investigated the morphologies at finer spatial scales.

Analysis 2: radial distribution of dendritic length

Before detailed spatial analysis, DL-Int-1 morphologies of newly emerged adults and foragers were coregistered to a common frame of reference (see Materials and Methods, Spatial registration) to establish spatial correspondence. Figure 2 compares the radial distributions of PDL_{shell} between newly emerged adults and foragers for WA, DB, and VB and highlights those spherical shells for which PDL_{shell} changed significantly during maturation, independent of registration parameters (see Materials
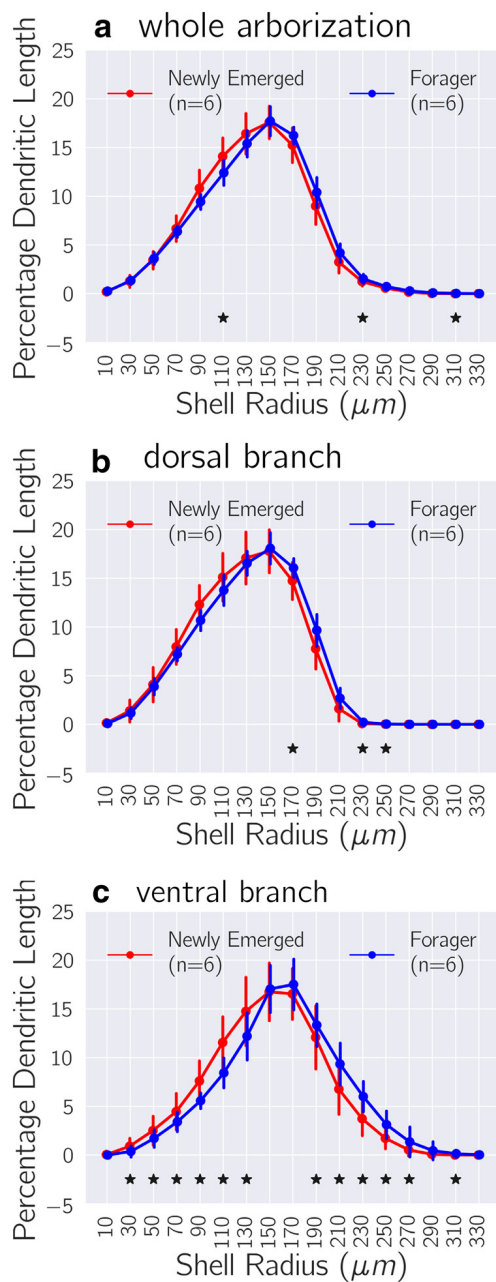
Figure 2. Changes in radial distribution of dendritic density. Comparison of PDL_{shell} calculated for dendrites contained in concentric spherical shells of thickness 20 μm for the WA, DB, and VB, respectively, in *a*, *b*, and *c*. Solid circles indicate means and error bars indicate SD, both of which were calculated by pooling PDL_{shell} values across registration parameters (Extended data Figure 2-1). Asterisks indicate a significant difference in PDL_{shell} between maturation levels independent of registration parameters (see Extended data Figure 2-1). ART two-way ANOVA was used for factor analysis with a p value cutoff of 5%. These comparisons indicate a redistribution of dendritic length during maturation, with reductions in proximal parts and increases in distal parts of DL-Int-1 morphologies.

and Methods, Morphological comparison using spherical shells). WA showed reductions in PDL_{shell} at 110 μm, whereas DB showed an increase at 170 μm during maturation. VB showed reductions up to 130 μm and increases for between 190 and 270 μm during maturation. These comparisons support a consistent redistribution of PDL_{shell} over shells, with reductions in proximal regions and increases in distal regions of the morphology.

To exclude that the observed pattern of proximal reduction and distal increase in dendritic density was a result of a residual scaling difference because of incomplete convergence of the iterative registration process, we repeated the coregistration of the morphologies with different starting conditions, using versions of the newly emerged adult morphologies that were artificially scaled up by 10 or 15%. In both cases, the results were the same as without the scaling (data not shown), confirming that the observed differences in the spatial distributions of dendritic length were not caused by scaling differences.

Analysis 3: local dendritic length

To investigate the observed changes in the radial distribution of dendritic length at finer spatial detail, we compared the morphologies at the scale of voxels of size 20 μm using PDL_{voxel} (see Materials and Methods, Morphological comparison using 3D voxels). Figure 3a–c visualizes the magnitude and spatial distribution of normalized change in PDL_{voxel} (see Materials and Methods, Morphological comparison using 3D voxels; Extended data Fig. 3-1) for voxels showing significant changes in the WA, DB, and VB using a color map (see Extended data Figure 3-1 for distributions). Consistent with indications from the previous analysis, some proximal voxels showed reductions in PDL_{voxel}, whereas some distal voxels showed increases. To quantify the observed changes more concretely, we divided the space containing the morphologies into proximal and distal partitions (Fig. 3d, Extended data Figure 3-2; see Materials and Methods, Morphological comparison using proximal and distal partitions). Pooling values across voxels in each partition, we used two-way ANOVA to test for significant changes in PDL_{voxel} during maturation independent of registration parameters (Fig. 3e, Extended data Figure 3-3, see Materials and Methods, Morphological comparison using proximal and distal partitions). WA, DB, and VB showed significant reductions of 8.5, 11.3, and 11.9%, respectively, in median PDL_{voxel} for the proximal partition. Whereas WA and DB did not show a significant change in median PDL_{voxel} for the distal partition, VB showed a significant reduction of 18.3%. Thus, there was a region-dependent reduction in the dendritic density of DL-Int-1 with more subregions showing a reduction for proximal parts of the arborization than for distal parts.

Electrophysiological adaptations

Comparison of time-resolved firing rate estimates of the responses of DL-Int-1 neurons (see Fig. 5a) indicated increased spontaneous activity and a remarkable increase in firing rate just after stimulus offset in foragers compared with newly emerged adults. These observations were quantified by comparing the firing rates during the four activity periods (Fig. 4b) as well as the spike timing during on-phasic response (Fig. 4c). Figure 5b summarizes the comparison of firing rates for the four periods. Average spontaneous firing rate showed a sig-
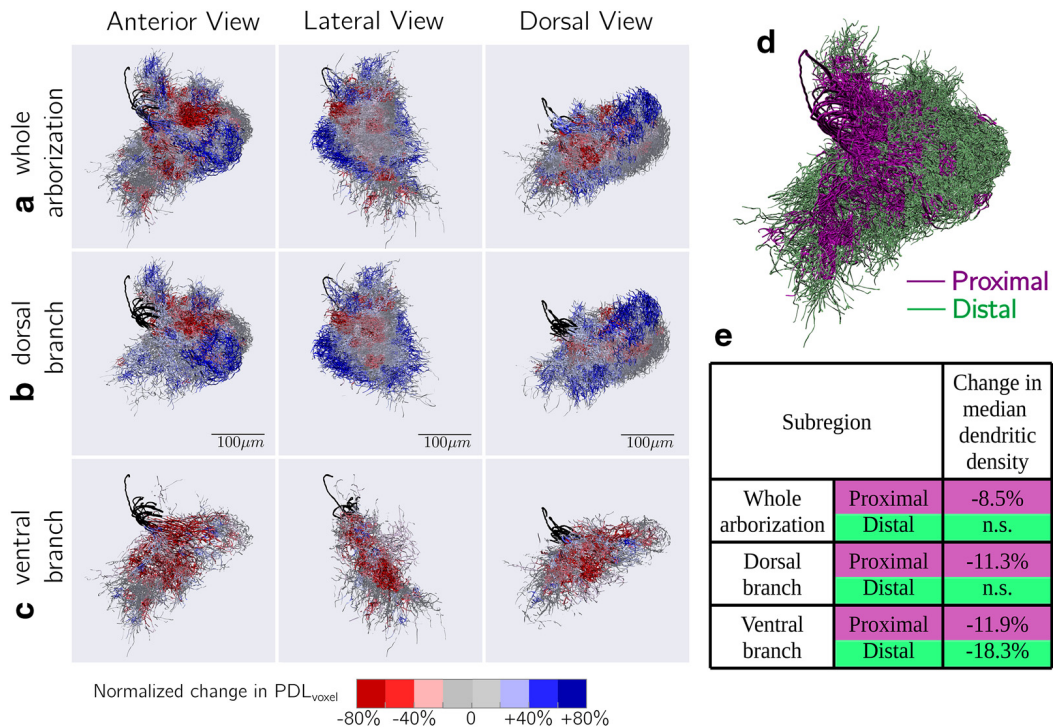
Figure 3. Region-dependent changes in dendritic density. All 12 DL-Int-1 morphologies visualized together after co-alignment, highlighting regions that show significant differences in PDL$_{voxel}$ during maturation. *a*, WA, *b*, DB, and *c*, VB. A voxel was highlighted if ART two-way ANOVA indicated that maturation had a significant effect on PDL$_{voxel}$ independent of registration parameters. The dendrites were colored with normalized change in PDL$_{voxel}$ (see Materials and Methods, Morphological comparison using 3D voxels; for distributions, see Extended data Figure 3-1). The MBs are colored in black. *d*, The space containing the morphologies was divided into proximal and distal partitions based on distances along the dendritic tree of a node from the root and terminals in its subtree (for detailed 3D view for all subregions, see Extended data Figure 3-2). *e*, Changes in median PDL$_{voxel}$ in proximal and distal partitions of each subregion. "n.s." indicates that maturation did not have a significant effect on PDL$_{voxel}$ independent of registration parameters when tested with ART two-way ANOVA (for distributions, see Extended data Figure 3-3).

nificant increase of 39.6%. Average firing rates during on-phasic and inhibitory response periods did not show significant changes, but average firing rate during rebound response nearly doubled, increasing by 94.75%. Thus, DL-Int-1 responses showed stronger spontaneous activity and rebound response.

DL-Int-1 is GABAergic and likely part of a disinhibitory network (Ai et al., 2017; Kumaraswamy et al., 2017). Therefore, increased spontaneous rate and poststimulus rebound in foragers compared with newly emerged adults is expected to result in enhanced strength of the inhibitory signal indicating antennal vibration. To quantify the signal strength of inhibition in DL-Int-1 relative to the level of spontaneous activity, we calculated Relative Inhibition (see Materials and Methods, Analysis of electrophysiology) by plotting the firing rates during the two response periods against each other (Fig. 5c). In general, higher spontaneous spiking was associated with higher spike rates during inhibition in DL-Int-1 neurons, but the difference in firing rates between spontaneous activity and inhibitory response was larger in foragers than in newly emerged adults. Quantitatively, Relative Inhibition was 0.42 ± 0.24 in newly emerged adults, but 0.66 ± 0.18 in foragers (mean $\pm$ SE; *p*-value: 1.34%, Welch's unequal variance *t* test). Additionally, least-squares regression in Figure 5c indicated that the difference became larger with

firing rate level in foragers (slope of 1.42 for foragers vs 1.06 for newly emerged adult), indicative of faster response dynamics in foragers compared with newly emerged adults.

In addition to changes in activity levels during different periods, comparison of firing rate profiles during on-phasic response (Fig. 5a, inset) indicated a change in the timing of the excitation peak. We investigated this by comparing the first spike latency, first interspike interval (ISI), second ISI, and third ISI during on-phasic response (Fig. 5d). All four spike-timing features showed a systematic reduction during maturation, with average values of first spike latency and first ISI showing significant reductions of 1.76 and 4.01 ms, respectively. Thus, spike timing of DL-Int-1 neurons during on-phasic excitation showed a systematic reduction indicative of response speed-up.

Discussion

In this study, we have compared morphological and physiological properties of an identified vibration-sensitive interneuron, DL-Int-1, between newly emerged adult and forager honeybees. Although comparisons of whole-cell scalar morphometric measures showed no major differences in broad dendritic structure and gross morphological features, detailed spatial analyses revealed region-dependent reduction in dendritic density
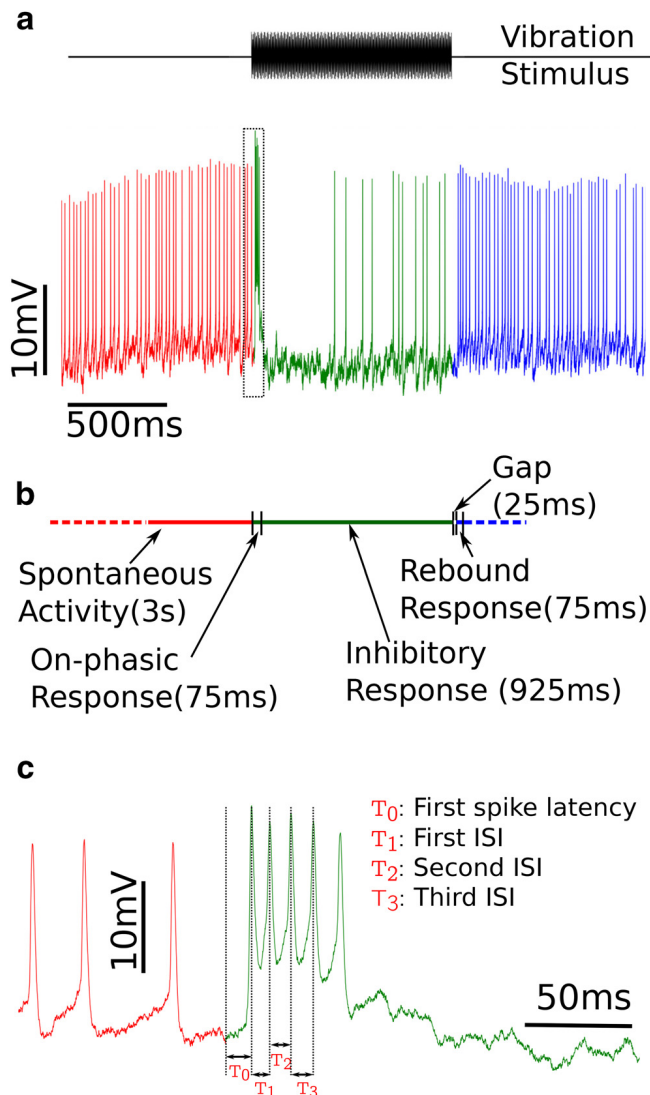
Figure 4. Definition of activity periods and spike timing features of electrophysiological responses. *a*, An example response of DL-Int-1 to 1 s long vibration stimulus of 265 Hz. Activity before stimulus is colored in red, activity during stimulus in green and activity after stimulus in blue. *b*, The definitions of the four activity periods used for analyzing electrophysiological properties of DL-Int-1. *c*, The trace contained in the dotted rectangle in *a* is magnified and the four spike timing features, T_0, T_1, T_2, and T_3 are defined on it.

with stronger reductions in proximal parts than in distal parts. This is consistent with findings from previous studies that investigated changes during maturation in the honeybee antennal lobe (Devaud and Masson, 1999) and mushroom body (Farris et al., 2004), which concluded that most of the process of dendritic maturation is completed before emergence, although minor age-dependent and age-independent changes continue for the first few weeks. Such region-dependent changes have also been shown in dendritic arborizations of Kenyon cells in the adult honeybee (Farris et al., 2001) as well as in the paper wasp (Jones et al., 2009). Comparison of the electrophysiological responses of DL-Int-1 to vibration stimuli between newly emerged adult and forager honeybees

showed increased spontaneous activity and stronger poststimulus rebound during maturation, whereas the qualitative pattern of response remained unchanged. Similar response enhancements have been reported for odor representation in honeybees (Wang et al., 2005), where odor-dependent activity patterns in antennal lobe glomeruli were similar in newly emerged adult and forager honeybees, with older neurons showing higher spiking rates and more active glomeruli.

Effect on network connectivity

Although the DB and VB subregions of DL-Int-1 showed reductions in dendritic density during maturation in the proximal parts, only VB showed reduction in dendritic density in the distal parts. The observed changes thus indicate region-dependent pruning in distal parts. DB and VB arborize in different sets of brain neuropils; the DB arborizes in the mPPL and the DL, whereas the VB arborizes in the DL and the dSEG. DB and VB could therefore be the areas where DL-Int-1 connects to different networks and the observed changes in morphology during maturation might reflect a refinement of the network connectivity.

The AMMC region of the honeybee brain is a center for multisensory integration, especially for waggle dance signals produced by wing beats (Ai and Hagio, 2013; Brockmann and Robinson, 2007). DL-Int-1 arborizes with fine terminals and boutons in the AMMC (Ai et al., 2009), indicating the presence of synaptic inputs and outputs in the region (Petralia et al., 2016). The observed decreases in dendritic density could be associated with changes in the synaptic ultra-structure, similar to that shown in the honeybee mushroom body (Groh et al., 2012; Muenz et al., 2015). However, more studies with synaptic labeling and higher resolution imaging are required to clarify such changes.

Enhanced inhibition

The observed changes in electrophysiological activity of DL-Int-1 could reflect an enhancement of features relevant for network processing of high-frequency components of waggle dance vibration signals in the honeybee primary mechanosensory center. Spontaneous firing rates were significantly higher in foragers than in newly emerged adults, while firing rates during inhibitory responses were similar. Thus, the inhibitory response to vibration stimuli was relatively stronger in foragers than in newly emerged adults. Because DL-Int-1 is itself inhibitory and possibly part of a disinhibitory network processing waggle dance air vibration signals (Ai et al., 2017, 2018a; Kumaraswamy et al., 2017), the observed strengthening of relative inhibition could result in more effective disinhibition. Furthermore, the strength of post-inhibitory rebound doubled during maturation. Because inhibition coupled with post-inhibitory rebound has been suggested to play an important role in processing temporal signals in insects (Ai et al., 2018a) and specifically in detecting temporal features (Hedwig 2016; Alluri et al., 2016; Naud et al., 2015; Yamada et al., 2018), our results suggest improved detection of information encoded in the temporal features of waggle dance air vibration signals in forager honeybees.
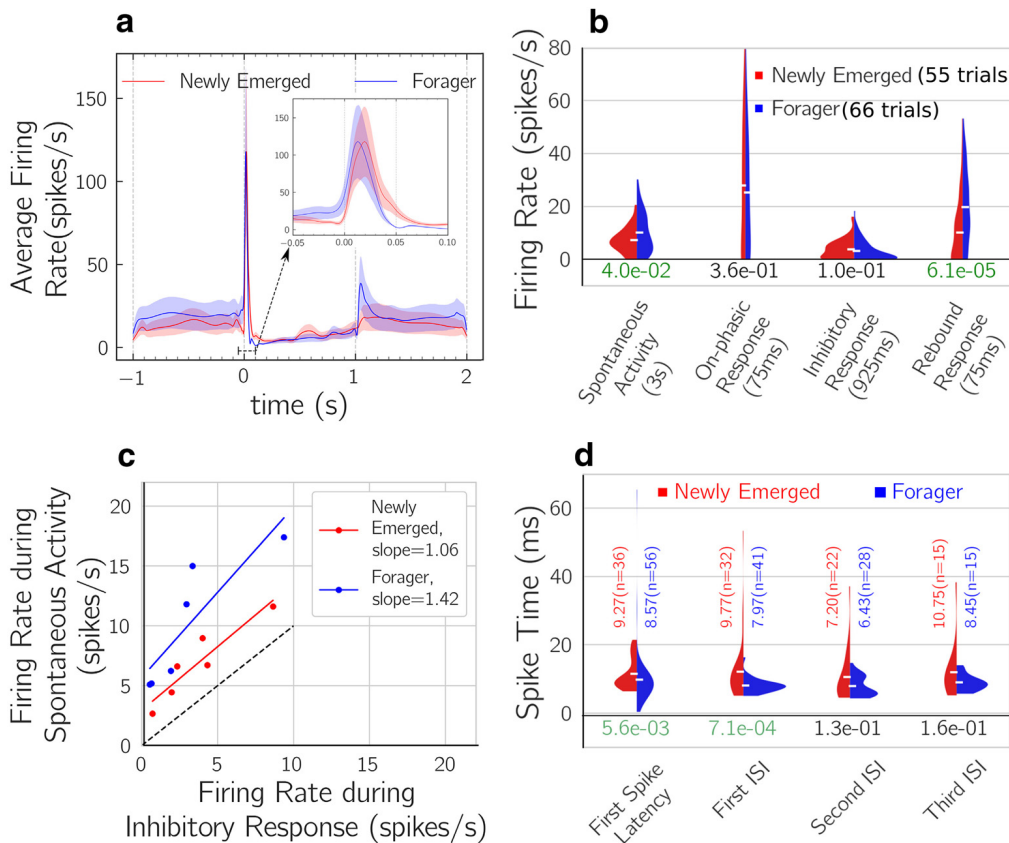
Figure 5. Analysis of electrophysiological properties. *a*, Comparison of the average firing rate profiles of newly emerged adult and forager DL-Int-1 neurons. Smoothed estimates of time-resolved average firing rates were calculated from responses aligned to stimulus onset using adaptive kernel density estimation (Shimazaki and Shinomoto, 2010). Solid lines indicate average firing rates, whereas shaded regions indicate 95% confidence intervals. Inset, Average firing rate during on-phasic response with expanded time scale. *b*, Comparison of firing rates during four activity periods. The filled areas represent firing rate distributions estimated using kernel density estimation (see Methods, Analysis of electrophysiology). The distributions were normalized to have equal areas. Horizontal white markers indicate mean values of the distributions. The numbers below the distributions are *p* values calculated using Mann–Whitney *U* test. *P*-values <5% are highlighted in green. Firing rates during spontaneous activity and rebound response showed significant increases. *c*, Comparison of the strength of inhibition relative to spontaneous activity by plotting the firing rates during the two periods against each other. Lines were fit using linear least-squares regression. The dashed line indicates the line of slope 1. *d*, Comparison of the timing of the first four spikes of the response using first spike latency, first ISI, second ISI, and third ISI. The distributions were estimated using Kernel Density estimation and normalized to have the same area. The numbers under the distributions are *p* values calculated using Mann–Whitney *U* test. Horizontal white markers indicate mean values, which are also shown above the distributions with sample numbers in parentheses. Spiking response was faster in foragers compared with newly emerged adults with significant reductions in first spike latency and first ISI.

Effects of morphological changes on physiology

The observed changes in neuron morphology of DL-Int-1 are consistent with a refinement process during maturation that may lead to improved propagation and processing of vibration signals in foragers compared with newly emerged adults. The broad structure of the DL-Int-1 did not show major changes during maturation, with the dendritic branches of the DB and VB extending to similar regions in the honeybee brain. Under this condition and assuming unchanged membrane parameters, reduced dendritic length in proximal regions could indicate lower electrical resistance, and thus, for passive propagation, lower signal attenuation through the DB and VB (Rall and Rinzel, 1973; Ferrante et al., 2013). However, clarification of these effects using multi-compartmental neuron simulations is currently limited by the lack of data about membrane parameters. The potential for such simulations is

nonetheless high because morphological reconstructions for several newly emerged adult and forager DL-Int-1 neurons are available.

Changes in response properties: neuron or network?

The response of DL-Int-1 neurons to vibration stimuli applied to the antennae is the combined effect of its inputs and its own intrinsic electrophysiological properties (Ai et al., 2017). In this study, significant increases were seen in spontaneous activity and the strength of inhibition relative to spontaneous activity, as well as in the strength of post-inhibitory rebound. These changes are likely because of maturation of the electrophysiological properties of DL-Int-1 as well as its connected neuronal network. Specifically, the adaptations in the strength of inhibition relative to spontaneous activity could have a stronger dependence on network factors as DL-Int-1 is inhibitory

and is believed to be inhibited in turn as part of a disinhibitory network in the honeybee primary mechanosensory center (Ai et al., 2017; Kumaraswamy et al., 2017). Further, the JO sensory neurons, which transduce antennal vibrations of the waggle dance and project close to the dendrites of DL-Int-1, show stronger responses to antennal deflection in foragers than in newly emerged adults (Tsujiuchi et al., 2007). This adaptation in the responses of JO neurons can also play a role in shaping the response properties of DL-Int-1 during maturation. Clarification of the contribution of these sources would be beneficial for further understanding the role of DL-Int-1 in networks that process air vibration jets of the waggle dance in the primary mechanosensory center of the honeybee.

Genetically programmed aging or foraging experience?

In this study we have quantified morphological and physiological changes in DL-Int-1 as honeybees mature from newly emerged adult bees (1–3 d old) to forager bees (>10 d old). There are two major factors that could cause such changes during maturation: genetically programmed aging and foraging experience. Further studies with age-controlled older honeybees with no foraging experience are required to elucidate the effect of these factors on DL-Int-1 maturation.

Linking observed changes to behavior

After successful foraging, honeybees return to their hive and perform the waggle dance, during which they produce patterns of air vibration pulses. Follower bees detect these pulses and gain information about the distance and direction of the advertised food sources (Michelsen et al., 1992; Landgraf, 2013). It has been argued that DL-Int-1 plays a role in the networks encoding information from air vibration jets of the waggle dance into neural signals (Ai et al., 2017; Kumaraswamy et al., 2017). The observed changes in DL-Int-1 suggest that neurons and networks processing waggle dance communication signals undergo functional and structural refinement as the honeybee matures that could prepare the bees to better process those important signals as foragers.

References

Ai H (2010) Vibration-processing interneurons in the honeybee brain. Front Syst Neurosci 3:19

Ai H (2013) Sensors and sensory processing for airborne vibrations in silk moths and honeybees. Sensors 13:9344–9363.

Ai H, Hagio H (2013) Morphological analysis of the primary center receiving spatial information transferred by the waggle dance of honeybees. J Comp Neurol 521:2570–2584.

Ai H, Nishino H, Itoh T (2007) Topographic organization of sensory afferents of Johnston's organ in the honeybee brain. J Comp Neurol 502:1030–1046.

Ai H, Rybak J, Menzel R, Itoh T (2009) Response characteristics of vibration-sensitive interneurons related to Johnston's organ in the honeybee, Apis Mellifera. J Comp Neurol 515:145–160.

Ai H, Kai K, Kumaraswamy A, Ikeno H, Wachtler T (2017) Interneurons in the honeybee primary auditory center responding to waggle dance-like vibration pulses. J Neurosci 37:10624–10635.

Ai H, Kumaraswamy A, Kohashi T, Ikeno H, Wachtler T (2018a) Inhibitory pathways for processing the temporal structure of sensory signals in the insect brain. Front Psychol 9:1517.

Ai H, Shinya T, Ayayo O, Koji H, Sakashi M, Naoyuki T (2018b) How do the honeybees learn waggle dance? International Union for the Study of Social Insects (IUSSI2018), Guarujá, Brazil, August.

Alluri RK, Rose GJ, Hanson JL, Leary CJ, Vasquez-Opazo GA, Graham JA, Wilkerson J (2016) Phasic, suprathreshold excitation and sustained inhibition underlie neuronal selectivity for short-duration sounds. Proc Natl Acad Sci U S A 113:E1927–E1935.

Andrione M, Timberlake BF, Vallortigara G, Antolini R, Haase A (2017) Morphofunctional experience-dependent plasticity in the honeybee brain. Learn Mem 24:622–629.

Arenas A, Ramírez GP, Balbuena MS, Farina WM (2013) Behavioral and neural plasticity caused by early social experiences: the case of the honeybee. Front Physiol 4:41.

Barth F, Hrncir M, Tautz J (2005) Vibratory and airborne-sound signals in bee communication (Hymenoptera). In: Insect Sounds and Communication, pp 421–436. Boca Raton, FL: CRC.

Bland JM, Altman DG (1995) Multiple significance tests: the Bonferroni method. BMJ 310:170

Brockmann A, Robinson GE (2007) Central projections of sensory systems involved in honey bee dance language communication. Brain, Behav Evol 70:125–136.

Brown SM, Napper RM, Mercer AR (2004) Foraging experience, glomerulus volume, and synapse number: a stereological study of the honey bee antennal lobe. Journal Neurobiol 60:40–50.

Cannon RC, Turner DA, Pyapali GK, Wheal HV (1998) An on-line archive of reconstructed hippocampal neurons. J Neurosci Methods 84:49–54.

Couvillon MJ (2012) The dance legacy of Karl von Frisch. Insectes Sociaux 59:297–306.

Cuntz H, Forstner F, Haag J, Borst A (2008) The morphological identity of insect dendrites. PLoS Comput Biol 4:1–7.

Devaud JM, Masson C (1999) Dendritic pattern development of the honeybee antennal lobe neurons: a laser scanning confocal microscopic study. J Neurobiol 39:461–474.

Dreller C, Kirchner WH (1993) Hearing in honeybees: localization of the auditory sense organ. J Comp Physiol 173:275–279.

Durst C, Eichmüller S, Menzel R (1994) Development and experience lead to increased volume of subcompartments of the honeybee mushroom body. Behav Neural Biol 62:259–263.

Fahrbach S, Darrell M, Capaldi EA, Farris SM, Robinson GE (1998) Experience-expectant plasticity in the mushroom bodies of the honeybee. Learn Mem 5:115–123.

Farris SM, Abrams AI, Strausfeld NJ (2004) Development and morphology of class ii kenyon cells in the mushroom bodies of the honey bee, Apis Mellifera. J Comp Neurol 474:325–339.

Farris SM, Robinson GE, Fahrbach SE (2001) Experience- and age-related outgrowth of intrinsic neurons in the mushroom bodies of the adult worker honeybee. J Neurosci 21:6395–6404.

Ferrante M, Migliore M, Ascoli GA (2013) Functional impact of dendritic branch-point morphology. J Neurosci 33:2156–65.

Ganeshina O, Schäfer S, Malun D (2000) Proliferation and programmed cell death of neuronal precursors in the mushroom bodies of the honeybee. J Comp Neurol 417:349–365.

Garcia S, Guarino D, Jaillet F, Jennings T, Pröpper R, Rautenberg PL, Rodgers CC, Sobolev A, Wachtler T, Yger P, Davison AP (2014) Neo: an object model for handling electrophysiology data in multiple formats. Front Neuroinform 8:10.

Garcia-Segura LM, Perez-Marquez J (2014) A new mathematical function to evaluate neuronal morphology using the Sholl analysis. J Neurosci Methods 226:103–109.

Groh C, Ahrens D, Rössler W (2006) Environment- and age-dependent plasticity of synaptic complexes in the mushroom bodies of honeybee queens. Brain Behav Evol 68:1–14.

Groh C, Lu Z, Meinertzhagen IA, Rössler W (2012) Age-related plasticity in the synaptic ultrastructure of neurons in the mushroom body calyx of the adult honeybee Apis Mellifera. J Comp Neurol 520:3509–3527.

Groh C, Meinertzhagen IA (2010) Brain plasticity in diptera and hymenoptera. Front Biosci 2:268–288.

Härdle W, Werwatz A, Müller M, Sperlich S (2004) Nonparametric and semiparametric models. Berlin; Heidelberg: Springer.

Hedwig BG (2016) Sequential filtering processes shape feature detection in crickets: a framework for song pattern recognition. Front Physiol 7:46

Hrncir M, Maia-Silva C, McCabe SI, Farina WM (2011) The recruiters excitement features of thoracic vibrations during the honey bees waggle dance related to food source profitability. J Exp Biol 214:4055–4064.

Hunt JH, Richard FJ (2013) Intracolony vibroacoustic communication in social insects. Insectes Sociaux 60:403–417.

Ikeno H, Kumaraswamy A, Kai K, Ikeno H, Wachtler T, Ai H (2018) A segmentation scheme for complex neuronal arbors and application to vibration sensitive neurons in the honeybee brain. Front Neuroinform 12:61

Jones TA, Donlan NA, ODonnell S (2009) Growth and pruning of mushroom body Kenyon cell dendrites during worker behavioral development in the paper wasp, *Polybia Aequatorialis* (Hymenoptera: Vespidae). Neurobiol Learn Mem 92:485–495.

Kirchner WH (1997) Acoustical communication in social insects. In: Orientation and Communication in Arthropods (Lehrer M, ed), pp 273–300. Basel, Switzerland: Birkhäuser; Springer.

Kirchner WH, Towne WF (1994) The sensory basis of the honeybee's dance language. Sci Am 270:74–80.

Kiya T, Kunieda T, Kubo T (2007) Increased neural activity of a mushroom body neuron subtype in the brains of forager honeybees. PLoS One 2:e371.

Kumaraswamy A, Kai K, Ai H, Ikeno H, Wachtler T (2018) Spatial registration of neuron morphologies based on maximization of volume overlap. BMC Bioinformatics 19:143.

Kumaraswamy A, Maksutov A, Kai K, Ai H, Ikeno H, Wachtler T (2017) Network simulations of interneuron circuits in the honeybee primary auditory center. bioRxiv 159533.

Landgraf, T (2013) RoboBee: a biomimetic honeybee robot for the analysis of the dance communication system. PhD thesis, Freie Universität Berlin.

Langhammer CG, Previtera ML, Sweet ES, Sran SS, Chen M, Firestein BL (2010) Automated Sholl analysis of digitized neuronal morphology at multiple scales: whole cell Sholl analysis versus Sholl analysis of arbor subregions. Cytometry A 77:1160–1168.

Luebke JI, Medalla M, Amatrudo JM, Weaver CM, Crimins JL, Hunt B, Hof PR, Peters A (2015) Age-related changes to layer 3 pyramidal cells in the rhesus monkey visual cortex. Cereb Cortex 25:1454–1468.

McDonald JH (2014) Handbook of biological statistics, Ed 3. Baltimore: Sparky House

Michelsen A (2003) Signals and flexibility in the dance communication of honeybees. J Comp Physiol 189:165–174.

Michelsen A, Andersen BB, Kirchner WH, Lindauer M (1989) Honeybees can be recruited by a mechanical model of a dancing bee. Naturwissenschaften 76:277–280.

Michelsen A, Andersen BB, Storm J, Kirchner WH, Lindauer M (1992) How honeybees perceive communication dances, studied by means of a mechanical model. Behav Ecol Sociobiol 30:143–150.

Michelsen A, Towne WF, Kirchner WH, Kryger P (1987) The acoustic near field of a dancing honeybee. J Comp Physiol A 161:633–643.

Minemoto TA, Saitoh H, Ikeno T, Isokawa N, Kamiura N, Matsui R, Kanzaki R (2009) SIGEN: system for reconstructing three-dimensional structure of insect neurons. Asia Simulation Conference, Shiga, Japan, October.

Morgan SM, Butz Huryn VM, Downes SR, Mercer AR (1998) The effects of queenlessness on the maturation of the honey bee olfactory system. Behav Brain Res 91:115–126.

Muenz TS, Groh C, Maisonnasse A, Le Conte Y, Plettner E, Rössler W (2015) Neuronal plasticity in the mushroom body calyx during adult maturation in the honeybee and possible pheromonal influences. Dev Neurobiol 75:1368–1384.

Naud R, Houtman D, Rose GJ, Longtin A (2015) Counting on disinhibition: a circuit motif for interval counting and selectivity in the anuran auditory system. J Neurophysiol 114:2804–2815.

Nieh JC (2010) A negative feedback signal that is triggered by peril curbs honey bee recruitment. Curr Biol 20:310–315.

O'Neill KM, Akum BF, Dhawan ST, Kwon M, Langhammer CG, Firestein BL (2015) Assessing effects on dendritic arborization using novel Sholl analyses. Front Cell Neurosci 9:285.

Peng H, Bria A, Zhou Z, Iannello G, Long F (2014) Extensible visualization and analysis for multidimensional images using Vaa3D. Nat Protoc 9:193–208.

Petralia RS, Wang YX, Mattson MP, Yao PJ (2016) The diversity of spine synapses in animals. NeuroMolecular Med 18:497–539.

Rall W, Rinzel J (1973) Branch input resistance and steady attenuation for input to one branch of a dendritic neuron model. Biophys J 13:648–687.

Scorcioni R, Polavaram S, Ascoli GA (2008) L-Measure: a web-accessible tool for the analysis, comparison and search of digital reconstructions of neuronal morphologies. Nat Protoc 3:866–876.

Seeley TD (1996) The wisdom of the hive: the social physiology of honey bee colonies. Cambridge, MA: Harvard UP.

Shimazaki H, Shinomoto S (2010) Kernel bandwidth optimization in spike rate estimation. J Compl Neurosci 29:171–182.

Sholl DA (1953) Dendritic organization in the neurons of the visual and motor cortices of the cat. J Anat 87:387–406.

Sigg D, Thompson CM, Mercer AR (1997) Activity-dependent changes to the brain and behavior of the honey bee, *Apis Mellifera* (L.). J Neurosci 17:7148–156.

Stoewer A, Kellner CJ, Benda J, Wachtler T, Jan G (2014) File format and library for neuroscience data and metadata. Front Neuroinform Abstr 27:00027.

Torben-Nielsen B (2014) An efficient and extendable python library to analyze neuronal morphologies. Neuroinformatics 12:619–622.

Tsujiuchi S, Sivan-Loukianova E, Eberl DF, Kitagawa Y, Kadowaki T (2007) Dynamic range compression in the honey bee auditory system toward waggle dance sounds. PLoS One 2:e234

Uylings HBM, van Pelt J (2002) Measures for quantifying dendritic arborizations. Network 13:397–414.

von Frisch K (1965) Tanzsprache und orientierung der bienen. Berlin; Heidelberg: Springer.

von Frisch K (1967) The dance language and orientation of bees. Cambridge, MA: Harvard UP.

Wang S, Zhang S, Sato K, Srinivasan MV (2005) Maturation of odor representation in the honeybee antennal lobe. J Insect Physiol 51:1244–1254.

Waskom M, Botvinnik O, O'Kane D, Hobson P, Ostblom J, Lukaus-kas S, Gemperline DC, Augspurger T, Halchenko Y, Cole JB, Warmenhoven J, de Ruiter J, Pye C, Hoyer S, Vanderplas J, Villalba S, Kunter G, Quintero E, Bachant P, Martin M, et al., (2018) Mwaskom/seaborn: V0.9.0 (July, 2018). Zenodo.

Wenner AM (1962) Sound production during the waggle dance of the honey bee. Animal Behav10:79–95.

Winnington AP, Napper RM, Mercer AR (1996) Structural plasticity of identified glomeruli in the antennal lobes of the adult worker honey bee. J Comp Neurol 365:479–490.

Withers GS, Fahrbach SE, Robinson GE (1995) Effects of experience and juvenile hormone on the organization of the mushroom bodies of honey bees. J Neurobio 26:130–144.

Withers GS, Fahrbach SE, Robinson GE (1993) Selective neuroanatomical plasticity and division of labour in the honeybee. Nature 364:238–240.

Wobbrock JO, Findlater L, Gergle D, Higgins JJ (2011) The aligned rank transform for nonparametric factorial analyses using only ANOVA procedures. Proceedings of the 2011 Annual Conference on Human Factors in Computing Systems–CHI 11, Vancouver, BC, Canada, May.

Wolschin F, Munch D, Amdam GV (2009) Structural and proteomic analyses reveal regional brain differences during honeybee aging. J Exp Biol 212:4027–4032.

Yamada D, Ishimoto H, Li X, Kohashi T, Ishikawa Y, Kamikouchi A (2018) GABAergic local interneurons shape female fruit fly response to mating songs. J Neurosci 38:4329–4347.

PUBLICATIONS 3 AND 4

Citations

3. Ai, H., Kai, K., Kumaraswamy, A., Ikeno, H., and Wachtler, T. (2017). "Interneurons in the honeybee primary auditory center responding to waggle dance-like vibration pulses." In: *The Journal of Neuroscience* 37.44, pp. 0044–17. doi: `10.1523/JNEUROSCI.0044-17.2017`

4. [preprint] Kumaraswamy, A., Maksutov, A., Kai, K., Ai, H., Ikeno, H., and Wachtler, T. (2017a). "Network simulations of interneuron circuits in the honeybee primary auditory center." In: *bioRxiv*. doi: `10.1101/159533`

Context

These publications are about a putative disinhibitory network in the PMC of the honeybee brain for encoding waggle dance signals. Note that the PMC is referred to as the primary auditory center (PAC) in these two publications. Publication 3 presents the experimental characterization of the morphology and physiology of 13 groups of vibration-sensitive interneurons. The publication also presents the immunohistochemistry of DL-Int-1, DL-Int-2 and a newly identified bilateral neuron along with the detailed investigation of their electrophysiological response features to behaviorally relevant vibration stimulus patterns. Publication 4 presents the modeling and simulation of this network and validates the simulated response traces against experimentally recorded traces. It also highlights the role of DL-Int-1 in the network. This computational study has been presented in brief in Publication 3 to support the proposed network as well as to clarify the role of different interneurons in this network.

Systems/Circuits

Interneurons in the Honeybee Primary Auditory Center Responding to Waggle Dance-Like Vibration Pulses

Hiroyuki Ai,[1] Kazuki Kai,[1] Ajayrama Kumaraswamy,[2] Hidetoshi Ikeno,[3] and Thomas Wachtler[2]

[1]Department of Earth System Science, Fukuoka University, Fukuoka 814-0180, Japan, [2]Department of Biology II, Ludwig-Maximilians-Universität München, 82152 Planegg-Martinsried, Germany, and [3]School of Human Science and Environment, University of Hyogo, Himeji 670-0092, Japan

Female honeybees use the "waggle dance" to communicate the location of nectar sources to their hive mates. Distance information is encoded in the duration of the waggle phase (von Frisch, 1967). During the waggle phase, the dancer produces trains of vibration pulses, which are detected by the follower bees via Johnston's organ located on the antennae. To uncover the neural mechanisms underlying the encoding of distance information in the waggle dance follower, we investigated morphology, physiology, and immunohistochemistry of interneurons arborizing in the primary auditory center of the honeybee (*Apis mellifera*). We identified major interneuron types, named DL-Int-1, DL-Int-2, and bilateral DL-dSEG-LP, that responded with different spiking patterns to vibration pulses applied to the antennae. Experimental and computational analyses suggest that inhibitory connection plays a role in encoding and processing the duration of vibration pulse trains in the primary auditory center of the honeybee.

Key words: brain; dance language; honeybee; Johnston's organ; primary auditory center; vibration; waggle dance

---

Significance Statement

The waggle dance represents a form of symbolic communication used by honeybees to convey the location of food sources via species-specific sound. The brain mechanisms used to decipher this symbolic information are unknown. We examined interneurons in the honeybee primary auditory center and identified different neuron types with specific properties. The results of our computational analyses suggest that inhibitory connection plays a role in encoding waggle dance signals. Our results are critical for understanding how the honeybee deciphers information from the sound produced by the waggle dance and provide new insights regarding how common neural mechanisms are used by different species to achieve communication.

Introduction

Karl von Frisch demonstrated that honeybees use a type of movement called the "waggle dance" to direct their nest mates to a remote food source (von Frisch, 1967). The duration of the phase of the "waggle" movement changes linearly with the distance to the food source, suggesting that this distance information is en-

coded in a physical parameter of the movement that changes with the duration (von Frisch, 1967). Although it is possible that substrate-borne vibration elicited by the waggle movement conveys spatial information regarding the food source (Michelsen, 2003), air-borne vibration is thought to be the most probable sensory cue delivered during waggle dance communication (Judd, 1995) where wing beats produce local air-jet flows. During the waggle phase of the dance, the wingbeats of the dancer produce a train of vibration pulses that pass from the tail end of the dancer to a follower bee, which follows behind the dancer. For a fixed target location, the duration of the waggle phase is constant, as are pulse rate (29 Hz) and waggle frequency (14.5 Hz), independent of the quality of the food source (Hrncir et al., 2011). However, the precise feature of the train of vibration pulses elicited during the waggle dance that encodes distance information is unclear. Two plausible parameters are (1) the duration of the train of vibration pulses and (2) the number of vibration pulses per waggle phase. These parameters are linearly related because the rate of the pulsed vibration is nearly constant.

Waggle dance followers detect air-borne vibrations via Johnston's organ (JO), which is located at the second segment (pedi-

cel) of the antenna (Towne and Kirchner, 1989; Kirchner et al., 1991; Dreller and Kirchner, 1993). The structural characteristics of the antenna and the response of JO neurons suggest that mature honeybee antennae and JO neurons are tuned to 250–300 Hz, which matches the frequency of sound generated during the waggle dance (Tsujiuchi et al., 2007). JO afferent fibers are spatially segregated in the medial posterior protocerebral lobe (mPPL) and the dorsal lobe (DL)-dorsal subesophageal ganglion (dSEG; Ai et al., 2007). The dSEG also receives sensory afferents from neck hairs that are thought to be gravity sensors (Brockmann and Robinson, 2007). This suggests that the dSEG integrates vector information about the waggle dance (i.e., distance information coded in air vibrations and direction information coded in the orientation of the dancer relative to gravity; Ai and Hagio, 2013).

Our goal is to understand how distance and direction information is encoded in the honeybee brain. Accordingly, we are interested in characterizing the distribution and location of neurons that exhibit appropriate response properties for processing distance or direction information. Recently, we identified two interneuron (Int) types, DL-Int-1 and DL-Int-2, that receive JO input and are located in the primary auditory center (PAC) of the honeybee. We demonstrated that these interneurons are responsive to antennal stimulation (Ai et al., 2009; Ai, 2010; Ai and Itoh, 2012). In the present report, we describe the above-mentioned interneurons as well as a newly identified neuron type, the bilateral DL-dSEG-lateral protocerebrum (LP). We investigated the morphology, GABA immunoreactivity, and physiology of these three cell types in the PAC, with a particular focus on their responses to trains of vibration pulses with temporal properties similar to those elicited during the waggle dance. This work represents a first step toward understanding the role of these neurons in the encoding of distance information in the honeybee brain.

Materials and Methods

Preparation. Honeybees (*Apis mellifera* L., NCBITaxon:7460) were reared in hives placed on the Fukuoka University campus. The data reported here were collected between the months of April and September from 2013 to 2015. Female worker bees that were returning to the hive after foraging and had pollen on their hindlegs were caught at the hive entrance and used in this study.

Intracellular recording and staining. To investigate the processing of the sound produced during the waggle dance, we collected auditory interneurons in the PAC, including the previously described interneuron types DL-Int-1 and DL-Int-2 (Ai et al., 2009). The procedure for each subject was as follows. An individual bee was immobilized by placing it in a cold environment and then mounting it in an acrylic chamber. The bee was then given a 1 M sucrose solution as food and kept overnight in a dark room with high humidity and a temperature of 20°C. The next day, the head of the bee was fixed in place with wax and the frontal surface of the brain was exposed by cutting away a small rectangular window between the compound eyes. The glands and tracheal sheaths on top of the brain were removed, and the mouthparts, including the mandibles, were cut off to expose and enable the removal of the esophagus. Small droplets of bee physiological saline (in mM: 137 NaCl, 3 KCl, 1 CaCl$_2$, 4 Na$_2$HPO$_4$, 2 KH$_2$PO$_4$, 100 sucrose, pH 6.7) were applied to wash away any residue in the esophagus and to enhance electrical contact with a platinum ground electrode placed in the head capsule next to the brain.

Borosilicate glass electrodes were pulled using a laser puller (P-2000, Sutter Instruments), and filled at the tip with 3% Lucifer Yellow CH dilithium salt (catalog #L0259, Sigma-Aldrich; PubChem substance accession identifier: 24896250) dissolved in 100 mM KCl, yielding DC resistances in the range of 150–300 MΩ. We also used a dextran-tetramethylrhodamine solution (3000 molecular weight, anionic, lysine fixable; catalog #D3308, Thermo Fisher Scientific) and Alexa Fluor 647 hydrazide (catalog #A20502, Thermo Fisher Scientific) for this injection. After removing a small section of the neural sheath and neurilemma, we

inserted electrodes into the DL-dSEG and the mPPL and began recording electrical activity from individual neurons. Electrical signals were amplified with an amplifier (MEZ 8301, Nihon Kohden) and were displayed on an oscilloscope. Data were recorded and analyzed using the data acquisition and analysis software Spike2 (Cambridge Electronic Design; RRID: SCR_000903). After recording electrical activity, we applied a hyperpolarizing current (2–5 nA for 2–10 min) to fill the neurons with Lucifer yellow. Thereafter, the brains were dissected out, fixed in 4% paraformaldehyde for 4 h at room temperature, then rinsed in phosphate buffer solution, dehydrated, and cleared in methyl salicylate for subsequent observation.

To identify vibration-sensitive neurons, we applied a continuous vibration to the right antenna and recorded the responses intracellularly. When a neuron was responsive to the vibration, we applied a continuous vibration at different frequencies. These frequencies included 265 Hz, which is the fundamental frequency of the waggle dance sound. We also applied single vibration pulses and trains of vibration pulses with varying pulse durations and intervals (see below). When the recording became unstable (e.g., fluctuating membrane potential or spike amplitude), we stopped applying the vibration stimuli and injected fluorescence dye into the neuron for morphological analysis.

Sensory stimulation. First, both antennal scapes of each honeybee were fixed to the acrylic chamber with wax. For vibratory stimulation of the JO, the right antenna was inserted into a glass capillary (length, 10 mm; inner diameter of the tip, 200 μm) up to the second segment of the flagellum and then fixed to the tip of the capillary with wax. The opposite tip of the capillary was connected to a piezo-actuator (Miniature Piezo Flexure NanoPositioners, catalog #P780.20, PI Japan). The piezo-actuator was programmed to move with a specific temporal pattern, which was controlled using the Spike2 software. This movement created a vibratory stimulation. We used vibrations with frequencies ranging from 100 to 400 Hz and amplitudes (peak to peak) ranging from 0 to 50 μm and 10 or 20 trains of vibration pulses with the interval ranging from 20 to 100 ms and with the duration ranging from 4 to 50 ms. The recorded neural activities and signals sent to the actuator were simultaneously recorded and stored on a PC.

GABA immunocytochemistry. After identifying the interneurons that had been filled with Lucifer yellow dye, the preparations including our marked target neurons were selected for GABA immunocytochemistry. The preparations were rehydrated through a series of ethanol steps and 0.1 M PBS containing 0.5% Triton X-100 (PBST), pH 7.4. The tissue was then sliced into 100-μm-thick vibratome sections. Next, the sections were incubated in 5% normal goat serum (NGS; catalog #G9023, Sigma-Aldrich) in PBST (PBST-NGS) for 1 h at room temperature to block nonspecific staining and then incubated in primary antiserum, rabbit anti-GABA (1:1000 in PBST-NGS; catalog #A2052, Sigma-Aldrich; RRID:AB_477652), and mouse anti-SYNORF1 (1:1000 in PBST-NGS; DSHB 3C11; RRID:AB_528479) for 3 d at 4°C in a shaking incubator. The anti-GABA was produced using GABA-bovine serum albumin (BSA; catalog #A2153-10G; Sigma-Aldrich) as the immunogen. The antibody was isolated from the antiserum using immunospecific methods of purification. Antigen-specific affinity isolation removes essentially all rabbit serum proteins, including Igs that do not specifically bind to GABA. Rabbit anti-GABA exhibited positive binding with GABA and GABA-keyhole limpet hemocyanin in a dot blot assay, and negative binding with BSA. We used 1 mM GABA to remove all background staining after preadsorption of the primary antibody. The sections were then washed in PBST and incubated in an Alexa Fluor 647-conjugated goat anti-rabbit IgG antibody (1:1000 in PBST-NGS; catalog #A11034, Thermo Fisher Scientific; RRID:AB_2576217) and an Alexa Fluor 555 goat anti-mouse IgG antibody (1:1000 in PBST-NGS; catalog #A21424, Thermo Fisher Scientific; RRID:AB_141780) overnight at 4°C. As controls, some preparations were processed without the anti-GABA antibody. Finally, after washing, the sections were mounted on slide glasses using VECTASHIELD (catalog #H-1000, Vector Laboratories; RRID:AB_2336789).

Confocal microscopy. The cleared specimens containing intracellularly stained neurons were viewed from the posterior side of the brain under a confocal laser-scanning microscope (LSM 510, Carl Zeiss) with a Zeiss Plan-Apochromat 25×/numerical aperture (NA) 0.8 oil lens objective

Table 1. List of PAC interneurons

Category	Group name	Neuron name	Arborized neuropils	Response pattern to continuous vibration	N_{total}	N_{ana}
Local interneurons	DL-Int-1	DL-Int-1	DL, dSEG, mPPL	On-off phasic E and tonic I	36	14
	DL-dSEG-mPPL	DL-dSEG-mPPL1	DL, dSEG, mPPL	Tonic I	17	6
		DL-dSEG-mPPL2		Tonic E	3	2
		DL-dSEG-mPPL3		On-phasic E	3	0
		DL-dSEG-mPPL4		On-phasic I	1	0
		DL-dSEG-mPPL5		No response	3	0
	DL-dSEG	DL-dSEG	DL, dSEG	Tonic I	5	2
	DL-mPPL	DL-mPPL	DL, mPPL	Tonic E	1	1
	DL-local	DL-local1	DL	Tonic E	3	3
		DL-local2		Tonic I	1	1
Output neurons	DL-Int-2	DL-Int-2	DL, dSEG, LP, cPPL	On phasic E or tonic E	14	5
	DL-LP	DL-LP	DL, LP	Tonic I	6	1
	DL-dSEG-LP	DL-dSEG-LP1	DL, dSEG, LP	Tonic I	3	2
		DL-dSEG-LP2		On-phasic E	2	0
		DL-dSEG-LP3		No response	1	0
	DL-whole PPL	DL-whole PPL1	DL, whole PPL	On-phasic I	2	0
		DL-whole PPL2		On-phasic E	1	0
		DL-whole PPL3		Tonic E	1	0
Bilateral neurons	Bilateral DL-dSEG-LP	Bilateral DL-dSEG-LP	DL, dSEG, LP	On-phasic E	12	8
	Bilateral DL-dSEG-mPPL	Bilateral DL-dSEG-mPPL	DL, dSEG, mPPL	Phasic tonic E	1	1
	Bilateral DL-dSEG-PPL	Bilateral DL-dSEG-PPL	DL, dSEG, PPL	Tonic E	1	1
	Bilateral mPPL-LP	Bilateral mPPL-LP	mPPL, LP	Tonic I	2	1

N_{total}, Number of preparations of PAC neurons responding to vibration stimuli; N_{ana}, Number of preparations with sufficient response data used for analysis; E, excitation; I, inhibition; cPPL, central posterior protocerebral lobe.

(working distance, 0.57 mm) for low-magnification images or with a Zeiss Plan-Apochromat 40×/NA 1.4 oil lens objective (working distance, 0.13 mm) for high-magnification images. Alexa Fluor 555 and Alexa Fluor 647 were excited by the 543 and 633 nm spectral lines of an HeNe laser, respectively, while Lucifer yellow was excited by the 488 nm spectral line of an argon laser. Optical sections were made at 3 μm (in low-magnification images) or 1.5 μm (in high-magnification images) throughout the entire depth of each specimen. The image resolution was 1024 × 1024 pixels.

Nomenclature. We use the terms proposed by Mobbs (1982) and Milde (1988) to describe the neuropilar regions in the SEG of the honeybee brain. The orientation of neuronal structures is given according to the body axis.

Experimental design and statistical analysis. To evaluate the significant responses induced by vibration of the antenna, we calculated time-resolved spike frequency rates before (0.5 s before the onset of each train), during, and after the stimulation, and statistically analyzed the differences between the responses (Wilcoxon signed rank test) using the software R version 3.4.0 (RRID:SCR_001905). To characterize the responses to different temporal patterns of pulse stimulation, we calculated the spike numbers, spike frequency, latency of the first spike, EPSPs, and IPSPs after the pulse stimulus for different pulse durations and intervals, and statistically analyzed the differences (Wilcoxon signed rank test). The criterion for all statistical tests was $p < 0.01$.

Modeling and simulation. Membrane potentials of DL-Int-1 and DL-Int-2 neurons were modeled using the Adaptive Exponential Integrate-and-Fire (AdExp) model (Brette and Gerstner, 2005; Fig. 8-1 available at https://doi.org/10.1523/JNEUROSCI.0044-17.2017.f8-1). Membrane potential calculations included synaptic input currents, which were calculated from synaptic conductances. Synaptic conductances were simulated using difference-of-exponentials functions (Fig. 8-1C available at https://doi.org/10.1523/JNEUROSCI.0044-17.2017.f8-1), based on the Exp2Syn model of the simulator NEURON (Carnevale and Hines, 2006; RRID:SCR_005393). Neuron and synapse parameters were adjusted to qualitatively reproduce the response properties of DL-Int-1 and DL-Int-2 neurons as determined in our electrophysiological experiments (Fig. 8-1B,D available at https://doi.org/10.1523/JNEUROSCI.0044-17.2017.f8-1). The network of DL-Int-1 and DL-Int-2 neurons was implemented using the simulator Brian version 2.0.1 (Stimberg et al., 2014; RRID:SCR_002998) in Python. The code is available at https://web.gin.g-node.org/ajkumaraswamy/HB-PAC_disinhibitory_network (doi: 10.12751/g-node.1090f8). An integration step size of 0.1 ms was used,

and all simulation runs had a "settling time" of 600 ms, after which stimuli were applied. Network inputs were modeled as spikes from JO sensory neurons spiking at the positive peak of the sinusoidal antennal vibration stimulus. Like the stimuli in our experiments, model stimuli were continuous sinusoidal vibrations with a frequency of 265 Hz and trains of sinusoidal pulses of 265 Hz vibrations with 16 ms pulse durations and 33 ms interpulse intervals (IPIs), values close to those observed in the honeybee waggle dance. In addition, pulse trains with 100 ms IPIs were used in the simulations to investigate the model results for longer pulse intervals, as used in the experiments.

Results

Categories of vibration pulse-sensitive interneurons arborizing in the PAC

We identified 119 vibration-sensitive interneurons arborizing in the PAC, DL, dSEG, and/or mPPL (Table 1). Of those, DL-Int-1 and DL-Int-2 neurons have been described previously (Ai et al., 2009), but the results reported here were obtained from neurons collected exclusively for the present study. We categorized the interneurons based on their arborization and on their response patterns to continuous vibration. Based on their general arborizing features, they were classified into the following three categories: PAC local interneurons, PAC output neurons, and PAC bilateral neurons.

PAC local interneurons
PAC interneurons had arborizations mainly inside the PAC (i.e., in the DL, dSEG, and/or mPPL). Based on arborization patterns, we identified five groups of neurons. These were further divided into subgroups based on response patterns (Table 1). Neurons in the largest group, DL-Int-1, showed arborizations in the DL, dSEG, and mPPL, and showed on-off phasic excitation and tonic inhibition to continuous vibration stimuli applied to the ipsilateral antenna. While DL-dSEG-mPPL neurons arborized in the same neuropils as DL-Int-1 neurons, individual DL-dSEG-mPPL neurons showed different response patterns to vibration stimuli, such as tonic inhibition, tonic excitation, on-phasic excitation, on-off phasic inhibition, or no response (Table 1). We found several other minor neuron groups in this category that arborized
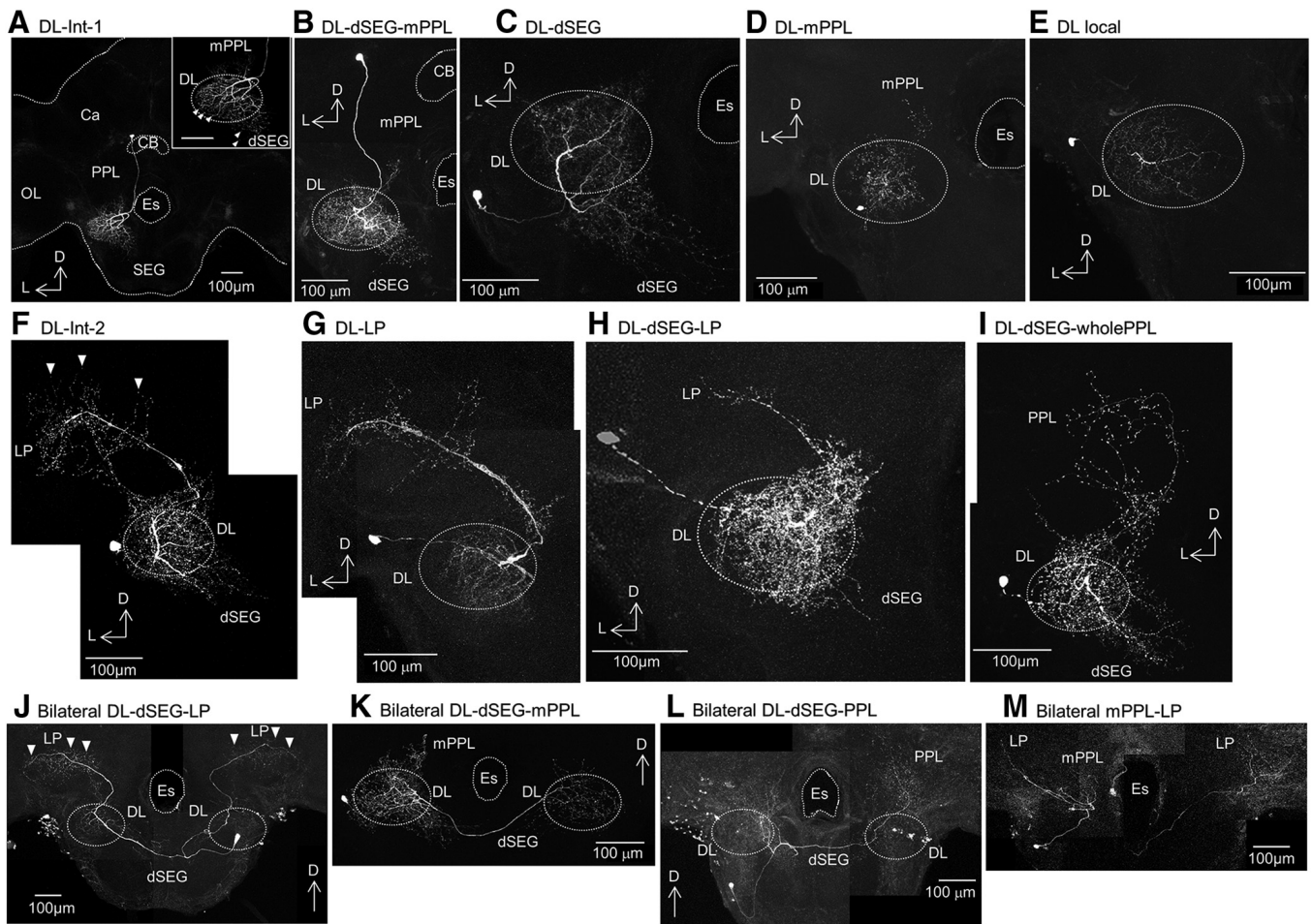
Figure 1. Morphology of PAC interneurons. Stained examples of the different neuron types investigated in this study (Table 1). *A–E,* Local interneurons arborized in the PAC neuropils DL, dSEG, and mPPL. *A,* DL-Int-1. This neuron type has dense arborizations in the DL and dSEG with fine spines and boutons (arrowhead), while in the medial PPL it has fine spines. The inset shows a magnification of the DL region. *B–E,* Four neuron types were named DL-dSEG-mPPL, DL-dSEG, DL-mPPL, and DL local according to the neuropils of arborization. *F–I,* Output neurons arborized in the PAC. Output neurons have dendritic arborizations in the PAC neuropils, DL, and/or dSEG, and axon terminals in the LP and/or PPL. *F,* DL-Int-2 has a soma in the lateral cell cluster of the DL and arborizes with fine spines in the DL and dSEG, and with boutons in the LP (arrowheads). *G–I,* Three neuron types named DL-LP, DL-dSEG-LP, and DL-dSEG-wholePPL according to the neuropils of arborization. *J–M,* Bilateral neurons arborized in the PAC. Bilateral neurons have dendritic arborization in the bilateral PAC, DL, dSEG, or mPPL. *J,* Bilateral DL-dSEG-LP neurons have symmetrical arborization in both the DL and LP. This neuron type has a spine branch in the DL-dSEG and terminals with boutons in the LP (arrowheads). *K–M,* Three neuron types named bilateral DL-dSEG-mPPL, bilateral DL-dSEG-PPL, and bilateral mPPL-LP according to the neuropils of arborization.

in different neuropils in the PAC (DL-dSEG, DL-mPPL, and DL local).

PAC output neurons
PAC output neurons had arborizations in the primary auditory center and sent their axons into the other neuropils of the PAC. Four groups were identified. Neurons in the main group, DL-Int-2, had arborizations in the DL and dSEG and sent their axons to the secondary auditory center, the LP. They showed excitatory responses to continuous vibration stimuli applied to the ipsilateral antenna. Moreover, we found several other minor neuron groups in this category (DL-LP, DL-dSEG-LP, and DL-whole PPL; Table 1).

PAC bilateral neurons
PAC bilateral neurons had arborizations in the PACs of both hemispheres and also sent their axons to the other neuropils in the PAC. Four groups were identified. Neurons in the main group, termed the bilateral DL-dSEG-LP, were newly identified in this study. These neurons had arborizations in both the DL and dSEG and sent their axons to both LPs. They showed on-phasic excitation to continuous vibration stimuli applied to the ipsilateral antenna. We found several other minor neuron groups in

this category (bilateral DL-dSEG-mPPL, bilateral DL-dSEG-PPL, and bilateral mPPL-LP; Table 1).

Categories of vibration pulse-sensitive interneurons arborizing in the PAC
In 48 of the 119 preparations, the recording was stable for sufficiently long to apply a number of stimulation pulses with different combinations of vibration frequency, pulse duration, and pulse intervals. The data from those 48 neurons were used for further analysis. Of those, 27 neurons were from one of the main groups, DL-Int-1, DL-Int-2, or bilateral DL-dSEG-LP. We focused on these neurons for our analysis. While we report findings for neurons from the other groups as well, in many cases, only one or two examples of these interneurons were recorded (Table 1).

Morphologies of PAC interneurons
The main PAC local interneurons, termed DL-Int-1 and DL-dSEG-mPPL (Fig. 1 A, B), connected the following neuropils in the PAC: the DL, the dSEG, and the mPPL. DL-Int-1 neurons had two branches. One branch arborized with fine terminals in the mPPL. The other branch arborized with fine terminals as well as
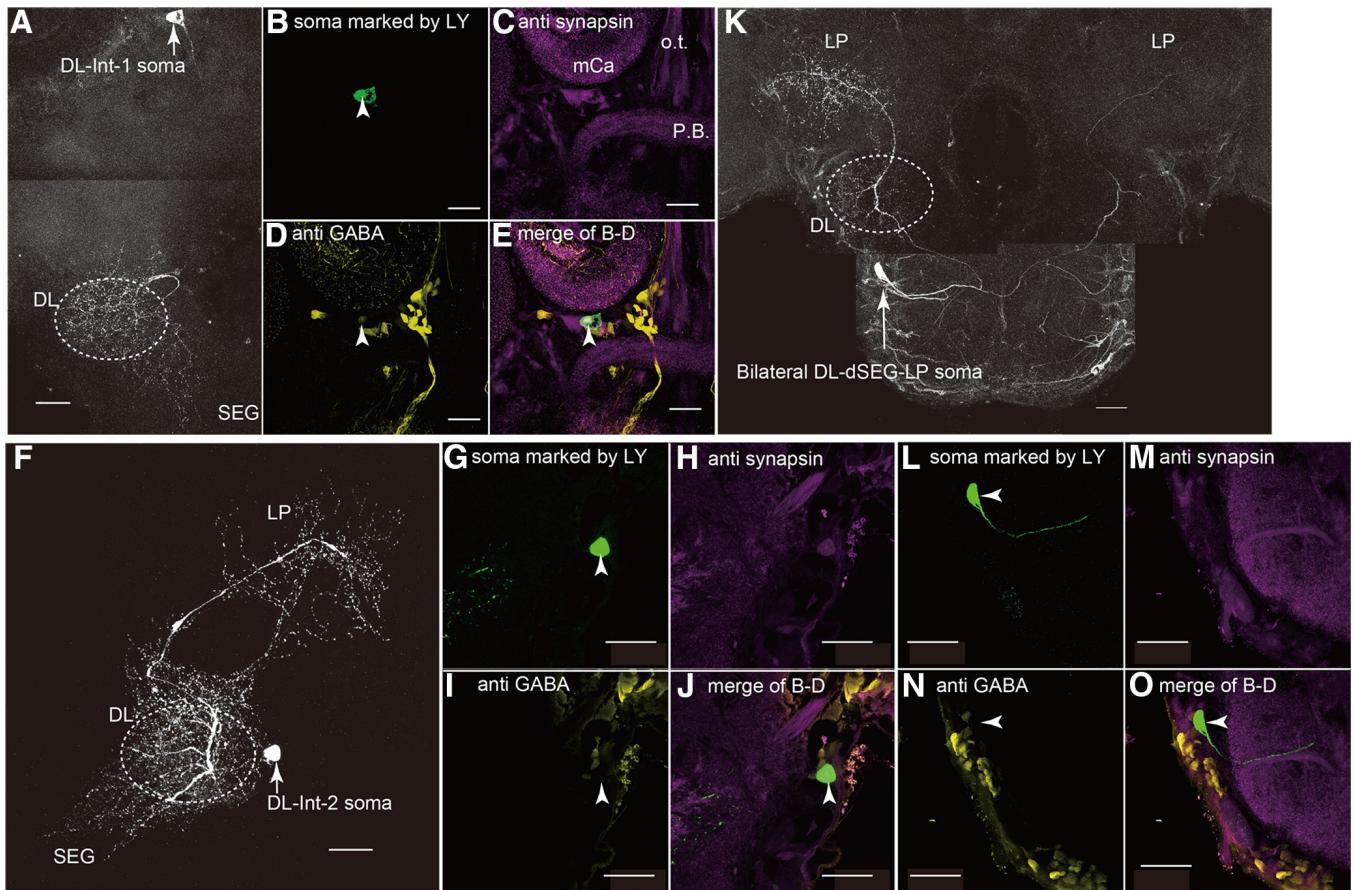
Figure 2. GABA immunoreactivity of PAC interneurons. Immunohistochemically stained examples of DL-Int-1, DL-Int-2, and bilateral DL-dSEG-LP neurons. *A*, Whole morphology of the DL-Int-1 neuron (preparation HB130822-1). *B–E*, GABA immunoreactivity of DL-Int-1; the same optical section is visualized using different staining techniques. *B*, Image of LY-injected soma of DL-Int-1 neuron. *C*, Anti-synapsin labeling. *D*, Anti-GABA labeling. *E*, Merged images of *B–D*. Arrows indicate the position of the DL-Int-1 soma. An anti-GABA-labeled spot coincides with the soma, suggesting that the DL-Int-1 is GABAergic. mCa, Medial calyx; o.t., ocellar tract; P.B., protocerebral bridge. *F*, Whole morphology of DL-Int-2 (preparation 131217-2). *G–J*, GABA immunoreactivity of DL-Int-2; the same optical section is visualized using different staining techniques. *G*, DL-Int-2 soma. *H*, Anti-Synapsin labeling. *I*, Anti-GABA labeling. *J*, Merged images of *G–I*. The DL-Int-2 soma location (arrow in *G* and *I*) does not overlap with GABA immunoreactivity, suggesting DL-Int-2 is not GABAergic. *K*, Whole morphology of a bilateral DL-dSEG-LP neuron (preparation 130612-3). *L–O*, GABA immunoreactivity of bilateral DL-dSEG-LP; the same optical section is visualized using different staining techniques. *L*, Bilateral DL-dSEG-LP soma. *M*, Anti-Synapsin labeling. *N*, Anti-GABA labeling. *O*, Merged images of *L–N*. The bilateral DL-dSEG-LP soma does not overlap with GABA immunoreactivity, suggesting that the bilateral DL-dSEG-LP is not GABAergic.

boutons in the DL and dSEG (Fig. 1*A*, inset). DL-dSEG-mPPL neurons had a similar arborization pattern. The somata of DL-Int-1 neurons were located dorsally from the central body, while the somata of DL-dSEG-mPPL neurons were located more laterally (Fig. 1*A*,*B*). The other local interneurons arborized in subsets of the PAC neuropils. DL-dSEG neurons had arborizations in the DL and dSEG but not in the mPPL. DL-mPPL neurons had arborizations in the DL and mPPL but not in the dSEG. DL-local neurons arborized inside the DL (Fig. 1*C*–*E*).

The PAC output neurons sent axons from the PAC to the other neuropils, mainly LP and PPL (Fig. 1*F*–*I*). All of the soma positions were located in the lateral DL. DL-Int-2 neurons had dense arborization in the DL-dSEG, with fine spines, and sparse and diverse arborization in the LP with boutons (Fig. 1*F*).

PAC bilateral neurons had dendritic arborizations in a PAC neuropil (either DL or mPPL) and sent processes to both hemispheres of the brain. Most of these neurons had arborizations in the DL, while two of them had arborizations in the mPPL, but not in the DL (Table 1). The neurons in this group arborized in the DL, dSEG, LP, and PPL. Most of these neurons were categorized as bilateral DL-dSEG-LP. Bilateral DL-dSEG-LP neurons had symmetrical arborizations in the DLs and LPs of both hemispheres, with fine spines in the DL and sparse and diverse ar-

borization in the LP, as well as boutons (Fig. 1*J*). We also found several other minor groups with different arborization patterns in this category (bilateral DL-dSEG-mPPL, bilateral DL-dSEG-PPL, and bilateral mPPL-LP; Fig. 1*K*–*M*).

GABA-immunohistochemistry of PAC interneurons
We performed GABA immunohistochemical experiments with the PAC interneuron preparations (Fig. 2). The soma of each DL-Int-1 neuron was clearly visible in the dorsoposterior protocerebrum (Fig. 2*A*), and the locations of these neurons coincided with a GABA-immunoreactive spot, indicating that DL-Int-1 neurons are anti-GABA positive (Fig. 2*B*–*E*). In contrast, the soma locations of DL-Int-2 (Fig. 2*F*–*J*) and bilateral DL-dSEG-LP neurons (Fig. 2*K*–*O*) did not overlap with a GABA-immunoreactive spot, indicating that DL-Int-2 and bilateral DL-dSEG-LP neurons are not anti-GABA positive.

Responses of PAC interneurons to trains of vibration pulses
Neurons of one of the major PAC local interneuron types, DL-Int-1, exhibited spontaneous activity, with rates ranging between 0 and 80 Hz, depending on the preparation (Ai et al., 2009). When a train of vibration pulses was applied to the antenna, DL-Int-1 neurons showed tonic inhibition (Fig. 3*A*): The spike rate was suppressed
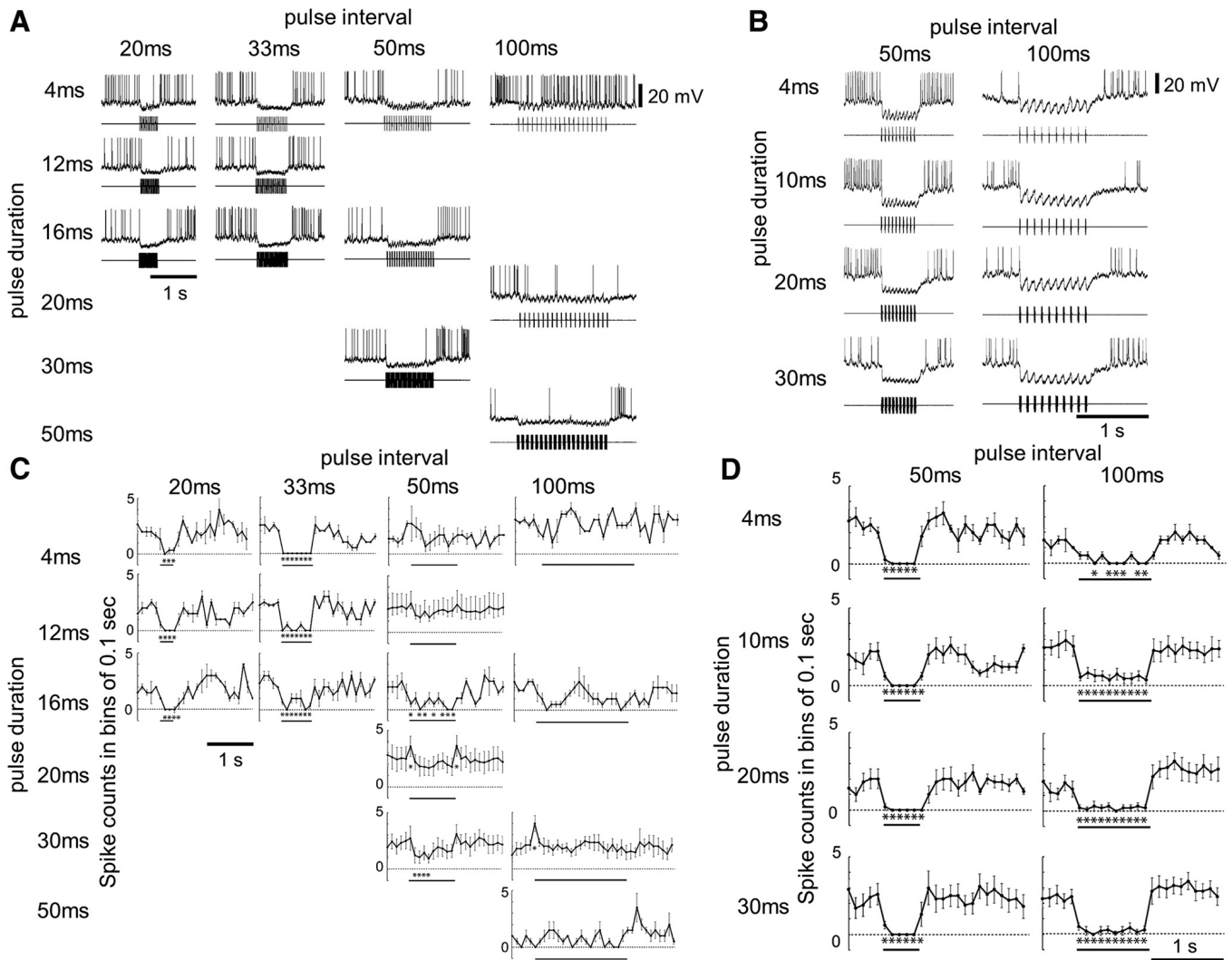
Figure 3. Responses of DL-Int-1 and DL-dSEG-mPPL neurons to trains of vibration pulses. Each of the records in **A** and **B** presents the data obtained from one animal. **A, B**, Single responses of two example neurons (preparations HB141121-1AL and HB130226-1Rh) to pulse stimuli applied to the antenna with different temporal patterns. Pulse durations were varied between 4 and 50 ms, and pulse intervals were varied between 20 and 100 ms. The carrier frequency of the pulse vibration was 265 Hz. DL-Int-1 neurons showed tonic inhibitory responses for shorter pulse durations (<50 ms), while DL-dSEG-mPPL neurons showed this response as well as a response to pulses with a longer pulse duration (100 ms). **C, D**, Instantaneous spike frequencies (spike counts in bins of 0.1 s) of DL-Int-1 (**C**) and DL-dSEG-mPPL neurons (**D**; $N = 7$). The horizontal bars indicate the duration of a train of pulses. Asterisks indicate statistical differences with the spontaneous activity in the 1 s interval before each record (*$p < 0.01$). DL-Int-1 neurons respond with a tonic inhibitory response to trains of pulses with a pulse interval up to 33 ms, while in DL-dSEG-mPPL neurons we also observed tonic inhibition for longer pulse durations, such as 100 ms. [Note that, owing to experimental conditions, responses to stimulation with shorter pulse durations (20 and 33 ms) were not recorded for DL-dSEG-mPPL neurons].

below the spontaneous level, and spikes were typically not observed during stimulation. We only observed intermittent spikes during trains of vibration pulses for pulse trains with long IPIs of 100 ms, which is far above the 14–30 ms IPI observed during the waggle dance. Statistical analysis revealed that spike rates significantly decreased during stimulation for pulse durations up to 16 ms and pulse intervals up to 33 ms (Wilcoxon signed rank test, $n = 14$; Fig. 3C).

Similar to DL-Int-1 neurons, DL-dSEG-mPPL neurons showed tonic inhibitory responses to trains of pulses. These responses were more pronounced for long-pulse intervals of 100 ms (Fig. 3B). Statistical analysis revealed that spike rates significantly decreased during stimulation for pulse intervals of ≥50 ms (Wilcoxon signed rank test, $n = 6$; Fig. 3D). It is not clear whether this tonic inhibition also occurs for pulse intervals <50 ms because data could not be obtained for these stimuli.

In contrast to DL-Int-1 and DL-dSEG-mPPL neurons, excitatory responses were observed in DL-Int-2 neurons (Fig. 4A). Specifically, the temporal response profiles of DL-Int-2 neurons showed remarkable on-phasic excitation up to rates of >70 Hz, as well as tonic excitatory responses to trains of pulses with durations of 16 ms and pulse intervals of 33 ms (Wilcoxon signed rank test, $n = 5$; Fig. 4B). Bilateral DL-dSEG-LP neurons also showed excitatory responses to trains of vibration pulses. In these neurons, each pulse onset elicited a single spike or EPSP, regardless of pulse duration and IPI (Fig. 5).

Response profiles of PAC neurons in response to a single pulse

To evaluate the response characteristics of PAC neurons, we analyzed the temporal response patterns induced by single pulses of different durations. We compared the spike counts, spike rates, and latencies of the first spikes of DL-Int-1 (Fig. 6A–E), DL-Int-2 (Fig. 6F–I), and bilateral DL-dSEG-LP neurons (Fig. 6J,K) evoked by single pulses with different pulse durations. The number of DL-Int-1 spikes elicited by a single vibration pulse gradually increased with the pulse duration up to 20 ms, and was saturated for pulse durations >20 ms (1.1 ± 0.6 at a pulse dura-
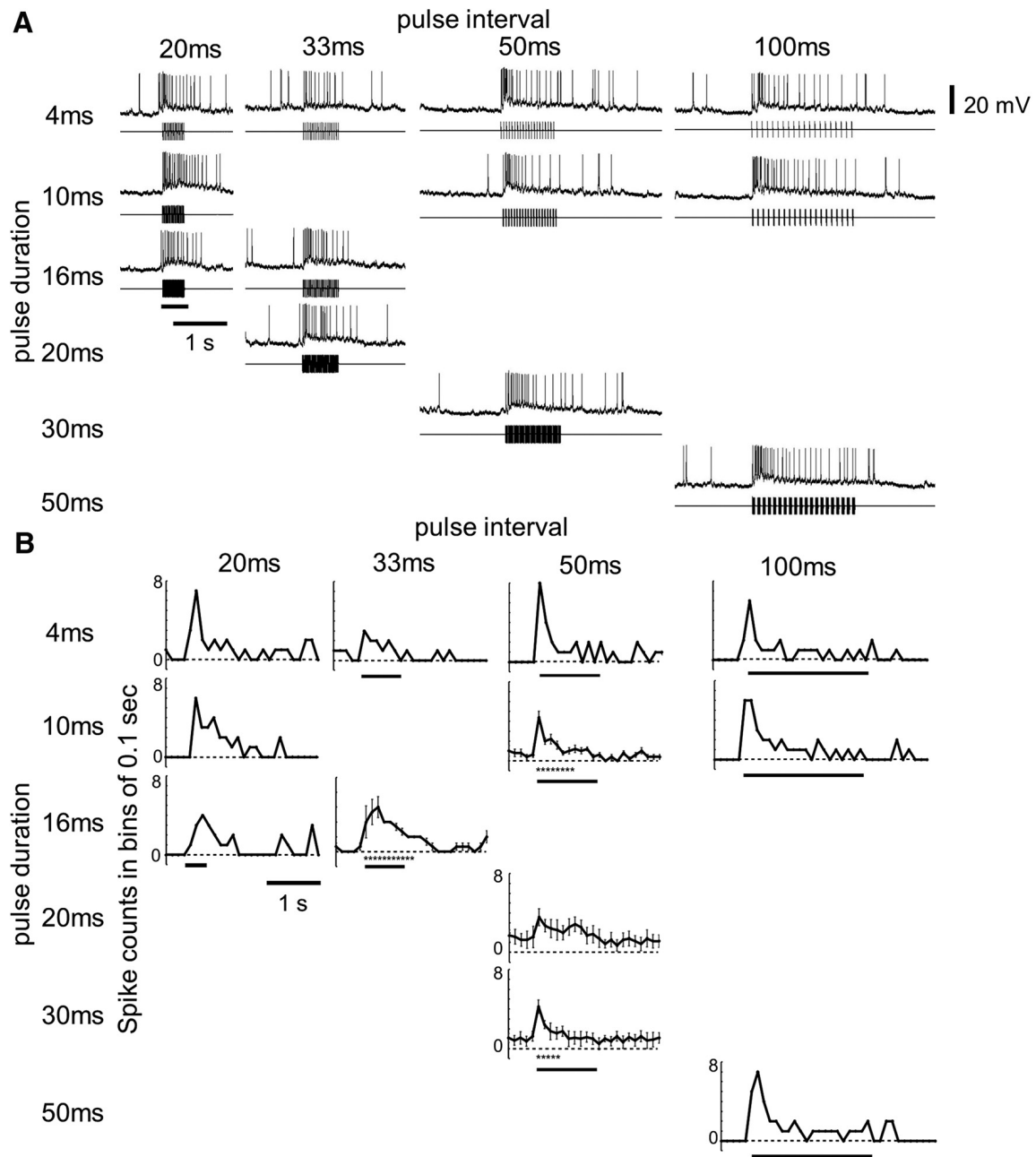
Figure 4. Responses of DL-Int-2 neurons to trains of vibration pulses. ***A***, Single responses of an example neuron to pulse train stimuli applied to the antenna with different temporal patterns (preparation HB140605-2Rh). All records present the data obtained in one animal. DL-Int-2 neurons showed tonic excitatory responses during trains of vibratory pulses with different temporal patterns. ***B***, Instantaneous spike frequencies of DL-Int-2 neurons before, during, and after the train of pulses (*N* = 6). The bin size was 0.1 s. The horizontal bars indicate the duration of a train of pulses. Asterisks indicate statistical differences compared with the spontaneous activity collected just before each record (**p* < 0.01). DL-Int-2 neurons responded with a tonic excitatory response to a train of pulses with a duration of 16 ms and interval of 33 ms. [Note that owing to experimental conditions, responses to stimulation with shorter (20 ms) and longer (100 ms) pulse intervals and with shorter (4 ms) pulse durations were recorded in only one preparation for DL-Int-2.]

tion of 4 ms and 2.8 ± 1.0 at pulse durations of 20, 30, and 50 ms, Fig. 6*B*; Wilcoxon signed rank test, *n* = 46). However, for values of >10 ms, the average spike rate for the phasic spikes gradually decreased as the pulse duration increased (180 ± 26 Hz at 10 ms pulse duration and 134 ± 53 Hz at 50 ms pulse duration; Fig. 6*C*; Wilcoxon signed rank test, *n* = 67), indicating the presence of tonic inhibition during the pulse stimulation. The latency of the first DL-Int-1 neuron spike after the onset of a single pulse (Fig. 6*A*) was constant, independent of pulse duration, for pulses <50 ms (7.5 ± 1.4 ms; Fig. 6*D*; Wilcoxon signed rank test, *n* = 34). The latency of the first spike after the offset of a single pulse was also constant, independent of pulse duration, for pulses of <50 ms

(57 ± 14 ms; Fig. 6*E*; Wilcoxon signed rank test, *n* = 34). For DL-Int-2 neurons, the number of spikes was significantly different for pulse durations of 4 versus 10 ms and was saturated for values of >10 ms (1.4 ± 1.0 at a pulse duration of 4 ms and 2.8 ± 0.5 for pulse durations of >10 ms; Fig. 6*G*; Wilcoxon signed rank test, *n* = 18), while spike rates and spike latency were constant independent of pulse duration (Fig. 6*F,H,I*; 107 ± 19 Hz spike frequency and 9.3 ± 1.7 ms for the latency of the first spike for DL-Int-2 neuron, Wilcoxon signed rank test, *n* = 49). The latencies of the EPSPs of bilateral DL-dSEG-LP neurons were also constant, independent of the pulse duration (5.2 ± 1.2 ms, Wilcoxon signed rank test; Fig. 6*J,K*).
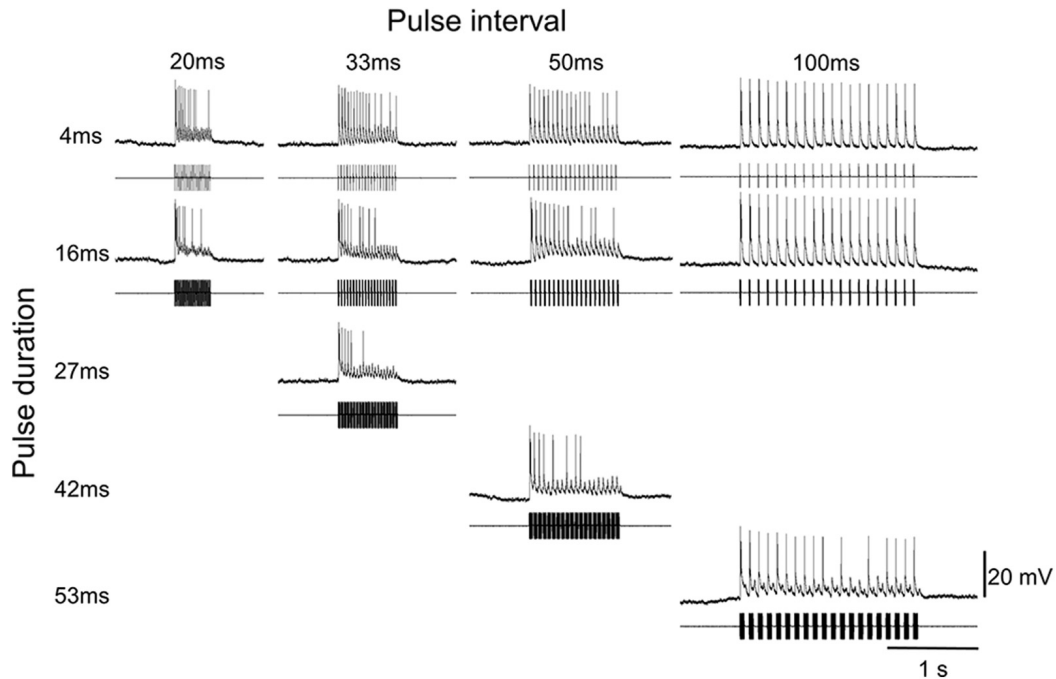
Figure 5. Responses of the bilateral DL-dSEG-LP neuron to trains of vibration pulses. Single responses of an example neuron to pulse train stimuli applied to the antenna with different temporal patterns (preparation HB140522-1AL). All records present the data obtained from the same neuron in one animal. This neuron type does not show spontaneous activity, but in response to pulse stimuli reliably shows EPSPs or spikes. Spikes or EPSPs were phase locked to the vibration pulses, even if the temporal pattern of stimuli changed (Fig. 7 H,I).
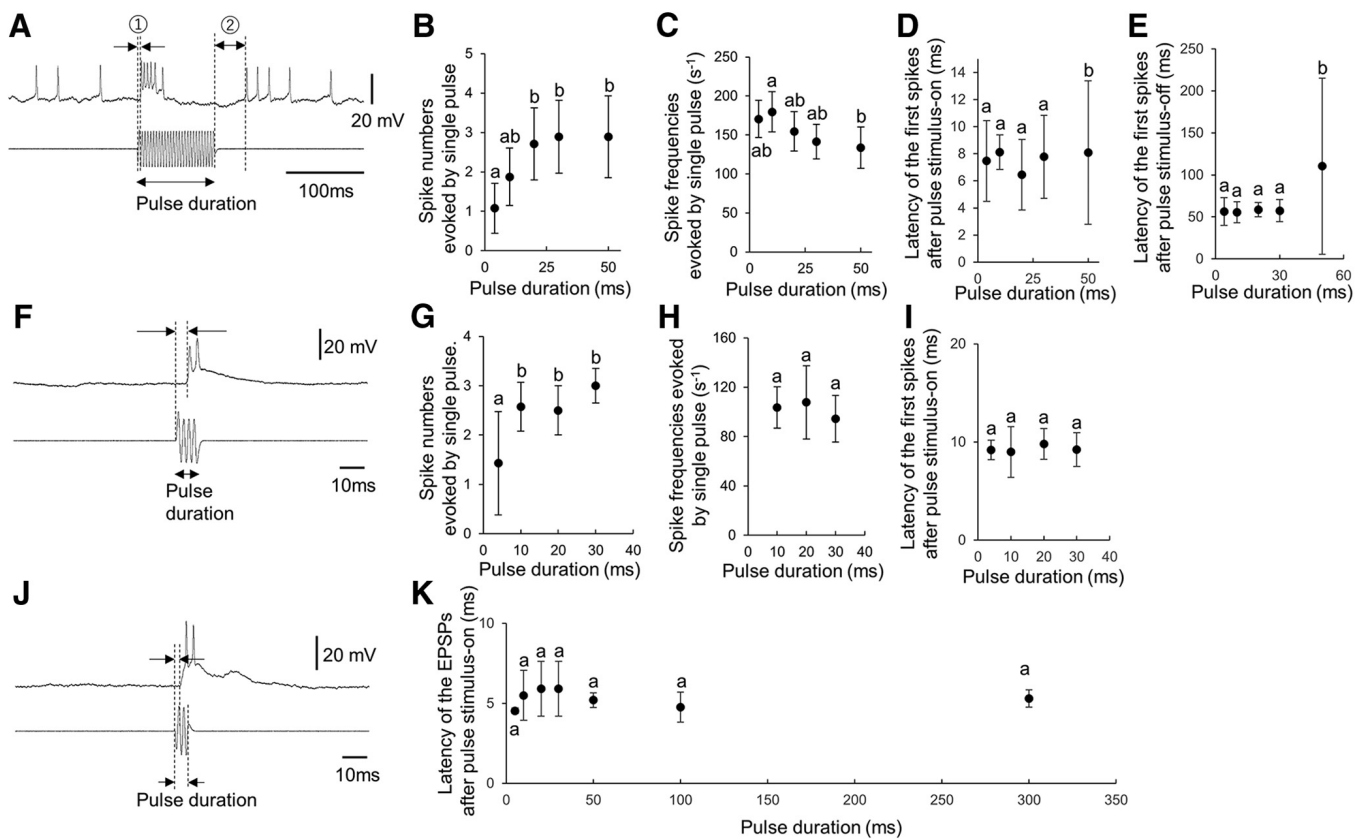

Figure 6. Characteristics of responses evoked by single pulses (A–E, DL-Int-1; F–I, DL-Int-2; J, K, bilateral DL-dSEG-LP). A, Example of the on-off phasic excitation of DL-Int-1 neuron to a single pulse with a duration 100 ms. Latencies of the spike after onset and offset of the pulse stimulus are indicated by ① and by ②, respectively. B, C, number (B) and frequency (C) of spikes evoked by a vibration pulse. Within each plot, different letters (a, b) indicate significant differences between values. D, E, Latencies of the spikes after stimulus-on (D) and stimulus-off (E) are not significantly different for the different pulse durations. F, Example of the response of DL-Int-2 neuron to a single pulse with a duration of 10 ms. The latency of the spike after pulse stimulus-on is indicated by the time lag between the two vertical dashed lines. G, H, Spike number (G) and spike frequency (H) evoked by single pulses with different durations. I, the latencies after pulse stimulus-on were not significantly different for different pulse durations. J, Example of the response of a bilateral DL-dSEG-LP neuron to a single pulse with a duration of 10 ms. The latency of the spike after pulse stimulus-on is indicated by the time lag between the two vertical dashed lines. K, The EPSP or spike latencies after pulse onset. Latencies were not significantly different for different pulse durations.
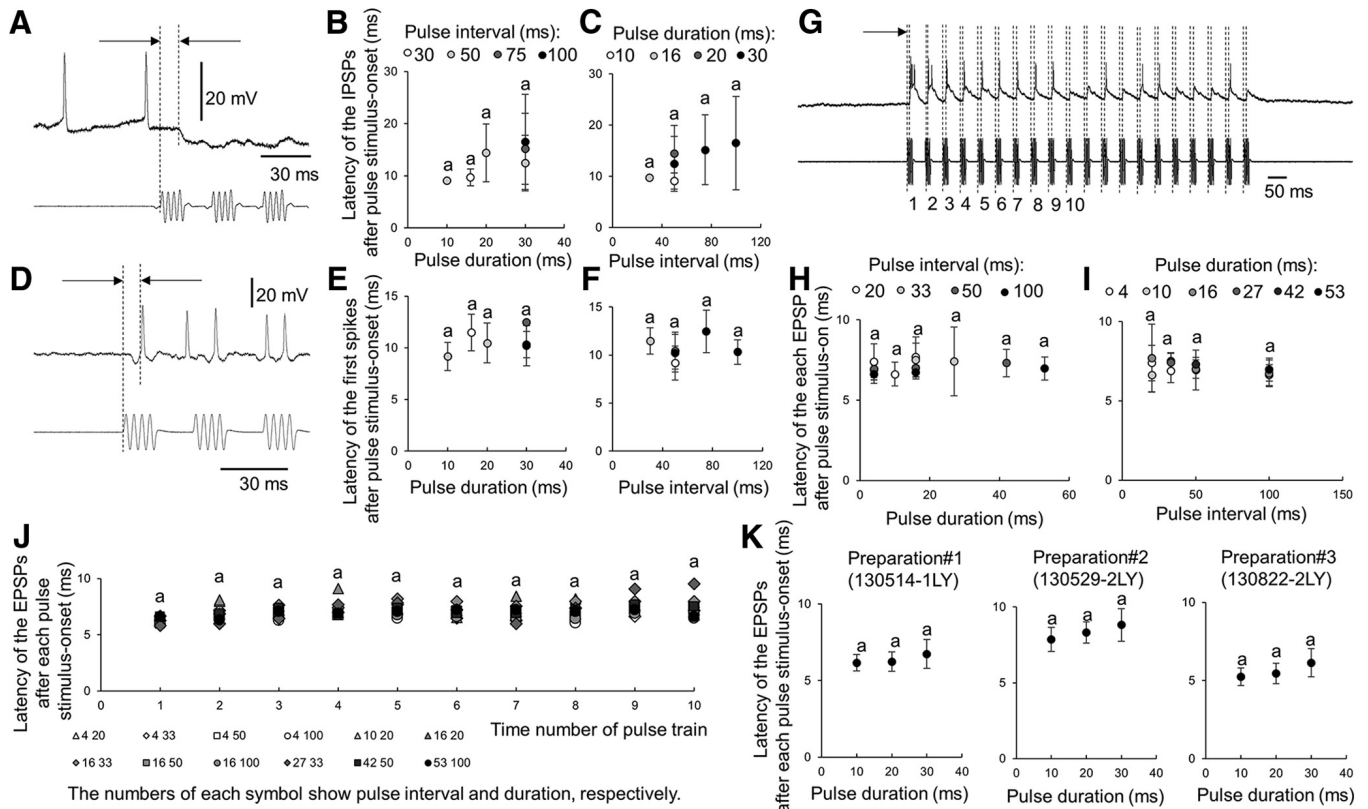
Figure 7. *A–K*, Response characteristics evoked by pulse trains (*A–C*, DL-Int-1; *D–F*, DL-Int-2; *G–K*, bilateral DL-dSEG-LP neurons). *A*, Example of the first IPSP of the DL-Int-1 neuron evoked by a train of 15 ms pulses. The latency of the IPSP is indicated by the time lag between the two vertical dashed lines. *B*, *C*, The mean latencies of the IPSPs over recordings from different preparations were not significantly different for different pulse durations (*B*) or pulse intervals (*C*). *D*, Example of the first spike of a DL-Int-2 neuron induced by a train of 15 ms pulses. The latency of the first spike is indicated by the time lag between the two vertical dashed lines. *E*, *F*, latencies were not significantly different for different pulse durations (*E*) or pulse intervals (*F*). *G*, Example of the response of a bilateral DL-dSEG-LP neuron to a train of 20 ms pulses. The latencies of the EPSPs after the pulse stimulus-on is indicated by the pairs of vertical dashed lines. *H*, *I*, The latencies of the EPSPs after pulse stimulus-on were not significantly different for different pulse durations (*H*) or intervals (*I*). *J*, latencies of the EPSPs after each pulse stimulus-on in a train of pulses (no significant differences). *K*, EPSP latencies of three different neurons for different pulse durations (no significant differences).

Response profiles of PAC neurons in response to pulse trains
For stimulation with trains of vibration pulses, the latencies of the first IPSPs of DL-Int-1 neurons (Fig. 7*A*) were constant (13.3 ± 6.3 ms), independent of either pulse duration (Fig. 7*B*; Wilcoxon signed rank test, $n = 35$) or pulse interval (Fig. 7*C*; Wilcoxon signed rank test, $n = 35$). The first spike latencies of DL-Int-2 neurons (Fig. 7*D*) were also constant, independent of pulse duration (10.4 ± 2.0 ms; Fig. 7*E*; Wilcoxon signed rank test, $n = 35$) or pulse interval (Fig. 7*F*; Wilcoxon signed rank test, $n = 35$). Bilateral DL-dSEG-LP neurons showed no spontaneous activity, but trains of vibration pulses applied to the antenna reliably elicited spikes or EPSPs during the pulsed vibration (Fig. 7*G*). The spikes or EPSPs corresponded in a one-to-one fashion to the vibration pulses and followed the pulses even if the temporal pattern of the stimulus changed. This indicates that bilateral DL-dSEG-LP neurons generate phase-locked spikes or EPSPs in response to trains of vibration pulses. EPSP latencies during a train of pulses were constant (20 pulse trains for each, $n = 5$), independent of pulse duration (Fig. 7*H*; Wilcoxon signed rank test, $n = 20$), pulse interval (Fig. 7*I*; Wilcoxon signed rank test, $n = 20$), or the number of pulses in the train (Fig. 7*J*; Wilcoxon signed rank test, $n = 10$). However, these latencies showed slight variations depending on individual preparations (6.4 ± 0.8 ms for preparation 130514–1LY; 8.3 ± 1.0 ms for preparation 130529–2LY; 5.6 ± 0.8 ms for preparation 130822–2LY; Fig. 7*K*; $p < 0.01$, Wilcoxon-signed rank test; 10 pulses for each individual).

Model of inhibitory network in the PAC
The projection patterns of DL-Int-1 and DL-Int-2 (Fig. 8*A*) along with their immunocytochemistry (Fig. 2) and response properties, including their relative onset latencies to single-pulse stimulations (Fig. 7*A,D,F,I*), suggest a network with inhibitory connections from DL-Int-1 to DL-Int-2. (Fig. 8*B,C*). The observed response properties of DL-Int-2, with tonic excitation decreasing for increasing pulse intervals, could be a result of disinhibition due to the decreasing tonic inhibition of DL-Int-1 (Fig. 8*D*). To test the plausibility of such a network in the PAC, we implemented a model of DL-Int-1 and DL-Int-2 neurons in a circuitry with corresponding excitatory and inhibitory connections (Fig. 8*C*) and investigated its responses to continuous and pulse train sinusoidal stimuli at waggle dance frequency (265 Hz).

When continuous vibration stimuli were used, model DL-Int-1 neurons in the network showed phasic excitation in response to vibration onset, followed by spikeless tonic inhibition (data not shown), in accordance with known properties of DL-Int-1 neurons (Ai et al., 2009). When the network was stimulated with vibration pulses with pulse intervals ∼30 ms, similar to waggle dance vibration pulses, model DL-Int-1 neurons exhibited no spikes during stimulation and weak rebound spikes after stimulation offset (Fig. 8*E*). When vibration pulses were separated by longer pulse intervals ∼100 ms, intermediate spikes occurred during stimulation pulses (Fig. 8*E*), similar to what was observed experimentally (Fig. 8*D*). Model DL-Int-2 neurons showed on-
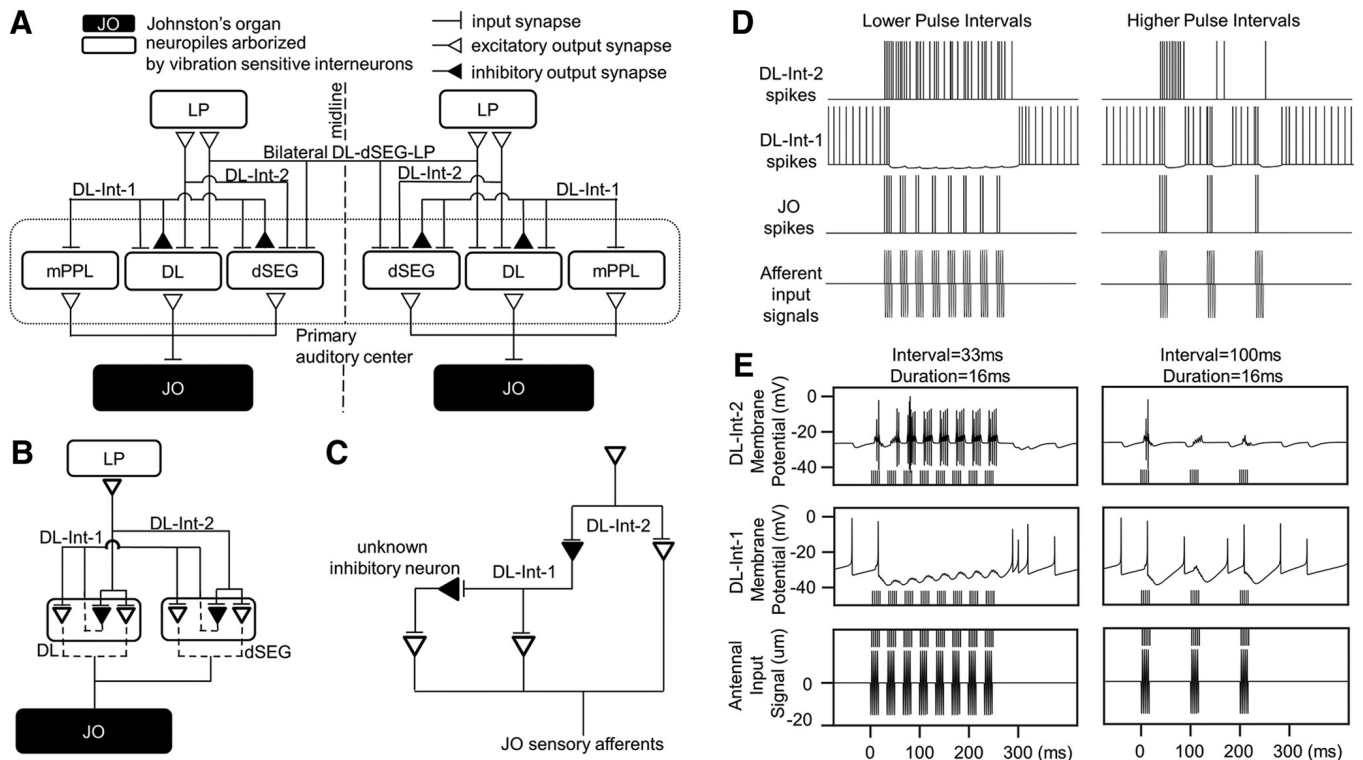
Figure 8. PAC network model based on the arborization and response patterns of interneurons. *A*, Summary of projection patterns of neurons arborizing in the PAC. Since DL-Int-1 neurons project to the DL-dSEG, where DL-Int-2 neurons arborize, DL-Int-1 neurons could have a synapse onto DL-Int-2 neurons. *B*, Subset of neural projections in *A* with putative synaptic connections (dotted lines). DL-Int-1 and DL-Int-2 neurons are assumed to have direct excitatory input from JO sensory afferents in the DL and dSEG. Since DL-Int-1 neurons are GABAergic, DL-Int-2 neurons are assumed to have an inhibitory synapse from DL-Int-1 in the DL and dSEG. *C*, Neurons and synapses in *B* represented as a network model. Synapses shown in *B* indicating the same connectivity in the DL and dSEG are represented by single synapses. An unknown inhibitory neuron is added between JO and DL-Int-1 to account for its inhibitory response. *D*, Summary of the experimental physiology of JO (bottom), DL-Int-1 (middle), and DL-Int-2 (top) neurons shown using schematic membrane traces for stimuli with shorter (~30 ms, left column) and longer (~100 ms, right column) pulse interval values. Note that the shorter intervals correspond to the vibration elicited during the honeybee waggle dance. JO sensory neurons tend to spike at a fixed phase of the input sinusoidal stimulus, showing spike frequency adaptation for later pulses. DL-Int-1 neurons show inhibition that is stronger for stimuli with shorter pulse intervals than those for stimuli with longer pulse intervals, and intermittent spikes occur during a train of pulses for long pulse intervals. DL-Int-2 neurons show on-phasic and tonic excitation, with the latter being weaker for stimuli with longer pulse intervals, suggesting that it arises from disinhibition due to the tonic inhibition of DL-Int-1. *E*, Simulation results of the network model in *C* for the same stimuli as in *D*. JO sensory neurons were assumed to spike regularly at a fixed phase of the sinusoidal stimulus applied to the antenna (bottom row). These spikes are indicated by vertical lines at the top in the bottom row and at the bottom in the middle and top rows. DL-Int-2 shows subthreshold EPSPs evoked by disinhibition through DL-Int-1. The network model could qualitatively reproduce the different spiking profiles for the two stimulus conditions.

phasic excitation and tonic spiking responses during pulse train stimulation with waggle dance-like short pulse intervals (Fig. 8E). For pulse trains with longer pulse intervals, the tonic component was reduced, and, while subthreshold EPSPs were present during stimulation, spikes occurred only sporadically (Fig. 8E). Thus, like for DL-Int-1, the response behavior of model DL-Int-2 neurons was similar to the experimentally observed responses. In summary, the activity of the model neurons qualitatively reproduced the experimental findings, indicating that the proposed network is compatible with the data.

Discussion
Extending previous work (Ai et al., 2009; Ai and Itoh, 2012), we investigated three main types of interneurons, DL-Int-1, DL-Int-2, and bilateral DL-dSEG-LP, using vibration pulses similar to those produced by honeybees during their waggle dance. DL-Int-1 neurons showed on-off phasic excitation and tonic inhibition, while DL-Int-2 and bilateral DL-dSEG-LP neurons showed on-phasic excitation. While the temporal responses differed qualitatively between these neuron types, their quantitative properties, including spike count, rate, and latencies, were largely independent of pulse parameters, suggesting that these auditory interneurons have a stereotyped response pattern. In particular, bilateral DL-

dSEG-LP neurons retained a precise response pattern, even throughout stimulation with trains of pulses. This indicates that the PAC might encode the temporal patterns of the sound produced by the waggle dance, along with other information that requires precise timing, such as the body angle of the follower relative to the direction of the waggle dance (see below).

That DL-Int-1 neurons exhibited a specific temporal response with a spike count that increased with pulse duration for short pulses but produced a constant number of evoked spikes for pulses >20 ms (Fig. 6B) suggests that these neurons receive not only excitatory input from JO afferents but also slow inhibitory input from a yet unknown inhibitory interneuron (Fig. 8C). This is also consistent with the disappearance of the on-off phasic excitation for pulse trains with short pulse intervals (Fig. 3A,C). The latencies of the first spikes produced by DL-Int-2 neurons (Fig. 6I), which were also constant and longer than those of DL-Int-1 neurons (Fig. 6D), suggest that DL-Int-2 neurons might receive input from DL-Int-1 neurons.

Possible neural mechanisms of the encoding of waggle dance information
Based on the current and previous experimental findings, we can speculate about the possible neural mechanisms underlying the

response behavior of the identified vibration-sensitive interneurons to waggle dance-like trains of vibration pulses.

Distance information
The duration of the waggle phase increases with the distance to the food source (von Frisch, 1967). During the waggle phase, the dancer produces vibration pulses during the moments at which her tail end passes in front of the follower. There are two possible parameters for encoding the distance: the duration of the train of vibration pulses and the number of pulses.

Based on the responses of DL-Int-1 neurons to continuous vibration, we previously proposed (Ai et al., 2009) that these neurons could encode the duration of vibration during the waggle phase. The present results demonstrate that the DL-Int-1 neuron also shows tonic inhibition during trains of vibration pulses and that it is an inhibitory interneuron, while the response pattern of the DL-Int-2 neuron is characterized by tonic excitation to a train of vibration pulses. Both neurons show precise latencies after the onset of a vibration pulse train (Fig. 7), but the response to stimulus offset is more precise in DL-Int-1 neurons than in DL-Int-2 neurons. This indicates that DL-Int-1 neurons are more accurate in encoding the waggle phase duration and that DL-Int-2 neurons might be postsynaptic to DL-Int-1 neurons. A previous spatial proximity analysis of dendrites indicated that DL-Int-2 neurons might receive direct input from JO afferents (Ai, 2010). Together, this may suggest that DL-Int-2 neurons receive disinhibitory input through DL-Int-1 neurons. As our model simulations (Fig. 8) indicate, the responses of these neurons are consistent with the presence of inhibition from DL-Int-1 neuron to DL-Int-2 neuron; however, further studies are needed to experimentally assess the synaptic contacts and transmission properties of PAC neurons. If honeybees use the duration of the waggle phase to describe the distance to the food source, then DL-Int-1 and DL-Int-2 neurons are potential candidates for processing this information.

Bilateral DL-dSEG-LP neurons reliably produced spikes or EPSPs in response to each pulse in a train-of-pulses stimulus and followed the vibration pulses even if the temporal pattern of the stimuli changed. The short onset latency suggests that this type of neuron receives direct inputs from JO afferents of both antennae. If honeybees use the number of pulses to encode distance, then the bilateral DL-dSEG-LP neuron is a potential candidate for processing this information. However, there is also a possible role for the bilateral DL-dSEG-LP neuron in encoding direction (see below).

Direction information
The waggle dancer communicates the direction of a profitable flower by the angle of the waggle run relative to the vertical, corresponding to the angle between the direction of the food source and the sun (von Frisch, 1967). The receivers of the information, the follower bees, are located at various positions around the line of wagging of the dancer and therefore must determine the difference between their body angle and that of the dancer during the waggle phase to decode the direction. Exactly how the follower bees achieve this computation is unclear. Michelsen (2003) hypothesized that the follower could perceive its orientation relative to the wagging run by assessing differences in the temporal patterns of airflow, specifically in terms of the difference in the intervals of the vibration pulses between both antennae. Such processing would require highly precise encoding and comparison of very short time lags. Since the bilateral DL-dSEG-LP neuron shows relatively precise spike timing in response to vibration

pulses, this neuron is a candidate for encoding information about the direction of the food source. To test this possibility, it is necessary to clarify whether the bilateral DL-dSEG-LP neuron can encode differences between the timing of the airflow at the two antennae.

Significance of an inhibitory network in the DL
DL-Int-1 IPSPs tend to occur with similar latencies as DL-Int-2 spikes (Fig. 7A–F). It is possible that a synaptic contact connects DL-Int-1 neurons to DL-Int-2 neurons and that the tonic excitation of DL-Int-2 neurons is caused by disinhibition from DL-Int-1 neurons. Interestingly, an inhibitory network has been found in the primary olfactory center [i.e., the antennal lobe (AL)] of the tobacco horn moth (Christensen et al., 1998), where a GABAergic inhibitory local interneuron induces phase-locked bursts of projection neurons encoding intermittent odor stimuli. An analogous inhibitory network might exist in the honeybee, consisting of DL-Int-1 and DL-Int-2 neurons, for encoding waggle dance vibration pulses.

The network model (Fig. 8B,C) qualitatively replicated the experimentally observed differences in the response behavior of DL-Int-1 and DL-Int-2 neurons (Fig. 8D,E). Thus, although further studies are needed to model the responses of these neurons in more quantitative detail, these results support the existence of an inhibitory network in the PAC.

Comparison of vibration-processing interneurons between the honeybee and other invertebrates
Invertebrate sensory processing typically consists of a rapid transition from coarse representations into perceptual and behavioral features over relatively few processing stages (Hildebrandt, 2014). It is very likely that a similar strategy is used for processing auditory signals in the honeybee. Our results indicate that neurons encoding different types of features arborize in the same region, the DL. Bilateral DL-dSEG-LP neurons closely follow stimuli with phase-locked spike responses, while the responses of DL-Int-1 and DL-Int-2 neurons are tuned to the behaviorally relevant features of waggle dance communication.

The interplay between excitation, delayed inhibition, and the resulting rebound depolarization have been shown in several species to be important in neural circuits that extract temporal features of sensory signals (Pollack, 2001; Large and Crawford, 2002; Alluri et al., 2016; Schöneich et al., 2015). In the honeybee, the DL-Int-1 neuron has a response consisting of on-phasic excitation, tonic inhibition, and rebound depolarization, which could result from the superimposition of an excitation and a delayed inhibition. These characteristics strongly indicate that the DL-Int-1 neuron is part of a network that extracts distance information that is temporally encoded in waggle dance communication signals.

A number of vibration-processing interneurons and neural pathways have been comprehensively identified in *Drosophila*, particularly in the PAC and the antennal mechanosensory and motor center (Kamikouchi et al., 2006; Lai et al., 2012; Vaughan et al., 2014; Matsuo et al., 2016). Some of these pathways are related to courtship song detection (Vaughan et al., 2014).

The male *Drosophila* produces an airborne vibration with a species-specific pulse song for attracting conspecific females (Ewing and Bennet-Clark, 1968; Cowling and Burnet, 1981). The honeybee uses pulses of airborne vibration for waggle dance communication. This analogy between the auditory behaviors of these two species suggests the presence of common characteristics in the central processing of vibration pulses. Comparison of the neurons involved in processing vibration signals in the two insects reveals a

number of common characteristics, such as inhibitory networks in the PAC, a secondary auditory center located in the lateral protocerebrum, which is also the secondary olfactory center, and bilateral interneurons connecting the PACs of both hemispheres.

However, further research is necessary to conclusively determine the role of interneurons in courtship song detection in the fly as well as the roles of DL-Int-1, DL-Int-2, and bilateral DL-dSEG-LP neurons in the encoding of vector information in the honeybee. Specifically, we hope to clarify the precise neural circuitry underlying the encoding of waggle dance vector information in the honeybee brain.

References

Ai H (2010) Vibration-processing interneurons in the honeybee brain. Front Syst Neurosci 3:19. CrossRef Medline

Ai H, Hagio H (2013) Morphological analysis of the primary center receiving spatial information transferred by the waggle dance of honeybees. J Comp Neurol 521:2570–2584. CrossRef Medline

Ai H, Itoh T (2012) The Auditory System of the Honeybee. In Honeybee neurobiology and behaviors, Ed 2 (Eisenhardt D, Galizia CG, Giurfa M, eds), pp 269–284. Berlin/Heidelberg, Germany: Springer.

Ai H, Nishino H, Itoh T (2007) Topographic organization of sensory afferents of Johnston's organ in the honeybee brain. J Comp Neurol 502:1030–1046. CrossRef Medline

Ai H, Rybak J, Menzel R, Itoh T (2009) Response characteristics of vibration-sensitive interneurons related to Johnston's organ in the honeybee, *Apis mellifera.* J Comp Neurol 515:145–160. CrossRef Medline

Alluri RK, Rose GJ, Hanson JL, Leary CJ, Vasquez-Opazo GA, Graham JA, Wilkerson J (2016) Phasic, suprathreshold excitation and sustained inhibition underlie neuronal selectivity for short-duration sounds. Proc Natl Acad Sci U S A 113:E1927–E1935. CrossRef Medline

Brette R, Gerstner W (2005) Adaptive exponential integrate-and-fire model as an effective description of neuronal activity. J Neurophysiol 94:3637–3642. CrossRef Medline

Brockmann A, Robinson GE (2007) Central projections of sensory systems involved in honey bee dance language communication. Brain Behav Evol 70:125–136. CrossRef Medline

Carnevale NT, and Hines ML (2006) The NEURON book. Cambridge, UK: Cambridge UP.

Christensen TA, Waldrop BR, Hildebrand JG (1998) Multitasking in the olfactory system: context-dependent responses to odors reveal dual GABA-regulated coding mechanisms in single olfactory projection neurons. J Neurosci 18:5999–6008. Medline

Cowling DE, Burnet B (1981) Courtship songs and genetic control of their acoustic characteristics in sibling species of the *Drosophila melanogaster* subgroup. Anim Behav 29:924–935. CrossRef

Dreller C, Kirchner WH (1993) Hearing in honeybees: localization of the auditory sense organ. J Comp Physiol A 173:275–279. CrossRef

Ewing AW, Bennet-Clark HC (1968) The courtship songs of Drosophila. Behaviour 31:288–301. CrossRef

Hildebrandt KJ (2014) Neural maps in insect versus vertebrate auditory systems. Curr Opin Neurobiol 24:82–87. CrossRef Medline

Hrncir M, Maia-Silva C, Mc Cabe SI, Farina WM (2011) The recruiter's excitement—features of thoracic vibrations during the honey bee's waggle dance related to food source profitability. J Exp Biol 214:4055–4064. CrossRef Medline

Judd TM (1995) The waggle dance of the honey bee: which bees following a dancer successfully acquire the information? J Insect Behav 8:343–354.

Kamikouchi A, Shimada T, Ito K (2006) Comprehensive classification of the auditory sensory projections in the brain of the fruit fly Drosophila melanogaster. J Comp Neurol 499:317–356. CrossRef Medline

Kirchner WH, Dreller C, Towne WF (1991) Hearing in honeybees: operant conditioning and spontaneous reactions to airborne sound. J Comp Physiol A 168:85–89. CrossRef

Lai JS, Lo SJ, Dickson BJ, Chiang AS (2012) Auditory circuits in the Drosophila brain. Proc Natl Acad Sci U S A 109:2607–2612. CrossRef Medline

Large EW, Crawford JD (2002) Auditory temporal computation: interval selectivity based on post-inhibitory rebound. J Comput Neurosci 13 2:125–142.

Matsuo E, Seki H, Asai T, Morimoto T, Miyakawa H, Ito K, Kamikouchi A (2016) Organization of projection neurons and local neurons of the primary auditory center in the fruit fly *Drosophila melanogaster.* J Comp Neurol 524:1099–1164. CrossRef Medline

Michelsen A (2003) Karl von Frisch lecture. Signals and flexibility in the dance communication of honeybees. J Comp Physiol A Neuroethol Sens Neural Behav Physiol 189:165–174. CrossRef Medline

Milde JJ (1988) Visual responses of interneurones in the posterior median protocerebrum and the central complex of the honeybee *Apis mellifera.* J Insect Physiol 34:427–436. CrossRef

Mobbs PG (1982) The brain of the honeybee *Apis mellifera.* I. The connections and spatial organization of the mushroom bodies. Philos Trans R Soc Lond B Biol Sci 298:309–354. CrossRef

Pollack GS (2001) Analysis of temporal patterns of communication signals. Curr Opin Neurobiol 11:734–738. CrossRef Medline

Schöneich S, Kostarakos K, Hedwig B (2015) An auditory feature detection circuit for sound pattern recognition. Sci Adv 1:e1500325. CrossRef Medline

Stimberg M, Goodman DF, Benichoux V, Brette R (2014) Equation-oriented specification of neural models for simulations. Front Neuroinform 8:6. CrossRef Medline

Towne WF, Kirchner WH (1989) Hearing in honey bees: detection of air-particle oscillations. Science 244:686–688. CrossRef Medline

Tsujiuchi S, Sivan-Loukianova E, Eberl DF, Kitagawa Y, Kadowaki T (2007) Dynamic range compression in the honey bee auditory system toward waggle dance sounds. PLoS One 2:e234. CrossRef Medline

Vaughan AG, Zhou C, Manoli DS, Baker BS (2014) Neural pathways for the detection and discrimination of conspecific song in. D. melanogaster. Curr Biol 24:1039–1049. CrossRef Medline

von Frisch K (1967) The tail-wagging dance as a means of communication when food sources are distant. In: The dance language and orientation of bees (von Frisch K, ed) pp 57–235. Cambridge, MA: Harvard UP.

Network simulations of interneuron circuits in the honeybee primary auditory center

Ajayrama Kumaraswamy[1, *], Aynur Makhsutov[2], Kazuki Kai[3], Hiroyuki Ai[3], Hidetoshi Ikeno[4], Thomas Wachtler[1, *]

[1] Department of Biology II, Ludwig-Maximilians-Universität München, 82152 Planegg-Martinsried, Germany
[2] Department of Biomedical Physics, Moscow Institute of Physics and Technology, Dolgoprudny, Russia
[3] Department of Earth System Science, Fukuoka University, 814-0180 Fukuoka, Japan
[4] School of Human Science and Environment, University of Hyogo, 670-0092 Himeji, Japan

* {ajayramak, wachtler}@bio.lmu.de

Abstract

Processing of airborne vibration signals in the auditory system is essential for honeybee communication through the waggle dance language. Properties of neurons in the honeybee primary auditory center suggest a circuitry of excitatory and inhibitory neurons encoding these communication signals. To test this assumption, we simulated this network and analyzed the predicted responses for different types of inputs. In particular, we investigated the effect of specific inhibitory connections in the network. The results indicate that the experimentally observed responses of certain interneuron types are compatible with an inhibitory network of vibration processing in the primary auditory center of the honeybee.

Introduction

Waggle dance and the honeybee primary auditory center

One of many fascinating behaviors of the honeybee is the "Waggle Dance", which is used by returning forager honeybees to advertise the location of beneficial resources like food, water and pollen among hive mates (Von Frisch 1967). The waggle dance consists of the "waggle phase" during which the honeybee walks in a specific direction wagging its body and flapping its wings, and a "return phase" during which it returns along a curved path to the start of the waggle phase. The waggle phase represents the flight path of the bee from the hive to resource, encoding the distance and direction of the resource in its duration and orientation, respectively. During the waggle phase, body and wing movements of the dancer honeybee produce pulses of air vibrations of specific frequency (≈265 Hz), duration (≈16 ms) and inter-pulse-interval (≈33 ms) (Wenner 1962). These "sounds" are important for successful recruitment of foragers (Barth et al. 2005; Michelsen 2003) and are sensed by follower bees using the Johnston's Organ (JO) in their antennae. Sensory neurons in the JO transduce air vibrations into neural signals (Tsujiuchi et al. 2007) and convey them to the honeybee brain, specifically to the Dorsal Lobe (DL), the dorsal Sub Esophageal ganglion (dSEG) and the medial Posterior Protocerebral Lobe (mPPL) (Ai et al. 2009), the regions forming the primary auditory center (PAC) of the honeybee brain.

Experimental results about PAC neurons

Experimental studies have identified several vibration-sensitive neurons in the honeybee PAC and characterized their morphological projections and physiological responses along with those of the JO sensory afferents (Ai et al. 2009; Ai et al. 2016; Ai et al. in prep.). The JO sensory afferents that project into the DL responded to sinusoidal vibration stimuli by producing spikes with high probability at a fixed phase of the input (unpublished data). DL-Int-1, a local inhibitory interneuron that arborizes in the DL, dSEG and mPPL, showed close proximity to JO sensory afferents (Ai and Hagio 2013) and responded to one-second-long continuous sinusoidal vibration with on-phasic excitation and tonic inhibition followed by post-inhibitory rebound (Ai et al. 2009). DL-Int-2, an excitatory output neuron that arborizes in the DL, dSEG, central PPL and the lateral protocerebrum (LP), also showed close proximity to JO sensory afferents (Ai and Hagio 2013). It responded to one-second-long continuous sinusoidal vibration with on-phasic and tonic excitation. For stimulation with trains of vibration pulses with different pulse duration and inter-pulse-interval (IPI) values (Ai et al. 2016; Ai et al. in prep.), DL-Int-1 showed a reduced spiking rate caused by strong inhibition for pulse trains of IPI shorter than 33 ms, which gradually increased for stimulus trains of higher IPIs. In contrast, DL-Int-2 showed higher spiking rates for pulse trains of IPI up to 33 ms, which reduced for pulse trains of higher IPI.

Putative Network model

The response properties, together with projection patterns and immunohistochemistry, suggested a disinhibitory network involving DL-Int-1 and DL-Int-2 (Fig 1A; Ai et al. in prep.). In this model, sensory afferents from the JO are assumed to form excitatory synapses onto both DL-Int-1 and DL-Int-2. The delayed tonic inhibition shown by DL-Int-1 is assumed to be the result of a local inhibitory neuron that is driven by JO sensory afferents. Since DL-Int-1 is GABAergic and has boutons in the DL and dSEG where DL-Int-2 arborizes (Ai et al. 2009), an inhibitory synapse is assumed from DL-Int-1 to DL-Int-2.

To test these assumptions and investigate the role of inhibition and disinhibition in vibration processing in the honeybee, we used phenomenological neuron models of DL-Int-1 and DL-Int-2 and simulated different interneuron circuits with variants of inhibitory connections.

Methods

Choice of neuron and synapse models

Since very little is known about the membrane properties of DL-Int-1 and DL-Int-2, point neuron models were chosen instead of more detailed models. The AdExp model is well understood (Touboul and Brette 2008) and can replicate a wide variety of neural responses with few parameters (Rossant et al. 2011; Kremer et al. 2011; Vogels et al. 2011). The double-exponential synaptic conductance model (Carnevale and Hines 2006) is a good approximation for experimentally observed synaptic traces (e.g.: Häusser and Roth 1997; Zsiros and Hestrin 2005). It provides parameters to independently control the rise and fall time constants and synaptic strength, which was specifically useful to implement the single-neuron properties of DL-Int-1 and DL-Int-2.
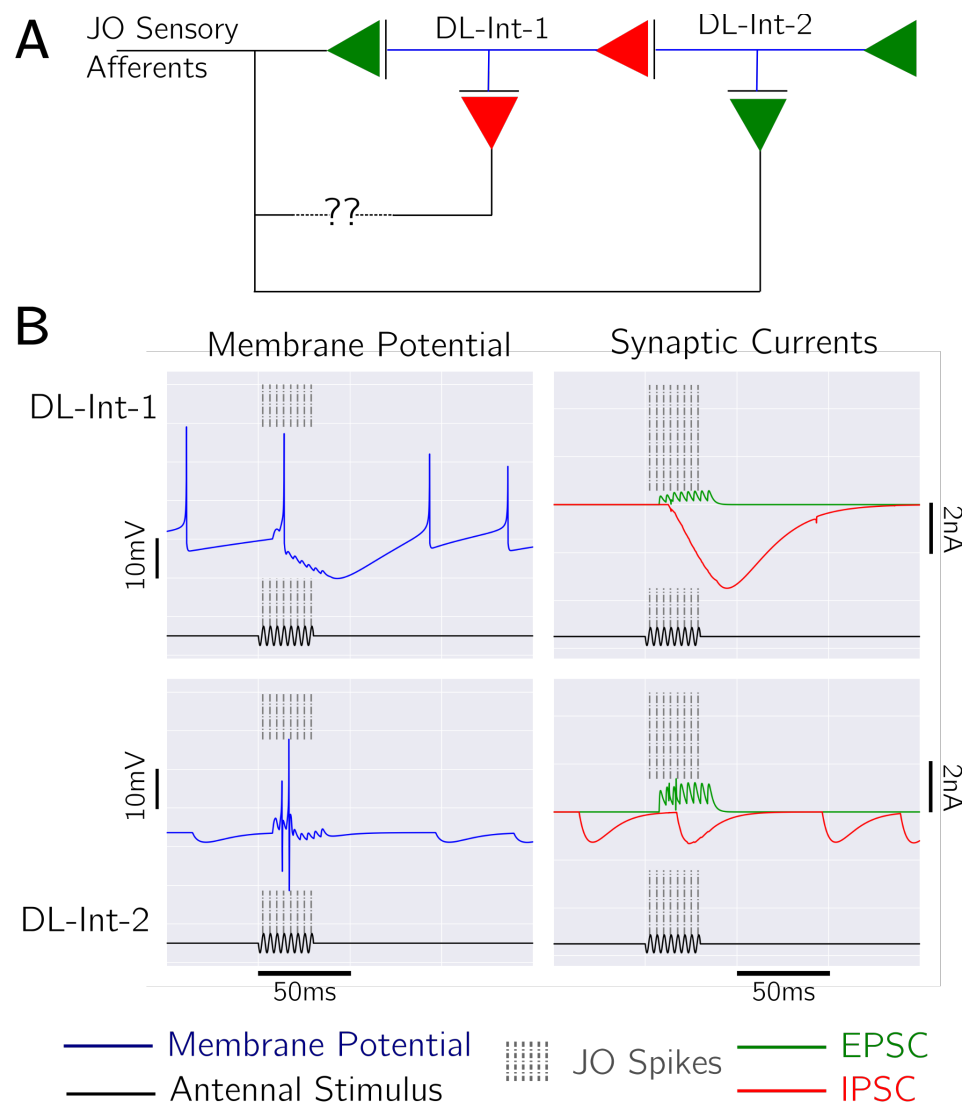
Figure 1. A, The network model used for the simulation. DL-Int-1 and DL-Int-2 were modeled as point neurons using the Adaptive Exponential Model and the synaptic conductances were modeled as difference of exponentials. **B,** Example simulation traces for a continuous sinusoidal stimulus of length 30 ms and frequency 265 Hz. The membrane potential traces for DL-Int-1 and DL-Int-2 are shown in the left column with their excitatory and inhibitory synaptic currents in the right column.

Model implementation

JO sensory neurons were assumed to spike at the positive peak of the input sinusoidal vibration stimulus. DL-Int-1 and DL-Int-2 were modeled as point neurons with their membrane potentials simulated using the Adaptive Exponential Integrate-and-fire (AdExp) model (Naud et al. 2008) (Fig 2). These membrane potential calculations included synaptic input currents, which which were calculated from their conductances. Synaptic conductances were simulated using difference of exponentials functions, based on the Exp2Syn model of the simulator NEURON (Carnevale and Hines 2006; RRID:SCR_005393)

(Fig 3).   78

Simulation setup and stimuli used   79

The network model described above was implemented using the simulator Brian version   80
2.0.1 (Stimberg et al. 2014; `RRID:SCR_002998`) in Python. An integration step size of   81
0.1 ms was used and all simulation runs had a "settling time" of 600 ms, after which   82
stimuli were applied. Similar to experimental studies (Ai et al. 2009; Ai et al. 2016; Ai   83
et al. in prep.), continuous sinusoidal stimuli with stimulus frequency 265 Hz and different 84
stimulus durations were used, along with trains of sinusoidal pulses of stimulus frequency 85
265 Hz and different combinations of pulse durations and IPI values. The pulse parameters   86
were chosen around the waggle dance parameters of 16ms pulse duration and 33 ms IPI.   87
    The code used to simulate this network is available on Github at   88
`https://github.com/wachtlerlab/HB-PAC_disinhibitory_network`.   89

Tuning model parameters   90

A

AdExp Model Equations:

$$C\frac{dV}{dt} = -g_L(V-E_L) + g_L s_F\left(\exp\left(\frac{V-V_t}{s_F}\right)\right)$$
$$-w + I_{inh} + I_{exc}$$

$$\tau_w \frac{dw}{dt} = a(V-E_L) - w$$

On Spike $\quad V \Leftarrow V_r \quad$ and $\quad w \Leftarrow w + b$

B

V	Membrane Potential	I_{inh}	Inhibitory input synaptic current
w	Adaptation Current	I_{exc}	Excitatory input synaptic current
E_L	Leak reversal potential	g_L	Membrane leak conductance
V_t	Spiking threshold potential	C	Membrane capacitance
V_r	Post-spike reset potential	τ_w	Decay time constant of "w"

C

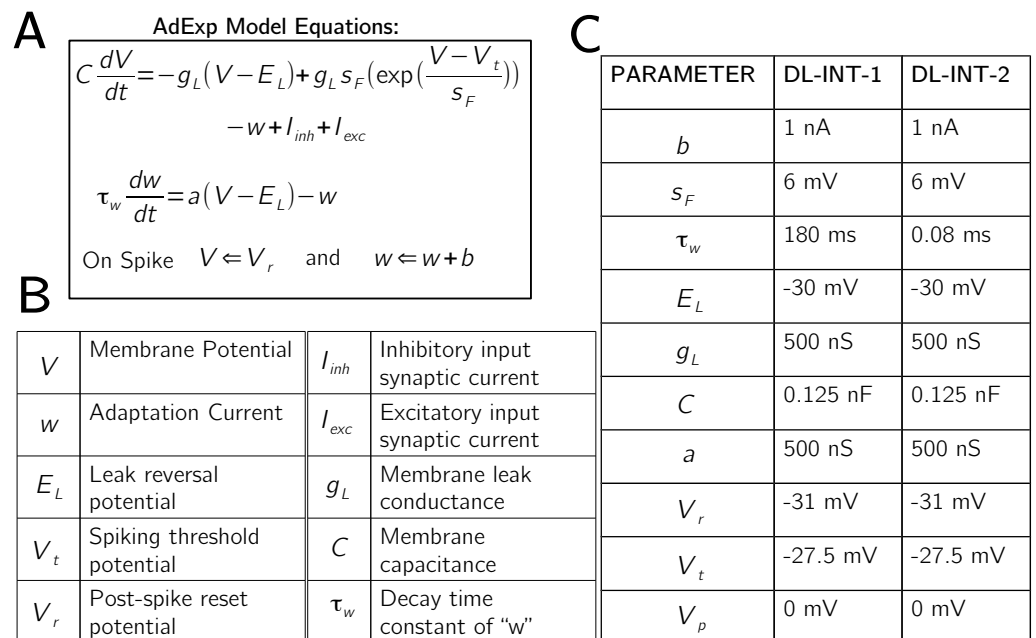| PARAMETER	DL-INT-1	DL-INT-2
b	1 nA	1 nA
s_F	6 mV	6 mV
τ_w	180 ms	0.08 ms
E_L	-30 mV	-30 mV
g_L	500 nS	500 nS
C	0.125 nF	0.125 nF
a	500 nS	500 nS
V_r	-31 mV	-31 mV
V_t	-27.5 mV	-27.5 mV
V_p	0 mV	0 mV

Figure 2. **A,** Equations of the Adaptive Exponential integrate-and-fire (AdExp) point neuron model used for DL-Int-1 and DL-Int-2. **B,** Description of the parameters of the equations in A. **C,** The set of parameters that were used in the simulations.

    Parameters of the DL-Int-1 model and its inputs synapses were chosen to qualitatively   91
reproduce the response characteristics of DL-Int-1. In particular, membrane and   92
adaptation parameters of DL-Int-1 were tuned to produce non-zero spontaneous firing   93
rate. The temporal dynamics of excitatory and inhibitory input synapses were adjusted by   94
controlling their rise and fall time constants and their delays to qualitatively reproduce the 95
temporal pattern of DL-Int-1's response to continuous sinusoidal pulses, i.e., its on-phasic 96
excitation, tonic inhibition and rebound. Further, the strengths of input synapses along   97
with the parameters that affect the neuron's excitability, viz., g_L and a, were adjusted to 98
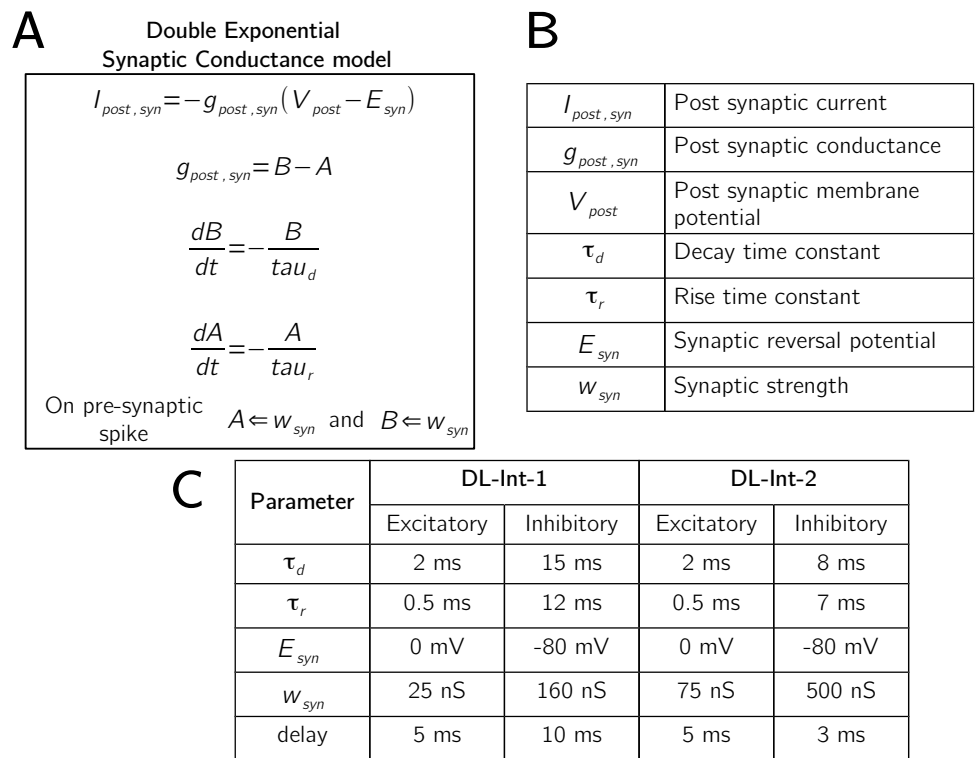
A

Double Exponential
Synaptic Conductance model

$$I_{post,syn} = -g_{post,syn}(V_{post} - E_{syn})$$

$$g_{post,syn} = B - A$$

$$\frac{dB}{dt} = -\frac{B}{tau_d}$$

$$\frac{dA}{dt} = -\frac{A}{tau_r}$$

On pre-synaptic spike $\quad A \Leftarrow w_{syn} \quad$ and $\quad B \Leftarrow w_{syn}$

B

$I_{post,syn}$	Post synaptic current
$g_{post,syn}$	Post synaptic conductance
V_{post}	Post synaptic membrane potential
τ_d	Decay time constant
τ_r	Rise time constant
E_{syn}	Synaptic reversal potential
w_{syn}	Synaptic strength

C

Parameter	DL-Int-1		DL-Int-2	
	Excitatory	Inhibitory	Excitatory	Inhibitory
τ_d	2 ms	15 ms	2 ms	8 ms
τ_r	0.5 ms	12 ms	0.5 ms	7 ms
E_{syn}	0 mV	-80 mV	0 mV	-80 mV
w_{syn}	25 nS	160 nS	75 nS	500 nS
delay	5 ms	10 ms	5 ms	3 ms

Figure 3. A, Equations of the difference of exponentials synaptic conductance model used for the excitatory and inhibitory synapses. **B,** Description of the model parameters. **C,** The set of parameters that were used for simulations.

qualitatively reproduce the response patterns of DL-Int-1 to trains of vibration pulses while retaining its tuned response to continuous pulses. Parameters of DL-Int-2 were assumed to be same as DL-Int-1 except for one adaptation parameter, τ_w, which was adjusted to account for the zero spontaneous firing rate and on-phasic and tonic excitation properties of this neuron type. The excitatory input synapse of DL-Int-2 had the same temporal dynamics as those of DL-Int-1, while its inhibitory input synapse was modified to have faster dynamics. The strengths of these synapses were tuned to qualitatively replicate DL-Int-2's response properties to trains of vibration pulses. All tuning parameters are listed along with their descriptions in Figs. 2 (neuron parameters) and 3 (synapse parameters).

99
100
101
102
103
104
105
106
107

Results

Qualitative replication of experimental results

Results for simulations of the neurons with a continuous sinusoidal vibration stimulus of 1 s are shown in Fig 4. The simulated membrane potential traces of DL-Int-1 showed non-zero spontaneous activity, on-phasic excitation, tonic inhibition and rebound, qualitatively very similar to experimental traces (see Figs 6 and 7 of Ai et al. 2009). The simulated membrane potential changes of DL-Int-2 showed zero spontaneous activity, on-phasic and tonic inhibition.
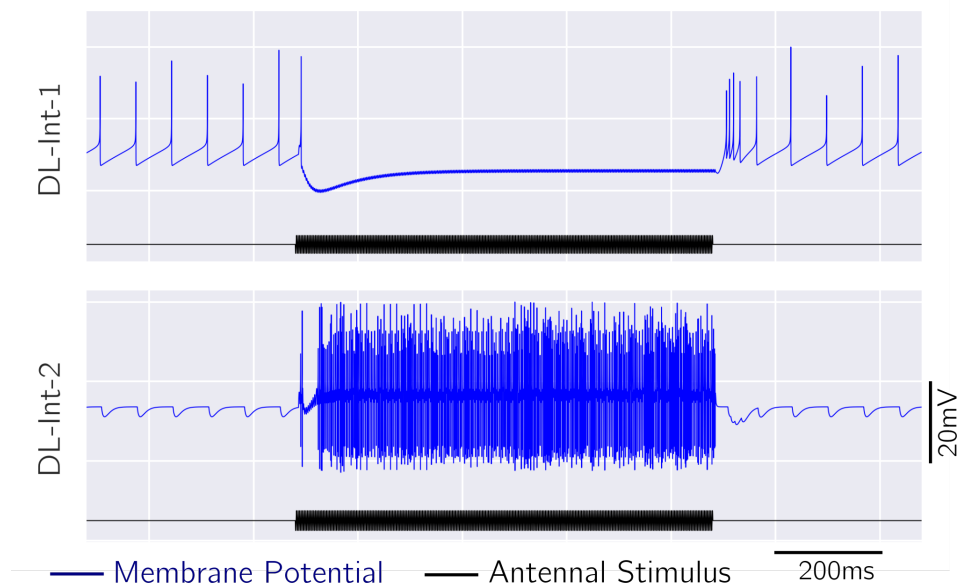
Figure 4. Responses of DL-Int-1 and DL-Int-2 to continuous sinusoidal vibration stimuli of frequency 265Hz. DL-Int-1 showed non-zero spontaneous activity, on-phasic excitation and tonic inhibition followed by post inhibitory rebound. DL-Int-2 showed zero spontanous activity, on-phasic and tonic excitation.

Membrane potential traces of DL-Int-1 for different trains of sinusoidal pulses are summarized in Fig. 5. Simulations showed low spiking rates for pulse trains of IPI shorter than 33 ms and increasingly higher spike rates for pulse trains with IPIs above 33 ms.

Significance of Inhibitory synapse from DL-Int-1 to DL-Int-2

A summary of simulated membrane potential traces of DL-Int-2 in response to pulse trains with different pulse parameters is shown in Fig. 6 (blue). DL-Int-2 responded to pulse trains with IPIs shorter than 33 ms with high spike rates, which reduced for trains with longer IPIs. The significance of the inhibitory connection from DL-Int-1 to DL-Int-2 was tested by silencing this inhibitory input in the model. With the inhibitory input from DL-Int-1 absent, DL-Int-2 showed high firing rates for all pulse parameters (Fig6, red). Since DL-Int-1 had low firing rate for pulse trains with short intervals, it did not affect the response of DL-Int-2 for these input parameters. However, DL-Int-1 showed higher spiking rate for pulse trains of IPI greater than 33 ms and hence could affect the response of DL-Int-2.
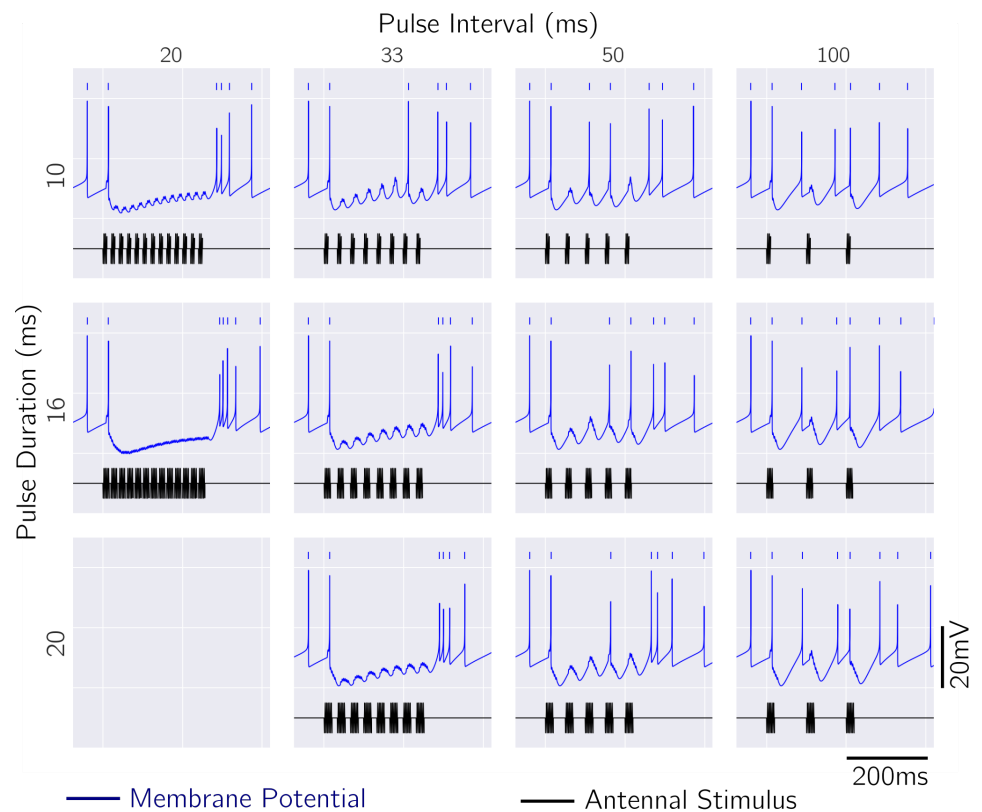
Figure 5. Simulated responses of DL-Int-1 to trains of vibration pulses of different pulse durations and pulse intervals. Spikes corresponding to the blue membrane potential traces are shown using short blue vertical lines. The model showed very low spiking rates for lower pulse intervals and higher spiking rates for higher pulse intervals. Increasingly stronger sub-threshold oscillations were observed for increasing pulse interval values.

Discussion

In this study, we simulated a hypothesized network of interneurons in the honeybee primary auditory center to test its consistency with experimentally observed responses. Simulations qualitatively reproduced the membrane potential traces of the interneurons to continuous vibration stimuli as well as trains of vibration pulses, suggesting that the hypothesized network model could underlie the experimental observations.

Since the simulation results of this study are only qualitative, and in particular the parameters of the model neurons were not directly measured experimentally, the results confirm the consistency, but do not imply the necessity, of the assumed circuitry. For example, the same behavior might potentially be observed in a network with different circuitry, possibly requiring different neuron properties. However, building and testing such models would require more experimental data.

This simulation study is a first step towards understanding the neural circuitry that underlies auditory processing in the honeybee. Although the simulated model provides instructive insights like the level of required excitability of the interneurons and the interplay between excitatory and inhibitory synaptic currents for producing the observed experimental traces, they do no explain all the observed features of experimental responses
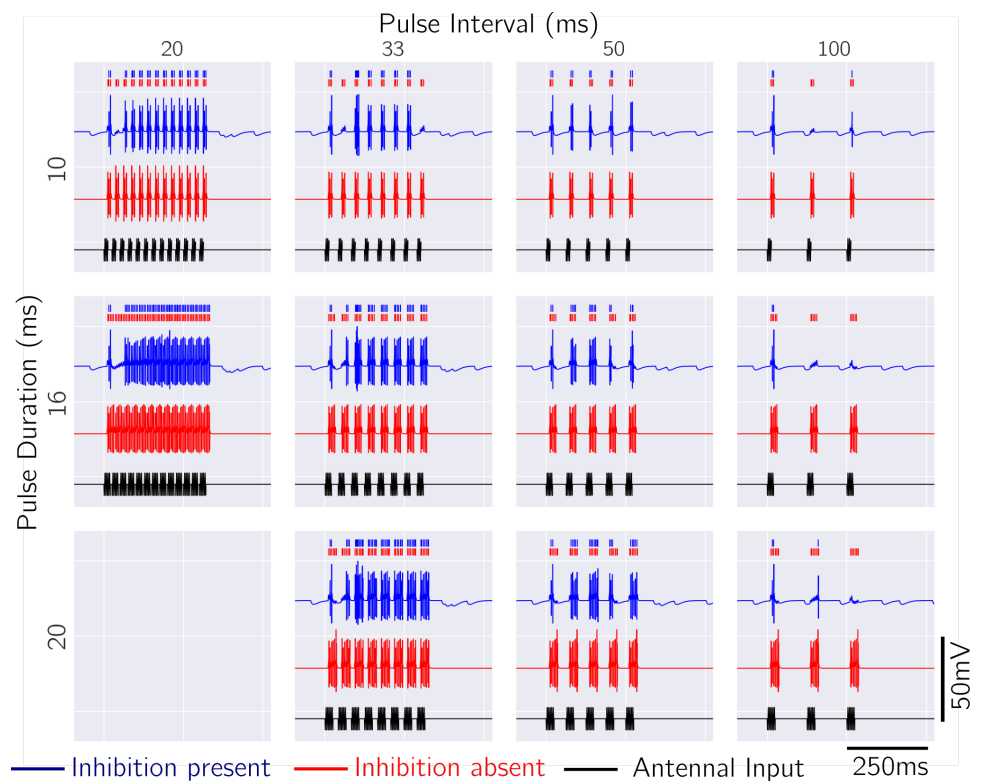
Figure 6. Simulated responses of DL-Int-2 to trains of vibration pulses of different pulse intervals and durations for the cases where the inhibition from DL-Int-1 is present (blue) and absent (red). Spikes corresponding to the membrane potential traces are shown using short vertical lines of corresponding colors. With the DL-Int-1 inhibition present (blue), the model showed high firing rate for short pulse intervals which gradually reduced for higher pulse intervals, consistent with experimental observations. Such a reduction in firing rate for higher pulse intervals is not seen for the case without DL-Int-2 inhibition (red).

to all the stimulus patterns used. More extensive testing and comparison of more complex models would be required, which however would require more information about synaptic connectivity and individual membrane properties of the interneurons of the honeybee primary auditory center.

Conclusion

We have simulated a network model of identified neurons in the primary auditory center of the honeybee brain, to investigate the potential role of inhibitory connections and in particular to test the assumption of a disihibitory network of auditory processing in the honeybee. The results show that such a network model is compatible with the experimental data. The principles underlying the network model could help to better understand auditory processing in the honeybee brain.

Acknowledgments [158]

References

Ai, H. and Hagio, H. (2013). "Morphological analysis of the primary center receiving spatial information transferred by the waggle dance of honeybees". In: *Journal of Comparative Neurology* 521.11, pp. 2570–2584. ISSN: 00219967. DOI: `10.1002/cne.23299`.

Ai, H., Kai, K., Kumaraswamy, A., Ikeno, H., and Wachtler, T. (in prep.). "Interneurons in the honeybee primary auditory center responding to waggle dance-like vibration pulses." in Preparation.

Ai, H., Kai, K., Kumaraswamy, A., Rautenberg, P. L., Wachtler, T., and Ikeno, H. (2016). "Interneurons of the primary auditory center of the honeybee brain responsive to pulsed vibration produced by the waggle dance". In: *Proceedings of 2016 Meeting of JSCPB*. URL: `https://www.jstage.jst.go.jp/article/hikakuseiriseika/33/4/33_145/_pdf`.

Ai, H., Rybak, J., Menzel, R., and Itoh, T. (2009). "Response characteristics of vibration-sensitive interneurons related to Johnston's organ in the honeybee, Apis mellifera". In: *Journal of Comparative Neurology* 515.2, pp. 145–160. ISSN: 00219967. DOI: `10.1002/cne.22042`.

Barth, F., Hrncir, M., and Tautz, J. (2005). "Vibratory and Airborne-Sound Signals in Bee Communication (Hymenoptera)". In: *Insect Sounds and Communication*. Contemporary Topics in Entomology. CRC Press, pp. 421–436. ISBN: 978-0-8493-2060-6. DOI: `doi:10.1201/9781420039337.ch32`. URL: `https://doi.org/10.1201/9781420039337.ch32`.

Carnevale, N. and Hines, M. (2006). *The NEURON Book.* Cambridge, UK: Cambridge University Press.

Häusser, M. and Roth, A. (1997). "Estimating the Time Course of the Excitatory Synaptic Conductance in Neocortical Pyramidal Cells Using a Novel Voltage Jump Method". In: *Journal of Neuroscience* 17.20, pp. 7606–7625. ISSN: 0270-6474. eprint: `http://www.jneurosci.org/content/17/20/7606.full.pdf`. URL: `http://www.jneurosci.org/content/17/20/7606`.

Kremer, Y., Leger, J.-F., Goodman, D., Brette, R., and Bourdieu, L. (2011). "Late Emergence of the Vibrissa Direction Selectivity Map in the Rat Barrel Cortex". In: *Journal of Neuroscience* 31.29, pp. 10689–10700. ISSN: 0270-6474. DOI: `10.1523/JNEUROSCI.6541-10.2011`. URL: `http://www.jneurosci.org/cgi/doi/10.1523/JNEUROSCI.6541-10.2011`.

Michelsen, A. (2003). *Karl von Frisch lecture. Signals and flexibility in the dance communication of honeybees.* eng. DOI: `10.1007/s00359-003-0398-y`.

Naud, R., Marcille, N., Clopath, C., and Gerstner, W. (2008). "Firing patterns in the adaptive exponential integrate-and-fire model". In: *Biological Cybernetics* 99.4-5, pp. 335–347. ISSN: 03401200. DOI: `10.1007/s00422-008-0264-7`.

Rossant, C., Goodman, D. F. M., Fontaine, B., Platkiewicz, J., Magnusson, A. K., and Brette, R. (2011). "Fitting neuron models to spike trains". In: *Frontiers in Neuroscience* 5.FEB, pp. 1–8. ISSN: 16624548. DOI: `10.3389/fnins.2011.00009`.

Stimberg, M., Goodman, D. F. M., Benichoux, V., and Brette, R. (2014). "Equation-oriented specification of neural models for simulations". In: *Frontiers in Neuroinformatics* 8.February, pp. 1–14. ISSN: 1662-5196. DOI: 10.3389/fninf.2014.00006. URL: http://journal.frontiersin.org/article/10.3389/fninf.2014.00006/abstract.

Touboul, J. and Brette, R. (2008). "Dynamics and bifurcations of the adaptive exponential integrate-and-fire model". In: *Biological Cybernetics* 99.4-5, pp. 319–334. ISSN: 03401200. DOI: 10.1007/s00422-008-0267-4.

Tsujiuchi, S., Sivan-Loukianova, E., Eberl, D. F., Kitagawa, Y., and Kadowaki, T. (2007). "Dynamic range compression in the honey bee auditory system toward waggle dance sounds". In: *PLoS ONE* 2.2. ISSN: 19326203. DOI: 10.1371/journal.pone.0000234.

Vogels, T. P., Sprekeler, H., Zenke, F., Clopath, C., and Gerstner, W. (2011). "Inhibitory Plasticity Balances Excitation and Inhibition in Sensory Pathways and Memory Networks". In: *Science* 334.6062, pp. 1569–1573. ISSN: 0036-8075. DOI: 10.1126/science.1211095. URL: http://www.sciencemag.org/cgi/doi/10.1126/science.1211095.

Von Frisch, K. (1967). *The dance language and orientation of bees.* Harvard University Press.

Wenner, A. M. (1962). "Sound production during the waggle dance of the honey bee". In: *Animal Behaviour* 10.1-2, pp. 79–95.

Zsiros, V. and Hestrin, S. (2005). "Background Synaptic Conductance and Precision of EPSP-Spike Coupling at Pyramidal Cells". In: *Journal of Neurophysiology* 93.6, 3248 LP –3256. URL: http://jn.physiology.org/content/93/6/3248.abstract.

3 | DISCUSSION

This doctoral research was part of the Ginjang project which investigates the neural mechanisms that underlie processing of waggle dance vibration signals in the honeybee brain. The main focus of this thesis was an identified vibration-sensitive interneuron, DL-Int-1. Specifically, the aim was to understand the function of DL-Int-1 in processing waggle dance vibrations and the work was divided into two sub-projects. Firstly, adaptations during maturation in morphology and physiology of DL-Int-1 were studied, since such adaptations can provide insights about functional adaptations for behavioral specialization. A new algorithm for spatial co-registration of neuron morphologies was developed for comparing DL-Int-1 morphologies from young and mature DL-Int-1 honeybees. Secondly, a putative network that included DL-Int-1 in the honeybee PMC was postulated based on morphological and immunohistochemical evidence and the network was simulated using behaviorally relevant stimuli to verify the consistency of the proposed network with observed electrophysiological responses. The following sections elaborate on the relevance of the results, challenges faced during the research and further research that can be undertaken based on current results.

RELEVANCE

Co-registration of morphologies

Publication 1 presents a novel algorithm for spatial co-registration of neuron morphologies, Reg-MaxS-N, along with a new multi-scale criterion for spatial similarity of neuron morphologies. The algorithm was validated by comparing its performance against that of six other state-of-the-art algorithms on five morphologically diverse datasets from Drosophila. This exercise not only demonstrated the strengths and shortcomings of Reg-MaxS-N but also provided insights that can help when choosing among such algorithms.

Reg-MaxS-N was designed based on a novel approach that draws from a couple of observations about neuron morphologies – the importance of the spatial region occupied by a dendritic arborization and lower spatial match between fine dendritic features of morphologies compared to gross features. Validation of the algorithm using multiple diverse datasets of insect morphologies confirmed the approach as well as the observations on which it was based. The validity of these notions for other invertebrate morphologies as well as vertebrate morphologies can be tested in a similar manner.

In the process of co-registration, Reg-MaxS-N compares morphologies at successively smaller scales and requires the specification of such a sequence of scales as a parameter. Repeated application of the algorithm with different sequences of scales and comparison of the similarity of the resulting co-registered morphologies can help in understanding the spatial similarity of the morphologies at different spatial scales.

Together with its application in Publication 2 for comparing DL-Int-1 morphologies, Publication 1 illustrates an approach for the detailed spatial comparison of neuron morphologies that show no major differences in global features, but possibly have differences in fine dendritic features. This approach can be more relevant for investigating spatially localized differences in invertebrate neurons, which are generally regarded as being more stereotypic than vertebrate neurons (Livneh and Mizrahi 2010).

Network role of DL-Int-1

A neuronal network consisting of DL-Int-1 and DL-Int-2 was proposed in Publication 3 based on the anatomical projection patterns and immunohistochemical screening of PMC neurons. Publication 4 presents models for neurons and synapses of the network along with simulations that demonstrate that simulated response traces of the neurons to continuous sinusoidal stimuli at 265 Hz were consistent with experimentally observed responses. Further, the model network was able to qualitatively reproduce differences in response patterns of DL-Int-1 and DL-Int-2 to pulse train stimuli with different inter-pulse-intervals.

The models used for neurons in Publication 4 were phenomenological, which use the black box approach to approximate the electrical behavior of neurons using simplified models as opposed to mechanistic models, which consist of mechanisms underlying neuronal activity such as membrane properties and ionic currents. The parameters used in Publication 4 are therefore relevant for understanding abstract features of the activity of DL-Int-1 and DL-Int-2 such as the level of excitability and the strengths of excitatory and inhibitory inputs.

Morphological adaptations in DL-Int-1 during maturation

Adaptations in morphology and physiology of neurons during maturation can provide insights about the accompanying changes in neural function. Publication 2 studied such adaptations in DL-Int-1 by comparing the neural structure and electrical activity between young, newly emerged adult and mature forager honeybees. Region-

dependent spatially localized changes in dendritic density were observed, which could indicate improved connectivity between DL-Int-1 and its neighboring neurons as well as improved electric conduction of signals through it.

Insect neural systems undergo a wider array of changes during metamorphosis than during adult life (Levine 1986). However, investigation of neural adaptations during adult life is important for clarifying whether such adaptations are relevant for behavioral specialization and whether experiences acquired during adult life shapes such adaptations (Tavosanis 2012). Devaud and Masson (1999) demonstrated in their seminal study that honeybee antennal lobe neurons acquire their overall structure approximately a week before emergence, while changes in fine dendritic structure continue for the first week of adult life. The results of Publication 2, which indicates preservation of broad arborization and branching characteristics along with region-specific outgrowth and pruning, reaffirm the conclusions of Devaud and Masson (1999). Only a handful of studies are currently available in insects that detail the effects of adult maturation on neuron morphology (Farris et al. 2001; Jones et al. 2009) and electrophysiology (Wang et al. 2005; Kiya et al. 2007) and the results of Publication 2 are in line with their results.

Function of DL-Int-1 and waggle dance

Publications 3 and 4 present a putative disinhibitory network of neurons in the honeybee PMC in which DL-Int-1 has an inhibitory synapse onto DL-Int-2. DL-Int-1 has a non-zero spontaneous activity, which inhibits the activity of DL-Int-1 and DL-Int-1 responds to vibration stimulus with tonic inhibition, which releases DL-Int-2 from inhibition. Strengthening during maturation of these response features – inhibition relative to spontaneous activity and rebound response presented in Publication 2 indicate that the disinhibitory role of DL-Int-1 in the putative network is more effective in foragers than in newly emerged adults.

The duration of the waggle phase of waggle dance communication increases proportionally with the distance of the food source advertised (von Frisch 1967). It has been hypothesized that DL-Int-1 could encode the duration of the waggle phase since it responds with persistent inhibition to continuous antennal vibrations at waggle dance frequency for the entire duration of the applied stimulus independent of stimulus length (Ai et al. 2009). Further, Publications 3 and 4 showed that DL-Int-1 was GABAergic, responded to waggle dance-like pulse stimuli with tonic inhibition and played a central inhibitory role in a putative neuronal network in the honey-

bee PMC for encoding waggle dance signals. Strengthening of the level of inhibition relative to spontaneous activity and the level of rebound response in DL-Int-1 during maturation could indicate better encoding of distance information from waggle dance vibration signals in mature foragers.

Antennal mechanosensory system in honeybees

The antennal mechanosensory system of the honeybee starts at the antenna, with JO sensory neurons transducing displacements of the flagellum in response to air vibrations. The JO sensory neurons project to the PMC of the honeybee brain, several vibration sensitive neurons arborizing in the PMC have been identified. The subject of this thesis, DL-Int-1, is a local neuron arborizing in the honeybee PMC while several other output, bilateral and descending neurons have also been identified. The neural processes by which the information about vibration stimuli contained in PMC neurons contributes to cognitive and motor functions of the honeybee are yet to be identified. Nonetheless, DL-Int-1 and other PMC neurons form the first stage of antennal mechanosensory processing that could accentuate and transform stimulus features in a way beneficial for honeybee air vibration perception and behavior.

Comparison with adaptations in
**   other sensory systems of the honeybee**

The mushroom body of the honeybee is the higher order sensory center for both olfactory and visual systems (Gronenberg 2001). Anatomical changes based on aging and experience have been reported in the lower order sensory centers of olfactory and visual systems as well as in the mushroom bodies of adult honeybees in the form of changes in the volume of neuropils and synaptic reorganization (Groh and Meinertzhagen 2010). Some of these changes have also been associated with the ability of the honeybee to distinguish and learn stimulus patterns. Adaptations observed in the morphology of DL-Int-1, which is a primary sensory neuron in the antennal mechanosensory system, could indicate changes in the structure and synaptic connectivity of the honeybee PMC, i.e., in the AMMC, SEG and PPL (see Section 1.2.3). The changes could also be relevant for the ability of the honeybee to learn and distinguish air vibration patterns, especially those which are related to waggle dance communication and flight.

Hearing in other insects

The antennae and the JO are specialized to detect near field air vibrations in many insect species (Yack 2004). In Drosophila, which is another insect species whose antennal mechanosensory system has been investigated in detail, several parallels in the projection patterns of JO sensory neurons and neurons arborizing in the PMC can be seen with those in the honeybee. A few neurons have been identified in Drosophila PMC that have features similar to DL-Int-1, namely, restriction of dendritic arborization within the PMC and GABAergic immunoreactivity (Vaughan et al. 2014). Some of these have also been shown to be crucial for eliciting courtship song behavior (Vaughan et al. 2014). Adaptations during maturation similar to that in DL-Int-1 could be expected in some local PMC neurons in Drosophila.

Results of Publications 2 and 3 indicate the importance of inhibition and rebound response features of a local GABAergic neuron in a disinhibitory network in the honeybee PMC. Similar mechanisms have been found to be important for processing temporal stimuli in crickets and moths (Ai et al. 2018) and in Drosophila (Yamada et al. 2018). This underlines the relevance of such mechanisms for temporal processing of stimuli in insects.

CHALLENGES

State of research

The vibration patterns produced during waggle dance communication in honeybees were recorded and characterized in detail by the early '60s (Wenner 1962; Esch 1961) leading to the suspicion that sound was essential for waggle dance communication (von Frisch 1967, Page 58). However, extensive evidence that particular sound patterns were crucial for waggle dance recruitment was available only by the early '90s (Kirchner 1993). Around the same time, it was also discovered that honeybees could perceive airborne sounds with the antenna and specifically, using the JO (Kirchner 1993). However, the investigation of the neural mechanisms underlying sound communication during waggle dance took off only during the late 2000s with the mechanical and neural characterization of the antenna and the JO (Tsujiuchi et al. 2007) as well as the topographic characterization of the JO sensory afferents in the honeybee brain (Ai et al. 2007). This was followed by the identification and characterization of neuron groups in the honeybee brain that were sensitive to antennal vibration and that arborized in the

same region as JO sensory afferents (Ai et al. 2009; Ai 2013). Thus, research into the neural substrates that process waggle dance vibration signals in the honeybee brain is currently at a nascent stage. The research presented in this thesis was part of the Japanese-German collaboration project "GinJang" (see Section 1.3.1), which continues this research, focusing on the identification and characterization of more vibration sensitive neurons in the honeybee brain, their network connectivity and their role in processing waggle dance vibration signals.

Challenges during experiments

Obtaining data for the characterization of vibration-sensitive neurons in the honeybee brain involved several challenging experimental techniques and conditions. At the Fukuoka University campus in Japan, where our experimental collaborators maintained the hives and conducted experiments, honeybees rarely ventured out of the hive during the period November-February due to cold temperatures and lack of flowers. This prevented experimentation for about a third of the year. Since the honeybee PMC is deep inside the brain, targeted insertion of electrodes into vibration sensitive neurons in the region was extremely challenging. Further, recording responses of neurons to antennal vibration required in-vivo experiments, which reduced the stability of recordings due to subtle head movements of the honeybee. These factors dragged down the rate at which experiments were successful in producing useful data to about ten percent.

**Challenges in segmenting and
    registering dendritic structures**

One of the goals of the doctoral research was the investigation of adaptations in the morphology of the vibration sensitive interneuron DL-Int-1 during maturation. DL-Int-1 has a dense arborization structure with dendrites from different secondary branches overlapping in the primary auditory center of the honeybee brain, specifically in the AMMC (see Figure 1.4a; also Figure 6E of Ikeno et al. (2018a)). This made the reconstruction of DL-Int-1 morphology using current automatic/semi-automatic neuron reconstruction methods challenging and led to the development of a new segmentation scheme for complex dendritic arbors (Ikeno et al. 2018a).
   Primary visual inspection of DL-Int-1 morphologies and comparison of morphometric measures indicated similar gross structure. However, fine-scale comparison of dendritic arborizations posed

challenges as individual morphologies had differing scales and rotations, due to differences in individual brains and tissue structures. This could be solved by transforming the morphologies such that they are spatially aligned. The Honeybee Standard Brain (Rybak 2010) could not be used for registering morphologies due to the lack of landmarks in the primary auditory center of the honeybee brain. As a result, a new method for registering neuron morphologies based on the maximization of volume overlap was developed, which is presented in Publication 1 (see Section 2.2).

LIMITATIONS

Sample number and statistical power

The success rate of experiments in generating useful data for Publication 2 from DL-Int-1 was low, about ten percent, due to experimental challenges and constraints. Further, the brains of newly emerged adult honeybees were soft and infirm, which made it difficult to maintain the electrode inside a DL-Int-1 neuron long enough to record sufficient electrophysiological data and inject a dye. The number of samples with usable data from newly emerged adult bees was therefore limited to six and we chose data of six forager DL-Int-1 to match them.

Studies with low sample size and issues with low statistical power are not uncommon in Neuroscience (Forstmeier et al. 2017; Button et al. 2013). The suggested course of action for studies like Publication 2 where low sample size is caused by experimental difficulties is to acknowledge the exploratory nature of the study along with its caveats and limitations.

In Publication 2, dendritic density in individual 3D voxels and average firing rates in different activity periods were statistically compared and the results for individual voxels and activity periods therefore suffer from low statistical power due to low sample size. However, the gross spatial pattern of change consisting of contiguous regions that show only increases or only decreases in dendritic density is more relevant than changes in individual voxels. Similarly, the change observed in the overall response pattern of DL-Int-1 is more relevant than the changes in firing rate of individual response periods.

Parameters of network simulations

The parameters used for network simulations in Publication 4 were tuned to qualitatively reproduce experimentally observed responses.

Although care was taken to maintain similarity between corresponding parameters for DL-Int-1 and DL-Int-2, the robustness and uniqueness of the parameters remain unclear and conducting more simulations that explore the effect of parameter perturbation on network behavior are required to address this issue.

Nature vs Nurture

The approach of Publication 2 is along the lines of the long-running "Nature vs Nurture" debate, which compares the effect of the environmental experiences and that of inherent genetic traits in shaping behavior (Institute of Medicine 2008). Adaptations presented in the morphology and physiology of DL-Int-1 during maturation can be caused by two factors – genetically programmed aging and foraging experience. Experiments with age-controlled honeybees that are caged throughout adulthood are needed to clarify the contribution of these two factors to the observed adaptations.

OUTLOOK

A large amount of data has been collected from different types of vibration sensitive honeybee neurons as part of the GinJang project between 2012 and 2014 (see Table 1 of Ai et al. 2017). A large part of this data has been analyzed to investigate the properties of DL-Int-1 and other interneurons and published in Publications 2, 3 and 4. However, more analyses are possible with the data for studying the properties of neurons that have not yet been published as well as some unanalyzed aspects of neurons that have been published. As part of publication 2, a data pipeline[1] has been developed in Python for parsing experimental metadata and electrophysiological traces as well as for annotating and organizing data to facilitate quick and easy analysis. This pipeline can be useful in analyzing existing and future data.

Electrophysiological data was recorded in the GinJang project using the software Spike2[2] (CED, Cambridge UK), which is proprietary. As none of the available free and open source alternatives was suitable for the visualization of the acquired data, a tool was developed during the thesis for this purpose[3]. This tool can be useful for quick inspection of recorded data.

Publication 4 proposes a putative disinhibitory network in the honeybee PMC for processing waggle dance sounds. This network

---

1 https://github.com/wachtlerlab/GJEphys
2 http://ced.co.uk/products/spkovin
3 https://github.com/wachtlerlab/GJEMSRDViewer

consists of DL-Int-1, DL-Int-2 and a yet-to-be-identified local inhibitory neuron. Analyses of collected data, as well as more experiments, are required to clarify the identity of this neuron and investigate more aspects of the proposed network.

BENEFITS OF OPEN TOOLS AND DATABASES

The need for promoting the use of open source tools and databases in neuroscience has been greatly discussed over the last two decades (Eckersley et al. 2003; Liu and Ascoli 2007; Herz et al. 2008; Teeters et al. 2008; Sejnowski et al. 2014; Ferguson et al. 2014; Morey et al. 2016; Gleeson et al. 2017). Benefits of a research culture based on public sharing of tools and data include better reproducibility of results, easier combination of data for tackling larger questions, increased tool reuse, improved cross-verification of results and easier collaboration. Recently, several open databases have come up[4], principles for standardizing research databases have been established (Wilkinson et al. 2016) and journals are encouraging authors to make their data and tools public. Issues hindering such an open research culture have been identified and recommendations have been submitted to the scientific community and funding agencies[5].

Most of the research for this thesis was done in close collaboration with the German Neuroinformatics Node (G-Node[6]), which provided me with an understanding of the need for the use of open source tools and databases in computational neuroscience research. Open data markup language (odML[7], Grewe et al. 2011) and Neuroscience information exchange format (NIX[8], Stoewer et al. 2014) were used to organize and label electrophysiological traces along with experimental metadata in a way that makes it quick and easy to fetch select parts of the recorded traces for analysis. G-Node data infrastructure service (GIN[9]) was used for data sharing among the members of the Ginjang project located in Japan and Germany. This service has been extremely helpful in the quick transfer of data during research and also as an easily sharable long term repository for all the data of the project.

The `neuromorpho.org` database for neuron morphologies (Ascoli 2006) was crucial during the development of Reg-MaxS-N

---

4 `http://home.earthlink.net/~perlewitz/database.html`
5 `http://www.potomacinstitute.org/images/stories/publications/`
`NeuroAndDataSharingReport2014.pdf`
6 `g-node.org`
7 `https://g-node.github.io/python-odml/`
8 `http://g-node.github.io/nix/`
9 `https://web.gin.g-node.org`

(see Section 2.2). The database provides access to a large number of morphologies with widely varying features, which played an important role in the exploration of ideas during the conception of the algorithm as well as during its validation. DL–Int-1 morphologies reconstructed for Publication 2 have been uploaded to the `neuromorpho.org` database. NBLAST (Costa et al. 2016) and its web service[10] from the Jefferis lab at the University of Cambridge was vital for the visualization and selection of Drosophila neurons for the validation of Reg-MaxS-N. Prof. Jefferis shared the data used for the NBLAST paper before it was published and this data played an important role in the validation of Reg-MaxS-N.

---

10 `http://flybrain.mrc-lmb.cam.ac.uk/si/nblast/www/`

REFERENCES

Acciai, L., Soda, P., and Iannello, G. (2016). "Automated Neuron Tracing Methods: An Updated Account." In: *Neuroinformatics* 14.4, pp. 353–367. doi: `10.1007/s12021-016-9310-0`.

Ai, H. (2013). "Sensors and Sensory Processing for Airborne Vibrations in Silk Moths and Honeybees." In: *Sensors* 13.7, pp. 9344–9363. doi: `10.3390/s130709344`.

Ai, H. and Itoh, T. (2012). "The Auditory System of the Honey Bee." In: *Honeybee Neurobiology and Behavior: A Tribute to Randolf Menzel*. Ed. by C. G. Galizia, D. Eisenhardt, and M. Giurfa. Springer Netherlands, pp. 269–283. doi: `10.1007/978-94-007-2099-2_21`.

Ai, H., Kai, K., Kumaraswamy, A., Ikeno, H., and Wachtler, T. (2017). "Interneurons in the honeybee primary auditory center responding to waggle dance-like vibration pulses." In: *The Journal of Neuroscience* 37.44, pp. 0044–17. doi: `10.1523/JNEUROSCI.0044-17.2017`.

Ai, H., Kumaraswamy, A., Kohashi, T., Ikeno, H., and Wachtler, T. (2018). "Inhibitory Pathways for Processing the Temporal Structure of Sensory Signals in the Insect Brain." In: *Frontiers in Psychology* 9. doi: `10.3389/fpsyg.2018.01517`.

Ai, H., Nishino, H., and Itoh, T. (2007). "Topographic organization of sensory afferents of Johnston's organ in the honeybee brain." In: *The Journal of Comparative Neurology* 502.6, pp. 1030–1046. doi: `10.1002/cne.21341`.

Ai, H., Rybak, J., Menzel, R., and Itoh, T. (2009). "Response characteristics of vibration-sensitive interneurons related to Johnston's organ in the honeybee,Apis mellifera." In: *The Journal of Comparative Neurology* 515.2, pp. 145–160. doi: `10.1002/cne.22042`.

Ascoli, G. A. (2006). "Mobilizing the base of neuroscience data: the case of neuronal morphologies." In: *Nature Reviews Neuroscience* 7.4, pp. 318–324. doi: `10.1038/nrn1885`.

Beggs, K. T., Glendining, K. A., Marechal, N. M., Vergoz, V., Nakamura, I., Slessor, K. N., and Mercer, A. R. (2007). "Queen pheromone modulates brain dopamine function in worker honey bees." In: *Proceedings of the National Academy of Sciences* 104.7, pp. 2460–2464. doi: `10.1073/pnas.0608224104`.

Briggman, K. L. and Bock, D. D. (2012). "Volume electron microscopy for neuronal circuit reconstruction." In: *Current Opin-*

ion in Neurobiology 22.1, pp. 154–161. doi: `10.1016/j.conb.2011.10.022`.

Button, K. S., Ioannidis, J. P. A., Mokrysz, C., Nosek, B. A., Flint, J., Robinson, E. S. J., and Munafò, M. R. (2013). "Power failure: why small sample size undermines the reliability of neuroscience." In: *Nature Reviews Neuroscience* 14.5, pp. 365–376. doi: `10.1038/nrn3475`.

Cannon, R., Turner, D., Pyapali, G., and Wheal, H. (1998). "An online archive of reconstructed hippocampal neurons." In: *Journal of Neuroscience Methods* 84.1-2, pp. 49–54. doi: `10.1016/s0165-0270(98)00091-0`.

Chen, E., McLeod, A. J., Baxter, J. S. H., and Peters, T. M. (2015). "Registration of 3D shapes under anisotropic scaling." In: *International Journal of Computer Assisted Radiology and Surgery* 10.6, pp. 867–878. doi: `10.1007/s11548-015-1199-9`.

Chen, Y. et al. (2017). "A biologically inspired, flapping-wing, hybrid aerial-aquatic microrobot." In: *Science Robotics* 2.11, eaao5619. doi: `10.1126/scirobotics.aao5619`.

Chittka, L. (2004). "Dances as Windows into Insect Perception." In: *PLOS Biology* 2.7. doi: `10.1371/journal.pbio.0020216`.

Claridge, M. (2005). "Insect Sounds and Communication — An Introduction." In: *Insect Sounds and Communication*. CRC Press, pp. 3–10. doi: `10.1201/9781420039337`.

Coskren, P. J., Luebke, J. I., Kabaso, D., Wearne, S. L., Yadav, A., Rumbell, T., Hof, P. R., and Weaver, C. M. (2014). "Functional consequences of age-related morphologic changes to pyramidal neurons of the rhesus monkey prefrontal cortex." In: *Journal of Computational Neuroscience* 38.2, pp. 263–283. doi: `10.1007/s10827-014-0541-5`.

Costa, M., Manton, J. D., Ostrovsky, A. D., Prohaska, S., and Jefferis, G. S. (2016). "NBLAST: Rapid, Sensitive Comparison of Neuronal Structure and Construction of Neuron Family Databases." In: *Neuron* 91.2, pp. 293–311. doi: `10.1016/j.neuron.2016.06.012`.

Cuntz, H., Forstner, F., Haag, J., and Borst, A. (2008). "The Morphological Identity of Insect Dendrites." In: *PLoS Computational Biology* 4.12. Ed. by K. J. Friston, e1000251. doi: `10.1371/journal.pcbi.1000251`.

Devaud, J. M. and Masson, C. (1999). "Dendritic pattern development of the honeybee antennal lobe neurons: a laser scanning confocal microscopic study." In: *Journal of Neurobiology* 39.4, pp. 461–474. doi: `10.1002/(SICI)1097-4695(19990615)39:4<461::AID-NEU1>3.0.CO;2-F`.

Donohue, D. E. and Ascoli, G. A. (2011). "Automated reconstruction of neuronal morphology: An overview." In: *Brain Research*

Reviews 67.1-2, pp. 94–102. doi: `10.1016/j.brainresrev.2010.11.003`.

Eckersley, P. et al. (2003). "Neuroscience data and tool sharing." In: *Neuroinformatics* 1.2, pp. 149–165. doi: `10.1007/s12021-003-0002-1`.

Esch, H. (1961). "Über die Schallerzeugung beim Werbetanz der Honigbiene." In: *Zeitschrift für Vergleichende Physiologie* 45.1, pp. 1–11. doi: `10.1007/bf00297754`.

Evans, A. C., Janke, A. L., Collins, D. L., and Baillet, S. (2012). "Brain templates and atlases." In: *NeuroImage* 62.2, pp. 911–922. doi: `10.1016/j.neuroimage.2012.01.024`.

Farina, W. M., Grüter, C., and Arenas, A. (2011). "Olfactory Information Transfer During Recruitment in Honey Bees." In: *Honeybee Neurobiology and Behavior*. Springer Netherlands, pp. 89–101. doi: `10.1007/978-94-007-2099-2_8`.

Farina, W. M. and Wainselboim, A. J. (2005). "Trophallaxis within the dancing context: a behavioral and thermographic analysis in honeybees (Apis mellifera)." In: *Apidologie* 36.1, pp. 43–47. doi: `10.1051/apido:2004069`.

Farris, S. M., Robinson, G. E., and Fahrbach, S. E. (2001). "Experience- and Age-Related Outgrowth of Intrinsic Neurons in the Mushroom Bodies of the Adult Worker Honeybee." In: *Journal of Neuroscience* 21.16, pp. 6395–6404. doi: `10.1523/JNEUROSCI.21-16-06395.2001`.

Feng, L., Zhao, T., and Kim, J. (2015). "neuTube 1.0: A New Design for Efficient Neuron Reconstruction Software Based on the SWC Format." In: *eNeuro* 2.1. doi: `10.1523/eneuro.0049-14.2014`.

Ferguson, A. R., Nielson, J. L., Cragin, M. H., Bandrowski, A. E., and Martone, M. E. (2014). "Big data from small data: Data-sharing in the 'long tail' of neuroscience." In: *Nature Neuroscience* 17.11, pp. 1442–1447. doi: `10.1038/nn.3838`.

Forstmeier, W., Wagenmakers, E.-J., and Parker, T. H. (2017). "Detecting and avoiding likely false-positive findings – a practical guide." In: *Biological Reviews* 92.4, pp. 1941–1968. doi: `10.1111/brv.12315`.

Gardner, K. E., Seeley, T. D., and Calderone, N. W. (2008). "Do honeybees have two discrete dances to advertise food sources?" In: *Animal Behaviour* 75.4, pp. 1291–1300. doi: `10.1016/j.anbehav.2007.09.032`.

Glaser, J. R. and Glaser, E. M. (1990). "Neuron imaging with neurolucida — A PC-based system for image combining microscopy." In: *Computerized Medical Imaging and Graphics* 14.5, pp. 307–317. doi: `10.1016/0895-6111(90)90105-k`.

Gleeson, P., Davison, A. P., Silver, R. A., and Ascoli, G. A. (2017). "A Commitment to Open Source in Neuroscience." In: *Neuron* 96.5, pp. 964–965. doi: `10.1016/j.neuron.2017.10.013`.

Grewe, J., Wachtler, T., and Benda, J. (2011). "A Bottom-up Approach to Data Annotation in Neurophysiology." In: *Frontiers in Neuroinformatics* 5. doi: `10.3389/fninf.2011.00016`.

Groh, C. and Meinertzhagen, I. A. (2010). "Brain plasticity in Diptera and Hymenoptera." In: *Frontiers in Bioscience* S2.1, pp. 268–288. doi: `10.2741/s63`.

Gronenberg, W. (2001). "Subdivisions of hymenopteran mushroom body calyces by their afferent supply." In: *Journal of Comparative Neurology* 435.4, pp. 474–489. doi: `10.1002/cne.1045`.

Henry, C. S. (2005). "Acoustic Communication in Neuropterid Insects." In: *Insect Sounds and Communication*. CRC Press, pp. 153–167. doi: `10.1201/9781420039337`.

Heran, H. (1959). "Wahrnehmung und Regelung der Flugeigengeschwindigkeit bei Apis mellifica L." In: *Zeitschrift für vergleichende Physiologie* 42.2, pp. 103–163. doi: `10.1007/BF00298733`.

Herz, A. V., Meier, R., Nawrot, M. P., Schiegel, W., and Zito, T. (2008). "G-Node: An integrated tool-sharing platform to support cellular and systems neurophysiology in the age of global neuroinformatics." In: *Neural Networks* 21.8, pp. 1070–1075. doi: `10.1016/j.neunet.2008.05.011`.

Hrncir, M., Maia-Silva, C., Cabe, S. I. M., and Farina, W. M. (2011). "The recruiter's excitement - features of thoracic vibrations during the honey bee's waggle dance related to food source profitability." In: *Journal of Experimental Biology* 214.23, pp. 4055–4064. doi: `10.1242/jeb.063149`.

Hrncir, M., Barth, F., and Tautz, J. (2005). "Vibratory and Airborne-Sound Signals in Bee Communication (Hymenoptera)." In: *Insect Sounds and Communication*. CRC Press, pp. 421–436. doi: `10.1201/9781420039337`.

Ikeno, H., Kumaraswamy, A., Kai, K., Wachtler, T., and Ai, H. (2018a). "A Segmentation Scheme for Complex Neuronal Arbors and Application to Vibration Sensitive Neurons in the Honeybee Brain." In: *Frontiers in Neuroinformatics* 12, p. 61. issn: 1662-5196. doi: `10.3389/fninf.2018.00061`.

Ikeno, H., Uenohara, Y., Goto, K., Tanaka, S., Kumaraswamy, A., Wachtler, T., Kai, K., and Ai, H. (2018b). "Construction of standard brain map of honeybee brain region related to vibration stimulus processing [version 1; not peer reviewed]." In: *Neuroinformatics 2018*. doi: `10.12751/incf.ni2018.0031`.

Institute of Medicine (2008). *From Molecules to Minds: Challenges for the 21st Century: Workshop Summary*. Ed. by M. Hougan

and B. Altevogt. The National Academies Press. doi: `10.17226/12220`.

Ishikawa, Y. and Kamikouchi, A. (2016). "Auditory system of fruit flies." In: *Hearing Research* 338, pp. 1–8. doi: `https://doi.org/10.1016/j.heares.2015.10.017`.

Jones, T. A., Donlan, N. A., and O'Donnell, S. (2009). "Growth and pruning of mushroom body Kenyon cell dendrites during worker behavioral development in the paper wasp, Polybia aequatorialis (Hymenoptera: Vespidae)." In: *Neurobiology of Learning and Memory* 92.4, pp. 485–495. doi: `10.1016/j.nlm.2009.06.007`.

Kirchner, W. H. (1993). "Acoustical communication in honeybees." In: *Apidologie* 24.3, pp. 297–307. doi: `10.1051/apido:19930309`.

Kiya, T., Kunieda, T., and Kubo, T. (2007). "Increased Neural Activity of a Mushroom Body Neuron Subtype in the Brains of Forager Honeybees." In: *PLoS ONE* 2.4. Ed. by M. Giurfa, e371. doi: `10.1371/journal.pone.0000371`.

Kumaraswamy, A. (2018a). *Library and scripts for analyzing morphologies of GinJang Project.* Github. Online code repository, version 0.2. url: `https://github.com/wachtlerlab/GJMorph`.

Kumaraswamy, A. (2018b). *Library and scripts for processing and analyzing electrophysiology data of Ginjang Project.* Github. Online code repository, version 0.2. url: `https://github.com/wachtlerlab/GJEphys`.

Kumaraswamy, A. (2018c). *Reg-MaxS and Reg-MaxS-N: Algorithms for co-registration of pairs and groups of neuron morphologies based on maximization of spatial overlap.* G-Node. Online Dataset. doi: `10.12751/g-node.feee47`.

Kumaraswamy, A., Ai, H., Kai, K., Ikeno, H., and Wachtler, T. (2019a). "Adaptations during maturation in an identified honeybee interneuron responsive to waggle dance vibration signals." In: *eNeuro* 6.5. doi: `10.1523/eneuro.0454-18.2019`.

Kumaraswamy, A., Ai, H., Kai, K., Ikeno, H., and Wachtler, T. (2019b). *Morphological reconstructions and electrophysiological recordings of vibration sensitive honeybee neurons belonging to two maturation levels.* G-Node. Online Dataset. doi: `10.12751/g-node.e70cb4`.

Kumaraswamy, A., Kai, K., Ai, H., Ikeno, H., and Wachtler, T. (2018). "Spatial registration of neuron morphologies based on maximization of volume overlap." In: *BMC Bioinformatics* 19, pp. 1–16. doi: `10.1186/s12859-018-2136-z`.

Kumaraswamy, A., Maksutov, A., Kai, K., Ai, H., Ikeno, H., and Wachtler, T. (2017a). "Network simulations of interneuron cir-

cuits in the honeybee primary auditory center." In: *bioRxiv*. doi: `10.1101/159533`.

Kumaraswamy, A., Maksutov, A., Kai, K., Ai, H., Ikeno, H., and Wachtler, T. (2017b). *Network simulations of interneuron circuits in the honeybee primary auditory center*. G-Node. Online Dataset. doi: `10.12751/g-node.1090f8`.

Landgraf, T. (2013). "RoboBee: A Biomimetic Honeybee Robot for the Analysis of the Dance Communication System." PhD thesis. Freie Universität Berlin. url: `https://refubium.fu-berlin.de/handle/fub188/10713`.

Landgraf, T., Rojas, R., Nguyen, H., Kriegel, F., and Stettin, K. (2011). "Analysis of the Waggle Dance Motion of Honeybees for the Design of a Biomimetic Honeybee Robot." In: *PLoS ONE* 6.8. Ed. by H. G. Krapp, e21354. doi: `10.1371/journal.pone.0021354`.

Langhammer, C. G., Previtera, M. L., Sweet, E. S., Sran, S. S., Chen, M., and Firestein, B. L. (2010). "Automated Sholl analysis of digitized neuronal morphology at multiple scales: Whole cell Sholl analysis versus Sholl analysis of arbor subregions." In: *Cytometry Part A* 77A.12, pp. 1160–1168. doi: `10.1002/cyto.a.20954`.

Levine, R. B. (1986). "Reorganization of the insect nervous system during metamorphosis." In: *Trends in Neurosciences* 9, pp. 315–319. doi: `https://doi.org/10.1016/0166-2236(86)90096-2`.

Lindauer, M. (1987). "Introduction." In: *Neurobiology and Behavior of Honeybees*. Springer Berlin Heidelberg, pp. 1–6. doi: `10.1007/978-3-642-71496-2_1`.

Liu, Y. and Ascoli, G. A. (2007). "Value Added by Data Sharing: Long-Term Potentiation of Neuroscience Research." In: *Neuroinformatics* 5.3, pp. 143–145. issn: 1559-0089. doi: `10.1007/s12021-007-0009-0`.

Livet, J., Weissman, T. A., Kang, H., Draft, R. W., Lu, J., Bennis, R. A., Sanes, J. R., and Lichtman, J. W. (2007). "Transgenic strategies for combinatorial expression of fluorescent proteins in the nervous system." In: *Nature* 450.7166, pp. 56–62. doi: `10.1038/nature06293`.

Livneh, Y. and Mizrahi, A. (2010). "A time for atlases and atlases for time." In: *Frontiers in Systems Neuroscience* 3, p. 17. doi: `10.3389/neuro.06.017.2009`.

Magliaro, C., Callara, A. L., Vanello, N., and Ahluwalia, A. (2017). "A Manual Segmentation Tool for Three-Dimensional Neuron Datasets." In: *Frontiers in Neuroinformatics* 11. doi: `10.3389/fninf.2017.00036`.

Maier-Hein, L., Franz, A. M., Santos, T. R. dos, Schmidt, M., Fangerau, M., Meinzer, H., and Fitzpatrick, J. M. (2012).

"Convergent Iterative Closest-Point Algorithm to Accomodate Anisotropic and Inhomogenous Localization Error." In: *IEEE Transactions on Pattern Analysis and Machine Intelligence* 34.8, pp. 1520–1532. doi: `10.1109/tpami.2011.248`.

Meijering, E. (2010). "Neuron tracing in perspective." In: *Cytometry Part A* 77A.7, pp. 693–704. doi: `10.1002/cyto.a.20895`.

Menzel, R., ed. (2012a). *Digital brain atlases*. Frontiers Media SA. doi: `10.3389/978-2-88919-031-7`.

Menzel, R. (2012b). "The honeybee as a model for understanding the basis of cognition." In: *Nature Reviews Neuroscience* 13.11, pp. 758–768. doi: `10.1038/nrn3357`.

Michelsen, A. (2003). "Signals and flexibility in the dance communication of honeybees." In: *Journal of Comparative Physiology A* 189.3, pp. 165–174. issn: 1432-1351. doi: `10.1007/s00359-003-0398-y`.

Michelsen, A., Andersen, B. B., Storm, J., Kirchner, W. H., and Lindauer, M. (1992). "How honeybees perceive communication dances, studied by means of a mechanical model." In: *Behavioral Ecology and Sociobiology* 30.3-4, pp. 143–150. doi: `10.1007/bf00166696`.

Mizrahi, A., Ben-Ner, E., Katz, M. J., Kedem, K., Glusman, J. G., and Libersat, F. (2000). "Comparative analysis of dendritic architecture of identified neurons using the Hausdorff distance metric." In: *The Journal of comparative neurology* 422.3, pp. 415–428. issn: 0021-9967. doi: `10.1002/1096-9861(20000703)422:3<415::AID-CNE8>3.0.CO;2-T`.

Morey, R. D. et al. (2016). "The Peer Reviewers' Openness Initiative: incentivizing open research practices through peer review." In: *Royal Society Open Science* 3.1, p. 150547. doi: `10.1098/rsos.150547`.

Munz, T. (2005). "The Bee Battles: Karl von Frisch, Adrian Wenner and the Honey Bee Dance Language Controversy." In: *Journal of the History of Biology* 38.3, pp. 535–570. doi: `10.1007/s10739-005-0552-1`.

O'Neill, K. M., Akum, B. F., Dhawan, S. T., Kwon, M., Langhammer, C. G., and Firestein, B. L. (2015). "Assessing effects on dendritic arborization using novel Sholl analyses." In: *Frontiers in Cellular Neuroscience* 9. doi: `10.3389/fncel.2015.00285`.

Peng, H., Hawrylycz, M., Roskams, J., Hill, S., Spruston, N., Meijering, E., and Ascoli, G. (2015). "BigNeuron: Large-Scale 3D Neuron Reconstruction from Optical Microscopy Images." In: *Neuron* 87.2, pp. 252–256. doi: `10.1016/j.neuron.2015.06.036`.

Peng, H., Ruan, Z., Long, F., Simpson, J. H., and Myers, E. W. (2010). "V3D enables real-time 3D visualization and quantitative

analysis of large-scale biological image data sets." In: *Nature Biotechnology* 28.4, pp. 348–353. doi: `10.1038/nbt.1612`.

Robinson, G. E. (1992). "Regulation of Division of Labor in Insect Societies." In: *Annual Review of Entomology* 37.1. PMID: 1539941, pp. 637–665. doi: `10.1146/annurev.en.37.010192.003225`.

Rybak, J. (2010). "The digital bee brain: integrating and managing neurons in a common 3D reference system." In: *Frontiers in Systems Neuroscience*. doi: `10.3389/fnsys.2010.00030`.

Sabo, C., Chisholm, R., Petterson, A., and Cope, A. (2017). "A lightweight, inexpensive robotic system for insect vision." In: *Arthropod Structure & Development* 46.5. From Insects to Robots, pp. 689–702. issn: 1467-8039. doi: `10.1016/j.asd.2017.08.001`.

Sanderson, M. J., Smith, I., Parker, I., and Bootman, M. D. (2014). "Fluorescence Microscopy." In: *Cold Spring Harbor Protocols* 2014.10, pdb.top071795–pdb.top071795. doi: `10.1101/pdb.top071795`.

Scorcioni, R., Polavaram, S., and Ascoli, G. A. (2008). "L-Measure: a web-accessible tool for the analysis, comparison and search of digital reconstructions of neuronal morphologies." In: *Nature Protocols* 3.5, pp. 866–876. doi: `10.1038/nprot.2008.51`.

Seeley, T. D. (1985). "The Honeybee Societies." In: *Honeybee Ecology*. Princeton University Press. doi: `10.1515/9781400857876.20`.

Seeley, T. D. (1996). *The Wisdom of the Hive: The Social Physiology of Honey Bee Colonies*. Harvard University Press. url: `http://www.hup.harvard.edu/catalog.php?isbn=9780674953765`.

Seeley, T. D., Mikheyev, A. S., and Pagano, G. J. (2000). "Dancing bees tune both duration and rate of waggle-run production in relation to nectar-source profitability." In: *Journal of Comparative Physiology A: Sensory, Neural, and Behavioral Physiology* 186.9, pp. 813–819. doi: `10.1007/s003590000134`.

Sejnowski, T. J., Churchland, P. S., and Movshon, J. A. (2014). "Putting big data to good use in neuroscience." In: *Nature Neuroscience* 17.11, pp. 1440–1441. doi: `10.1038/nn.3839`.

Sholl, D. A. (1953). "Dendritic organization in the neurons of the visual and motor cortices of the cat." In: *Journal of Anatomy* 87.4, pp. 387–406. url: `https://www.ncbi.nlm.nih.gov/pmc/articles/PMC1244622`.

Sigrist, S. J. and Sabatini, B. L. (2012). "Optical super-resolution microscopy in neurobiology." In: *Current Opinion in Neurobiology* 22.1, pp. 86–93. doi: `10.1016/j.conb.2011.10.014`.

Srinivasan, M. V. (2010). "Honey Bees as a Model for Vision, Perception, and Cognition." In: *Annual Review of Entomology* 55.1, pp. 267–284. doi: `10.1146/annurev.ento.010908.164537`.

Srinivasan, M. V. (2011). "Honeybees as a Model for the Study of Visually Guided Flight, Navigation, and Biologically Inspired Robotics." In: *Physiological Reviews* 91.2, pp. 413–460. doi: `10.1152/physrev.00005.2010`.

Stoewer, A., Kellner, C., Benda, J., Wachtler, T., and Grewe, J. (2014). "File format and library for neuroscience data and metadata." In: *Frontiers in Neuroinformatics* 8. doi: `10.3389/conf.fninf.2014.18.00027`.

Tavosanis, G. (2012). "Dendritic structural plasticity." In: *Developmental Neurobiology* 72.1, pp. 73–86. doi: `10.1002/dneu.20951`.

Taylor, G. J., Luu, T., Ball, D., and Srinivasan, M. V. (2013). "Vision and air flow combine to streamline flying honeybees." In: *Scientific Reports* 3.1. doi: `10.1038/srep02614`.

Teeters, J. L., Harris, K. D., Millman, K. J., Olshausen, B. A., and Sommer, F. T. (2008). "Data Sharing for Computational Neuroscience." In: *Neuroinformatics* 6.1, pp. 47–55. doi: `10.1007/s12021-008-9009-y`.

Thom, C., Gilley, D. C., Hooper, J., and Esch, H. E. (2007). "The Scent of the Waggle Dance." In: *PLoS Biology* 5.9. Ed. by L. Chittka, e228. doi: `10.1371/journal.pbio.0050228`.

Torben-Nielsen, B. (2014). "An Efficient and Extendable Python Library to Analyze Neuronal Morphologies." In: *Neuroinformatics* 12.4, pp. 619–622. doi: `10.1007/s12021-014-9232-7`.

Tsujiuchi, S., Sivan-Loukianova, E., Eberl, D. F., Kitagawa, Y., and Kadowaki, T. (2007). "Dynamic Range Compression in the Honey Bee Auditory System toward Waggle Dance Sounds." In: *PLoS ONE* 2.2. Ed. by M. Giurfa, e234. doi: `10.1371/journal.pone.0000234`.

Turner, J. N., Swann, J. W., Szarowski, D. H., Smith, K. L., Carpenter, D. O., and Fejtl, M. (1993). "Chapter 13 Three-Dimensional Confocal Light Microscopy of Neurons: Fluorescent and Reflection Stains." In: *Methods in Cell Biology*. Elsevier, pp. 345–366. doi: `10.1016/s0091-679x(08)61010-9`.

Uylings, H. B. M. and Pelt, J. van (2002). "Measures for quantifying dendritic arborizations." In: *Network: Computation in Neural Systems* 13.3, pp. 397–414. doi: `10.1088/0954-898x_13_3_309`.

Vaughan, A. G., Zhou, C., Manoli, D. S., and Baker, B. S. (2014). "Neural Pathways for the Detection and Discrimination of Conspecific Song in D. melanogaster." In: *Current Biology* 24.10,

pp. 1039–1049. doi: `https://doi.org/10.1016/j.cub.2014.03.048`.

Visscher, P. K. (2007). "Group Decision Making in Nest-Site Selection Among Social Insects." In: *Annual Review of Entomology* 52.1, pp. 255–275. doi: `10.1146/annurev.ento.51.110104.151025`.

von Frisch, K. (1965). *Tanzsprache und Orientierung der Bienen*. Springer Berlin Heidelberg. doi: `10.1007/978-3-642-94916-6`.

von Frisch, K. (1967). *The Dance Language and Orientation of Bees*. Harvard University Press. doi: `10.4159/harvard.9780674418776`.

von Frisch, K. (1973). *Erinnerungen eines Biologen*. Springer Berlin Heidelberg. doi: `10.1007/978-3-642-61968-7`.

Wan, Y., Long, F., Qu, L., Xiao, H., Hawrylycz, M., Myers, E. W., and Peng, H. (2015). "BlastNeuron for Automated Comparison, Retrieval and Clustering of 3D Neuron Morphologies." In: *Neuroinformatics* 13.4, pp. 487–499. doi: `10.1007/s12021-015-9272-7`.

Wang, S., Zhang, S., Sato, K., and Srinivasan, M. V. (2005). "Maturation of odor representation in the honeybee antennal lobe." In: *Journal of Insect Physiology* 51.11, pp. 1244–1254. doi: `10.1016/j.jinsphys.2005.07.003`.

Wenner, A. M. (1962). "Sound production during the waggle dance of the honey bee." In: *Animal Behaviour* 10.1-2, pp. 79–95. doi: `10.1016/0003-3472(62)90135-5`.

Wilkinson, M. D. et al. (2016). "The FAIR Guiding Principles for scientific data management and stewardship." In: *Scientific Data* 3, p. 160018. doi: `10.1038/sdata.2016.18`.

Xing, B. and Gao, W.-J. (2014). "Bee Inspired Algorithms." In: *Innovative Computational Intelligence: A Rough Guide to 134 Clever Algorithms*. Cham: Springer International Publishing, pp. 45–80. isbn: 978-3-319-03404-1. doi: `10.1007/978-3-319-03404-1_4`.

Yack, J. E. (2004). "The structure and function of auditory chordotonal organs in insects." In: *Microscopy Research and Technique* 63.6, pp. 315–337. doi: `10.1002/jemt.20051`.

Yamada, D., Ishimoto, H., Li, X., Kohashi, T., Ishikawa, Y., and Kamikouchi, A. (2018). "GABAergic Local Interneurons Shape Female Fruit Fly Response to Mating Songs." In: *The Journal of Neuroscience* 38.18, pp. 4329–4347. doi: `10.1523/jneurosci.3644-17.2018`.

ASSOCIATED PUBLISHED RESOURCES

PAPERS

1. Kumaraswamy, A., Ai, H., Kai, K., Ikeno, H., and Wachtler, T. (2019a). "Adaptations during maturation in an identified honeybee interneuron responsive to waggle dance vibration signals." In: *eNeuro* 6.5. doi: `10.1523/eneuro.0454-18.2019`

2. Ikeno, H., Kumaraswamy, A., Kai, K., Wachtler, T., and Ai, H. (2018a). "A Segmentation Scheme for Complex Neuronal Arbors and Application to Vibration Sensitive Neurons in the Honeybee Brain." In: *Frontiers in Neuroinformatics* 12, p. 61. issn: 1662-5196. doi: `10.3389/fninf.2018.00061`

3. Ai, H., Kumaraswamy, A., Kohashi, T., Ikeno, H., and Wachtler, T. (2018). "Inhibitory Pathways for Processing the Temporal Structure of Sensory Signals in the Insect Brain." In: *Frontiers in Psychology* 9. doi: `10.3389/fpsyg.2018.01517`

4. Kumaraswamy, A., Kai, K., Ai, H., Ikeno, H., and Wachtler, T. (2018). "Spatial registration of neuron morphologies based on maximization of volume overlap." In: *BMC Bioinformatics* 19, pp. 1–16. doi: `10.1186/s12859-018-2136-z`

5. Ai, H., Kai, K., Kumaraswamy, A., Ikeno, H., and Wachtler, T. (2017). "Interneurons in the honeybee primary auditory center responding to waggle dance-like vibration pulses." In: *The Journal of Neuroscience* 37.44, pp. 0044–17. doi: `10.1523/JNEUROSCI.0044-17.2017`

6. [preprint] Kumaraswamy, A., Maksutov, A., Kai, K., Ai, H., Ikeno, H., and Wachtler, T. (2017a). "Network simulations of interneuron circuits in the honeybee primary auditory center." In: *bioRxiv*. doi: `10.1101/159533`

DATASETS

1. Kumaraswamy, A., Ai, H., Kai, K., Ikeno, H., and Wachtler, T. (2019b). *Morphological reconstructions and electrophysiological recordings of vibration sensitive honeybee neurons belonging to two maturation levels.* G-Node. Online Dataset. doi: `10.12751/g-node.e70cb4`

CODE REPOSITORIES

1. Kumaraswamy, A. (2018b). *Library and scripts for processing and analyzing electrophysiology data of Ginjang Project.* Github. Online code repository, version 0.2. url: `https://github.com/wachtlerlab/GJEphys`

2. Kumaraswamy, A. (2018a). *Library and scripts for analyzing morphologies of GinJang Project.* Github. Online code repository, version 0.2. url: `https://github.com/wachtlerlab/GJMorph`

3. Kumaraswamy, A. (2018c). *Reg-MaxS and Reg-MaxS-N: Algorithms for co-registration of pairs and groups of neuron morphologies based on maximization of spatial overlap.* G-Node. Online Dataset. doi: `10.12751/g-node.feee47`

4. Kumaraswamy, A., Maksutov, A., Kai, K., Ai, H., Ikeno, H., and Wachtler, T. (2017b). *Network simulations of interneuron circuits in the honeybee primary auditory center.* G-Node. Online Dataset. doi: `10.12751/g-node.1090f8`

ACKNOWLEDGMENTS

Ajayrama Kumaraswamy

Curriculum vitae

Education

2013–present **Doctoral Studies**, **Ludwig-Maximilians-Universität**, München, Germany.
Specialization — Computational Neuroscience

2011–2013 **Master of Engineering**, **Indian Institute of Science**, Bangalore, India, *GPA: 6.8/8.0*.
Specialization — Signal Processing.

2007–2011 **Bachelor of Technology**, **National Institute of Technology**, Surathkal, India, *GPA: 9.23/10.0*.
Specialization — Electrical and Electronics Engineering.

Research Experience

Doctoral Thesis

2013–present **Analysis of honeybee interneurons responsive to waggle dance vibration signals: adaptations during maturation and network simulations**.
under the supervision of PD Dr. Thomas Wachtler, Dept. Biologie II, LMU

- Comparing electrical responses and 3D structures of nerve cells from young and mature honeybees

- Developed and validated an algorithm for spatially aligning 3D strutures of nerve cells in Python; journal paper published

- Developed a pipeline for processing 1D electrical response data of nerve cells using metadata management, filtering and reliable peak detection

- Set up and ran multiple nerve cell simulations using local desktops and remote high performance compute servers

- Proposed and supervised three short-term student projects

Visiting Researcher

March 2017 –July 2017	**Reconstruction of neuronal structures and computational consulting**.

at the lab of Prof. Hiromu Tanimoto at Tohoku University, Sendai Japan

- Developed a framework for pre-processing and segmenting 3D images to compare 22 state-of-the-art algorithms in Python
- Drove the development of a preprocessing pipeline for 3D images; proposed and implemented scheme for measuring pipeline performance
- Enabled researchers to use new computational tools and methods

Conference Presentations

Poster	Kumaraswamy et al., "Spatial co-registration of neuron morphologies based on maximization of volume overlap", *Neuroinformatics Meeting 2018*, Kuala Lumpur, Malaysia
Student Talk	Kumaraswamy et al., "Evidence for morphological refinement of neurons encoding waggle dance communication signals in the honeybee", 11th *Göttigen Meeting of the German Neuroscience Society 2015*, Göttingen, Germany
Poster	Kumaraswamy et al., "Method for comparing and classifying morphologies of neurons based on spatial alignment", *Bernstein Conference 2014*, Tübingen, Germany
Paper	Kumaraswamy et al., "A USB-based Multi-channel Frequency Recorder For Power System Applications", *Centenary Conference of the Electrical Engineering Dept., IISc 2011*, Bangalore, India

Journal Publications

2018	[preprint] Kumaraswamy et al. "Adaptations during maturation in an identified honeybee interneuron responsive to waggle dance vibration signals". *bioRxiv*. `https://doi.org/10.1101/469502`.
2018	Kumaraswamy et al. "Spatial Registration of Neuron Morphologies Based on Maximization of Volume Overlap." *BMC Bioinformatics*. `https://doi.org/10.1186/s12859-018-2136-z`.
2017	[preprint] Kumaraswamy et al. "Network Simulations of Interneuron Circuits in the Honeybee Primary Auditory Center." *bioRxiv*. `https://doi.org/10.1101/159533`.
2017	Ai, Kumaraswamy, et al., "Interneurons in the Honeybee Primary Auditory Center Responding to Waggle Dance-like Vibration Pulses." *The Journal of Neuroscience*. `https://doi.org/10.1523/JNEUROSCI.0044-17.2017`
2018	Ai, Kumaraswamy et al. "Inhibitory Pathways for Processing the Temporal Structure of Sensory Signals in the Insect Brain." *Frontiers in Psychology*. `https://doi.org/10.3389/fpsyg.2018.01517`.

2018	Ikeno, Kumaraswamy et al. "A Segmentation Scheme for Complex Neuronal Arbors and Application to Vibration Sensitive Neurons in the Honeybee Brain." *Frontiers in Neuroinformatics*. `https://doi.org/10.3389/fninf.2018.00061`.
2014	Rautenberg, Kumaraswamy A, et al. "NeuronDepot — Keeping your colleagues in sync by combining modern cloud storage services, local the file system, and user-friendly web techniques", *Frontiers in Neuroinformatics 8:55*. `https://doi.org/10.3389/fninf.2014.00055`.

Awards and Honors

2012	Was awarded **two gold medals** for securing the **highest CGPA** in the B.Tech. (Electrical and Electronics Engineering) batch of 2010-2011 at NITK, Surathkal.
2009	Won **First Prize** in Symphony, a controller-circuit design contest for a musical water fountain, in Engineer 2009, annual technical festival of NITK, Surathkal.

Computer skills

Python	*Advanced*
C/C++	*Good*
Microsoft/Libre Office	*Advanced*
Linux and Windows setup and usage	*Advanced*
Matlab	*Advanced*
R	*Beginner*

Languages

English	Fluent	*Complete education in this medium*
German	Intermediate	*B1 telc exam; attended B2 classes*
Kannada	Fluent	*Mother Tongue and Formally educated as a language*
Hindi	Intermediate	*Formally educated as a language*
Sanskritam	Intermediate	*Formally educated as a language*

Other Interests

Sports	Badminton, Squash and Table Tennis at recreation centers.
Music	Hard Rock and Carnatic Classical, trained in Indian classical Flute, performed in a band at many locations in Munich.
Literature	Kannada and English Novels.
Traveling	Exploring new cities, landscapes and cultures.